Allosteric regulation of the ligand-binding ability of Zn-porphyrin

(亜鉛ポルフィリン軸配位能の
アロステリック抑制)

理学研究科
物質分子系専攻

平成 27 年度

Yoshikazu Ninomiya
(二宮　美雄)

Contents

~Chapter 1~
General introduction

1-1. Allosteric regulation

"Allosteric" regulation is an essential mechanism for *in vivo* metabolic control. Allosteric regulation is a non-competitive function control mechanism. "Allosteric" is neoterized from the Greek words "*allos*" and "*stereos*"; these words mean "other" and "solid," respectively.[1a] In the allosteric mechanism, the activity of compounds with functional units (catalyst, receptor, etc.) is regulated by the conformational changes in the compounds triggered by the binding of a small molecule or an ion to a specific site. This specific site is known as "allosteric site." The chemical species is known as "effector" or "stimulus." When the binding of the effector activates or strengthens the activity of the compound, the effect is called "positive allosteric effect" or "allosteric activation." When the binding of the effector inactivates or weakens the activity of the compound, the effect is called "negative allosteric effect" or "allosteric inhibition." Allosteric regulation is also categorized by the type of effector and substrate. When effector and substrate are different materials, the allosteric system is categorized as "heterotropic." In contrast, when effector and substrate are the same material, the allosteric system is categorized as "homotropic." In allosteric systems with multiple active sites, they sometimes act as the allosteric site for another active site. In this case, the effect is called "cooperative effect."[1]

Recently, artificial allosteric systems have attracted much interest from the viewpoint of the application to smart catalysts, drug-delivery reagents, and molecular machines.[1] Pre-organized, self-locking, and shielding strategies are frequently used for the construction of artificial allosteric systems. In the pre-organized strategy, the steric configuration of the active site is confined to the active or inactive form by the binding of the effector.[2–4] Nabeshima *et al.* reported an allosteric receptor with an oligo ethylene glycol chain and two bipyridine units as the active site and allosteric site, respectively (Figure 1-1).[2a] The conformation of the oligo ether chain changed from a linear form to a cyclic form by adding Cu^+ ions. The cyclic form of the oligo ethylene glycol chain is advantageous for bonding alkali metal ions.

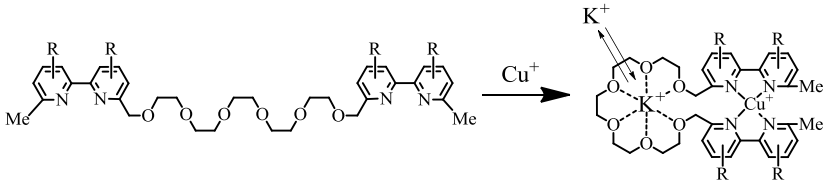

Figure 1-1. Allosteric receptor based on the pre-organized strategy.

In the self-locking strategy, the active site is blocked by a part of the compound itself similar to a competitive inhibition in the inactive form.[5] In the shielding strategy, the active site is covered by a

shielding unit in the inactive form.[6] For the activation, the binding of the effector must remove the shielding unit from the active site. When the binding of the effector stabilizes the shielding unit around the active site, the activity of the system is inhibited. Mirkin *et al.* reported an activation-type allosteric catalysis system with an aluminium salen unit as the catalytic centre based on the shielding strategy.[6a] They successfully demonstrated the ON/OFF switching of the polymerization of ε-caprolactone by regulating the catalytic activity of the aluminium centre by adding and removing Cl^- (Figure 1-2). The inactive form of the allosteric system has a three-layer structure where bulky shielding units were fixed above and below the salen units. Therefore, the catalytic activity of the aluminium salen unit decreased because the accessibility of the substrate to the aluminium centre is considerably reduced. In contrast, addition of Cl^- results in the cleavage of the Rh–N bond and the removal of the shielding unit from the salen unit, thus enhancing the catalytic ability. Most of the previously reported allosteric systems exhibited allosteric activation. Allosteric inhibition-type systems are of interest from a scientific point of view and important for various applications.

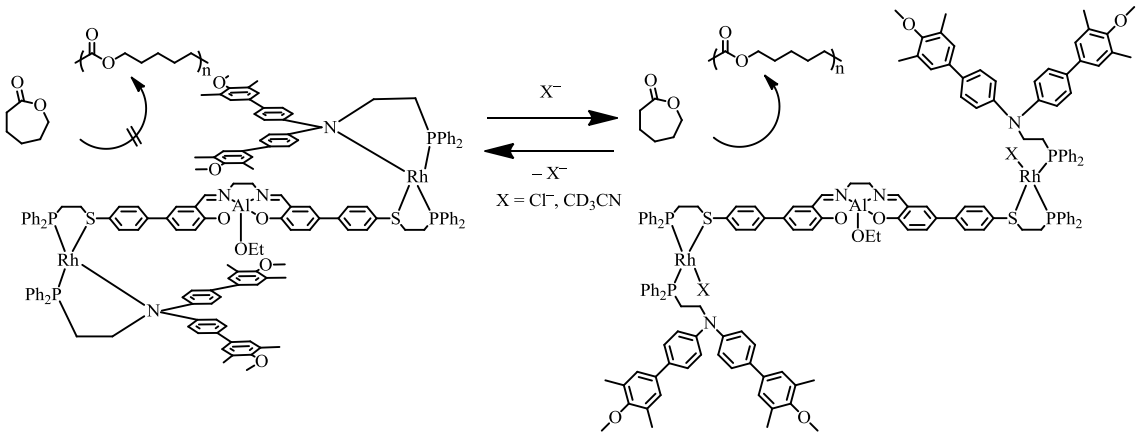

Figure 1-2. Allosteric salen catalyst based on the shielding strategy.

1-2. Porphyrins

Porphyrins are organic compounds with a cyclic π-conjugated system. (Figure 1-3, M = 2H) Metalloporphyrins (metal complex of porphyrins, Figure 1-3, M = metal ion) show various functions depending on the metal centre. Porphyrin derivatives and analogues are widely found in natural catalysts and receptors *in vivo*.[7a] These porphyrins are known as one of the most versatile functional units and act as receptors, electron donors, visible-light absorbers, and catalysts.[7] The regulation of the activity of porphyrin units by external stimulus afforded several types of smart functional materials where the activity changes in response to an external environment.

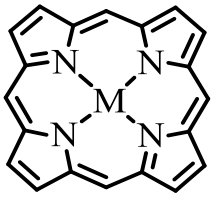

Figure 1-3. Chemical structure of porphyrin.

Schmittel *et al.* reported an activation-type allosteric receptor with a Zn porphyrin unit as the ligand-binding site based on the self-locking strategy.[5a,5b] They successfully demonstrated the ON/OFF switching of the organocatalytic process by regulating the axial coordination of the catalyst to Zn porphyrin unit. In the inactive form, it is difficult for the catalyst to ligate the Zn porphyrin of the receptor because of the intramolecular coordination of the pyrimidinyl terminal to the Zn porphyrin unit. After the addition of both Cu(I) ions and a phenanthroline-type ligand, the intramolecular coordination was prevented because of the formation of a Cu complex. Therefore, the catalyst bound to the Zn porphyrin unit, and the concentration of the active catalyst decreased considerably (Figure 1-4).

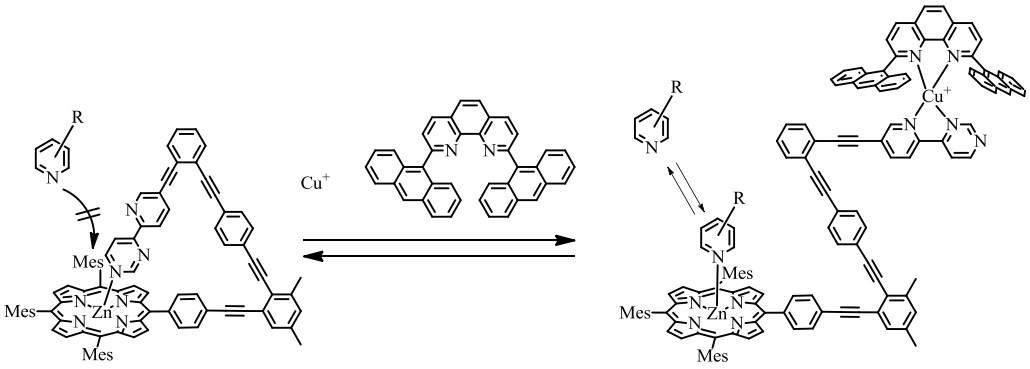

Figure 1-4. Self-locking type allosteric receptor.

1-3. Previous studies

The pre-organized strategy has been used for the allosteric regulation of the axial binding properties of metalloporphyrins.[3b] As described above, the self-locking strategy is important for the allosteric regulation of the axial binding ability of metalloporphyrins. Because the self-locking strategy depends on the receptor ability of an active site, it is difficult to use the allosteric regulation of the catalytic activity of metalloporphyrins. The shielding strategy is applied to allosteric regulation of the various activities of metalloporphyrins. However, the shielding strategy has not been investigated in detail for use in the allosteric regulation of axial binding, or for regulating the catalytic activity of metalloporphyrins.

Previously, our research group reported a unique method for inducing a large conformational change in alkyl chains by metal complexation.[6b] This conformational change was applied to the construction of the allosteric receptor shown in Figure 1-5 in which the steric environment around the porphyrin unit was switched by metal complexation. Herein, the shielding strategy was used for allosteric regulation.

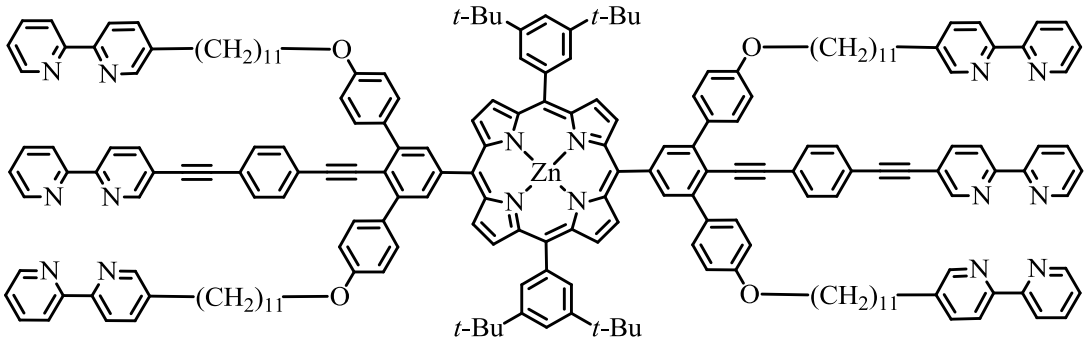

Figure 1-5. Chemical structure of allosteric receptor in previous study.

The allosteric receptor affords two [M(bpy)$_3$]-type complexes with Fe ions at each terminal of the central rigid chain. In the Fe complex, the conformation of the alkyl chains is fixed, and the steric crowding above and below the porphyrin ring is reduced. Therefore, the axial binding ability of the Zn porphyrin was enhanced by adding Fe ions. Unfortunately, the conformational change had only a limited effect on the binding constant (1.2 times enhancement by Fe(II)), probably because of the large separation between the Zn porphyrin unit and alkyl chains.

1-4. Strategy and abstract of this study

The results of a previous study show the important factors to achieve more effective allosteric regulation using the shielding strategy: The Zn porphyrin unit should be located at a position where the conformational change of alkyl chains strongly affects the steric environment. Allosteric receptor **1** was designed to enhance the allosteric regulation of the axial binding ability of Zn porphyrins by metal complexation (Figure 1-6). Because Zn porphyrin units are incorporated in the middle of the conjugated chains, the alkyl chains effectively shield above and below the porphyrin ring in the Fe complex of receptor **1**. Therefore, the axial binding ability of the Zn porphyrin is allosterically inhibited by Fe ions. To the best of our knowledge, such an approach has not been applied to allosteric systems with metalloporphyrins as the active site.

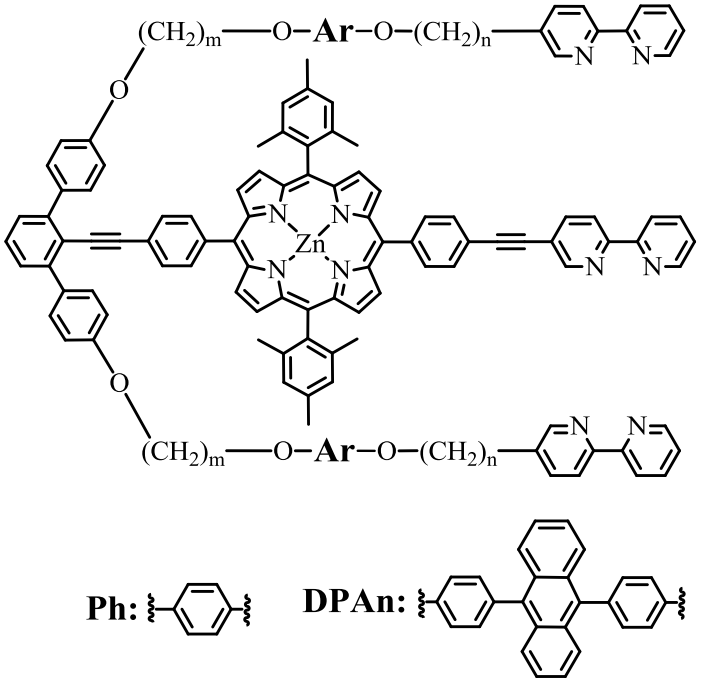

1a : n = 11, m = 12, Ar = **Ph**
1b : n = 9, m = 10, Ar = **Ph**
1c : n = 7, m = 8, Ar = **Ph**
1d : n = 5, m = 6, Ar = **Ph**
1e : n = 5, m = 4, Ar = **DPAn**

Figure 1-6. Chemical structures of allosteric receptor **1**.

In **chapter 2**, the design and synthesis of artificial allosteric receptor **1a** are described. The analytical method used for evaluating the degree of allosteric inhibition of the axial binding ability of receptor **1** is described. The Fe complexation of receptor **1a** was confirmed by both UV–visible spectroscopic titration and ESI-MS spectrum. The axial binding ability of receptor **1a** before and after the Fe complexation was determined by UV–visible spectroscopic titration to evaluate the degree of allosteric inhibition. In **chapter 3**, three allosteric receptors with shorter alkyl chains were designed (**1b**, **1c**, and **1d**; Figure 1-6.) The alkyl chain length was selected using molecular mechanics force field (MMFF) calculations to form stable 1:1 complexes with Fe ions and for the effective shielding of the Zn porphyrin unit. Based on the calculation results, receptors **1b** and **1c** were selected as the synthetic targets. The receptors were synthesized, and their properties as the allosteric receptor were evaluated. Several types of axial ligands were prepared to study the effect of the structural difference in axial ligands on the allosteric inhibition of receptor **1**. The binding constants of allosteric receptors **1a**, **1b**, and **1c** with these axial ligands were determined to estimate the degree of allosteric inhibition.

In **chapter 4**, allosteric receptor **1e** with sterically bulky shielding units was designed. After the MMFF calculations, receptor **1e** was synthesized, and its superior properties as an allosteric receptor were established. Moreover, the thermodynamic parameters of axial ligand binding reactions before and after the addition of Fe ions were determined.

1-5. References

(1) (a) Kremer, C.; Lützen A. *Chem. Eur. J.* **2013**, *19*, 6162−6196. (b) Nabeshima, T. *Bull. Chem. Soc. Jpn.* **2010**, *83*, 969−991. (c) Shinkai, S.; Ikeda, M.; Sugasaki A.; Takeuchi, M. *Acc. Chem. Res.* **2001**, *34*, 494−503. (d) Brown, R. A.; Diemer, V.; Webb S. J.; Clayden *J. Nature Chem.* **2013**, *5*, 853−860. (e) Clayden, J.; Vassiliou, N. *Org. Biomol. Chem.* **2006**, *4*, 2667−2678. (f) Kovbasyuk, L.; Krämer, R. *Chem. Rev.* **2004**, *104*, 3161−3188. (g) Balzani, V.; Venturi, M.; Credi, A. Molecular Devices and Machines: *A Journey into the Nanoworld*, Wiley-VCH, Weinheim: Germany, **2003**. doi: 10.1002/3527601600.

(2) (a) Nabeshima, T.; Inaba, T.; Furukawa, N.; Hosoya, T.; Yano, Y. *Inorg, Chem.* **1993**, *32*, 1407−1416. (b) Kobuke, Y.; Satoh, Y. *J. Am. Chem. Soc.* **1992**, *114*, 789−790. (c) Nabeshima, T.; Yoshihira, Y.; Saiki, T.; Akine, S.; Horn, E. *J. Am. Chem. Soc.* **2003**, *125*, 28−29. (d) Nabeshima, T.; Hanami, T.; Akine, S.; Saiki, T. *Chem. Lett.* **2001**, 560−561.

(3) (a) Robertson, A.; Ikeda, M.; Takeuchi, M.; Shinkai, S. *Bull. Chem. Soc. Jpn.* **2001**, *74*, 883−888. (b) Ayabe, M.; Ikeda, A.; Kubo, Y.; Takeuchi, M.; Shinkai, S. *Angew. Chem. Int. Ed.* **2002**, *41*, 2790−2792.

(4) (a) Baldes, R.; Schneider, H.-J. *Angew. Chem. Int. Ed. Engl.* **1995**, *34*, 321−323. (b) Inouye, M.; Konishi, T.; Isagawa, K. *J. Am. Chem. Soc.* **1993**, *115*, 8091−809.

(5) (a) Schmittel, M.; De S.; Pramanik, S. *Angew. Chem. Int. Ed.* **2012**, *51*, 3832−3836. (b) Pramanik, S.; De, S.; Schmittel, M. *Angew. Chem., Int. Ed.* **2014**, *53*, 4709−4713. (c) Durola, F.; Rebek, J. Jr., *Angew. Chem. Int. Ed.* **2010**, *49*, 3189−3191.

(6) (a) Yoon, H. J.; Kuwabara, J.; Kim, J.-H.; Mirkin, C. A. *Science* **2010**, 330, 66−69. (b) Kato, M.; Hashimoto, E.; Kozaki, M.; Suzuki S.; Okada, K. *Tetrahedron Lett.* **2012**, *53*, 309−312.

(7) (a) K. M. Kadish, K. M. Smith and R. Guliard eds. *Porphyrin Handbook*; Academic Press, **2000**, Vol. 4. (b) Collman, J. P.; Boulatov, R.; Sunderland C. J.; Fu, L. *Chem. Rev.* **2004**, *104*, 561−588. (c) Gopalaiah, K. *Chem. Rev.* **2013**, *113*, 3248−3296. (d) Kozaki, M.; Suzuki, S.; Okada K. *Chem. Lett.* **2013**, 1112−1118.

~Chapter 2~
Development of allosteric receptor using Fe(II) ion as an external stimulus

2-1. Introduction

In this chapter, molecule **1a** was designed as an artificial allosteric receptor (Figure 2-1). Receptor **1a** contains a Zn porphyrin as the active (axial ligand binding) site in the middle of the rigid conjugated chain. A bipyridine unit was attached at one end of the rigid chain. The other end of the chain was separated and attached to two other bipyridine units through flexible alkyl chains. These bipyridine units form a $[Fe^{II}(bpy)_3]$-type complex when Fe(II) is used as the external stimulus. In the iron complex, the alkyl chain bridges are expected to shield the Zn porphyrin unit and inhibit its axial ligand-binding ability (Scheme 2-1).

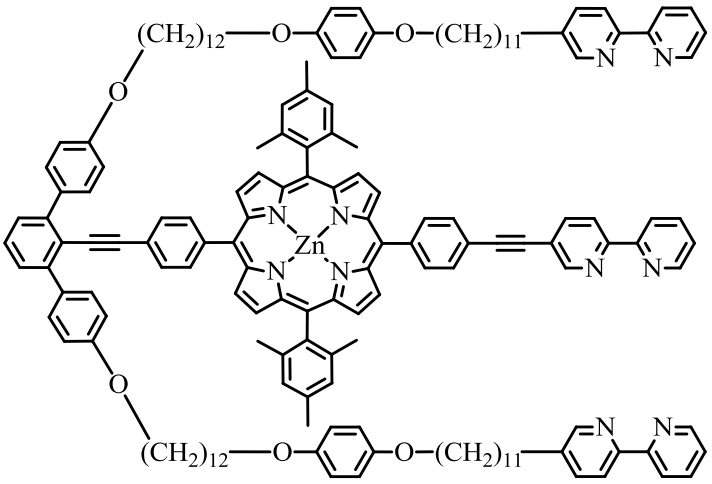

Figure 2-1. Chemical structure of receptor **1a**.

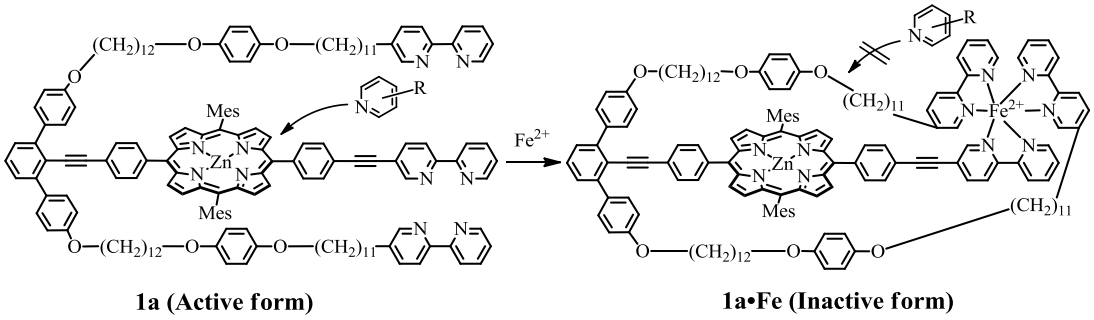

Scheme 2-1. Expected mechanism of allosteric inhibition in receptor **1a**.

2-2. Synthesis of side chain 7a

Alkyl chain **7a** was synthesized as shown in Scheme 2-2. A mixture of 1,12-dibromododecane and pinacol borate **2** was heated under basic conditions in anhydrous DMF, affording pinacol borate **3a** in 66% yield. The treatment of 5-methyl-2,2′-bipyridine (**4**)[2] with LDA followed by reaction with 1,10-dibromodecane afforded **5a** in 56% yield.[3] In these reactions, excess dibromoalkanes were used to avoid the formation of the corresponding disubstituted alkane derivatives as a by-product. These bromoalkanes **5a** and **3a** were attached to hydroquinone stepwise by heating under basic conditions in anhydrous DMF, affording side chain **7a** in 32% yield (two steps). In the synthesis of **6a**, an excess amount of hydroquinone was used to suppress the formation of the corresponding disubstituted by-product.

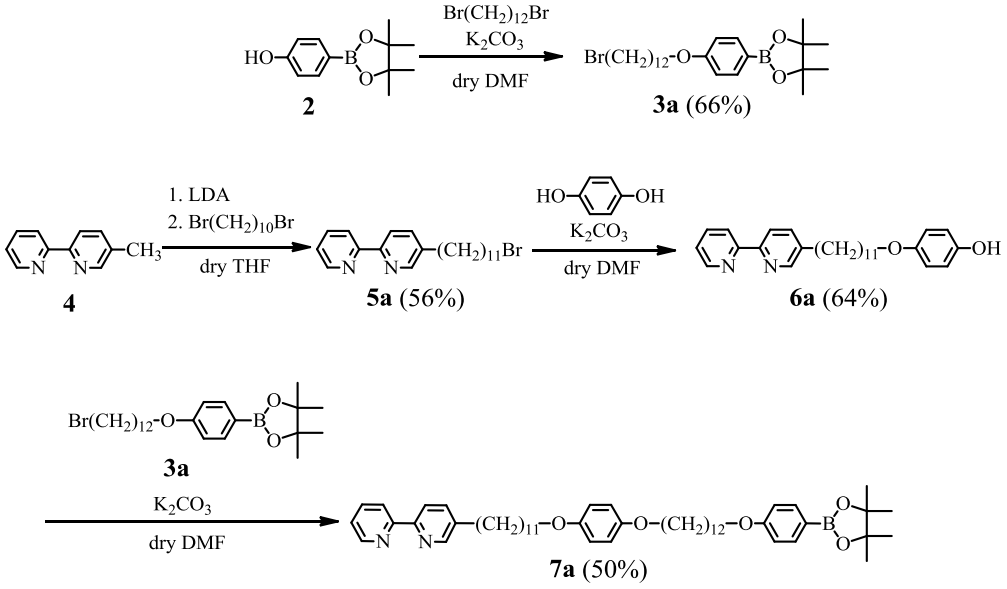

Scheme 2-2. Synthesis of side chain **7a**.

2-3. Synthesis of receptor 1a and main chain 11

Main chain **11** and receptor **1a** were synthesized as shown in Scheme 2-3. The three-component Sonogashira cross-coupling reaction of Zn porphyrin **8**[4] with 1,3-dibromo-2-ethynylbenzene (**9**)[5] and 5-ethynyl-2,2′-bipyridine (**10**)[2] afforded main chain **11** in 41% yield.[6] The Suzuki–Miyaura cross-coupling reaction of main chain **11** with side chain **7a** afforded **1a** as a purple solid in 67% yield.[7]

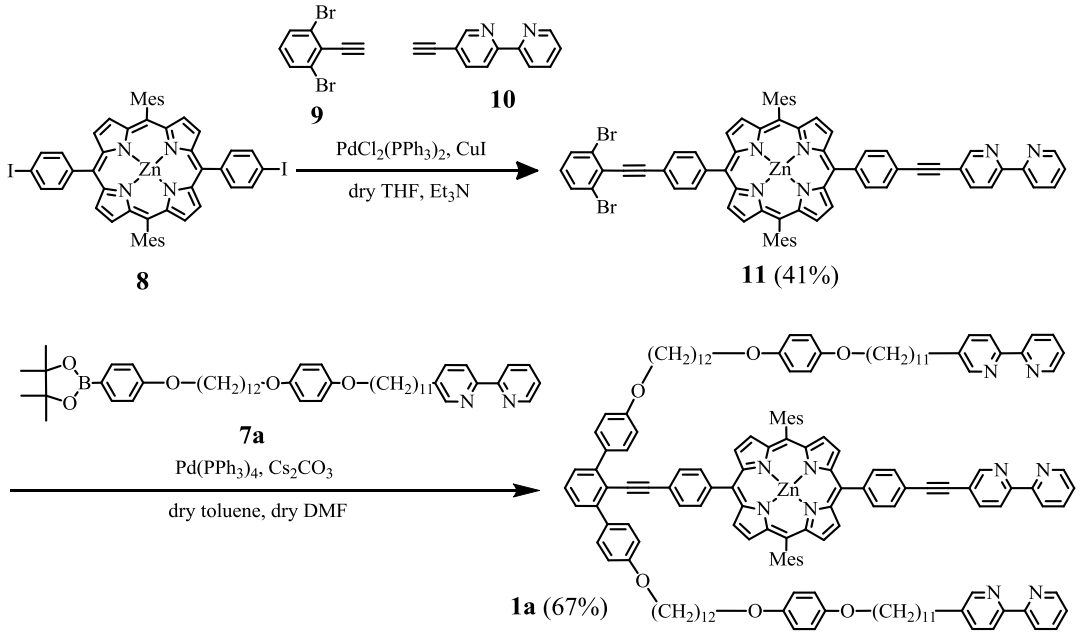

Scheme 2-3. Synthesis of receptor **1a** and main chain **11**.

2-4. Iron complexation

It was conformed that allosteric receptor 1a formed a stable 1:1 complex with Fe(II) ions in a mixture of toluene/acetonitrile (1:1 v/v). A solution of **1a** (2×10^{-5} M) exhibited the characteristic Soret band (440 nm) and Q-band (550−630 nm) absorption of the Zn porphyrin skeleton. As shown in Figure 2-2a, when Fe(II) ions were added to a solution of **1a** (2×10^{-5} M), the characteristic metal-to-ligand charge transfer (MLCT) absorption band of the Fe(II)$(bpy)_3$-type complex appeared at ~500 nm.[8] The absorption owing to the MLCT band at 500 nm linearly increased in proportion to the amount of Fe(II) ions until the concentration of Fe(II) reached equivalent to **1a** (Figure 2-2b). These results indicate the almost quantitative formation ($K_{1a\cdot Fe} > 10^6$ M^{-1}) of Fe(II)$(bpy)_3$-type complex **1a·Fe**. The formation of 1:1 complex **1a·Fe** was supported by ESI-MS spectrum (Figure 2-3). The peak at m/z = 2534 can be assigned to $[(\mathbf{1a\cdot Fe})\cdot\mathbf{BF_4}]^+$ (MW = 2534, calcd for $C_{160}H_{170}BF_4FeN_{10}O_6Zn$). The observed isotope pattern was consistent with the theoretical pattern.

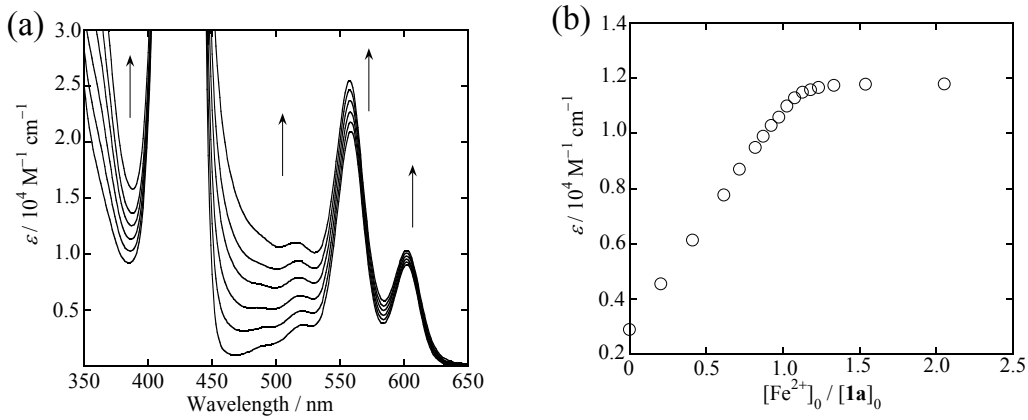

Figure 2-2. (a) UV–vis spectral change resulting from the titration of **1a** (2×10^{-5} M) with $Fe(BF_4)_2$•$6H_2O$ (3×10^{-4} M) in a toluene/acetonitrile (1/1 (v/v)) solution at 20 °C. (b) The change in the molar extinction coefficient at 500 nm. $[Fe^{2+}]_0$: The concentration of Fe^{2+} when complexation is ignored. $[\mathbf{1a}]_0$: The initial concentration of **1a**.

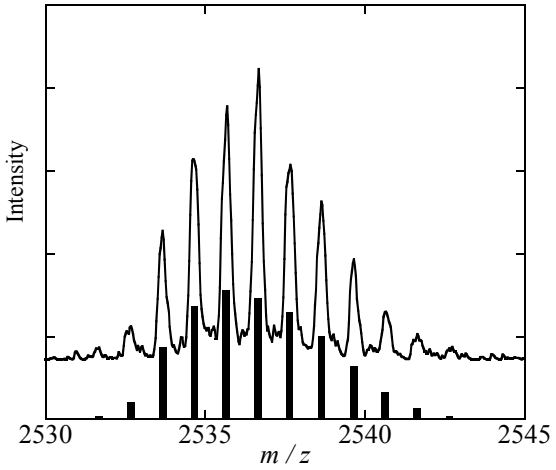

Figure 2-3. ESI-Mass spectrum of **1a** with $Fe(BF_4)_2$•$6H_2O$ in a toluene/acetonitrile (1/1 (v/v)) solution. Line is observed spectrum. The block height is calculated isotope pattern of $[(\mathbf{1a•Fe})•\mathbf{BF_4}]^+$, calcd for $C_{160}H_{170}BF_4FeN_{10}O_6Zn$: 2534.

2-5. Axial binding and allosteric inhibition

The binding constant of active receptor **1a** with an axial ligand ($K_{\mathbf{1}\text{-}\mathbf{L}}$) was determined by the UV–visible spectroscopic titration in a mixture of toluene/acetonitrile (1:1 v/v). When a solution of **LP1** (4-phenylpyridine, Figure 2-4, 6×10^{-2} M) was added to a solution of **1a** (5×10^{-5} M), the porphyrin Q-band red-shifted (to λ_{Max} = 565, 608 nm, from λ_{Max} = 559, 603 nm) because of the axial coordination of **LP1** to the porphyrin zinc centre (Figure 2-5). The red shift of an absorption band

due to the axial coordination to a porphyrin Zn centre has been reported.[9] The binding constants of allosteric receptor **1a** with **LP1** ($K_{\mathbf{1a}\cdot\mathbf{LP1}}$) was determined to be 8.67 ± 0.14 × 10^3 M^{-1} by the curve fitting of experimental data (see section 2-7-2).

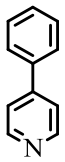

LP1

Figure 2-4. Chemical structure of axial ligand **LP1**.

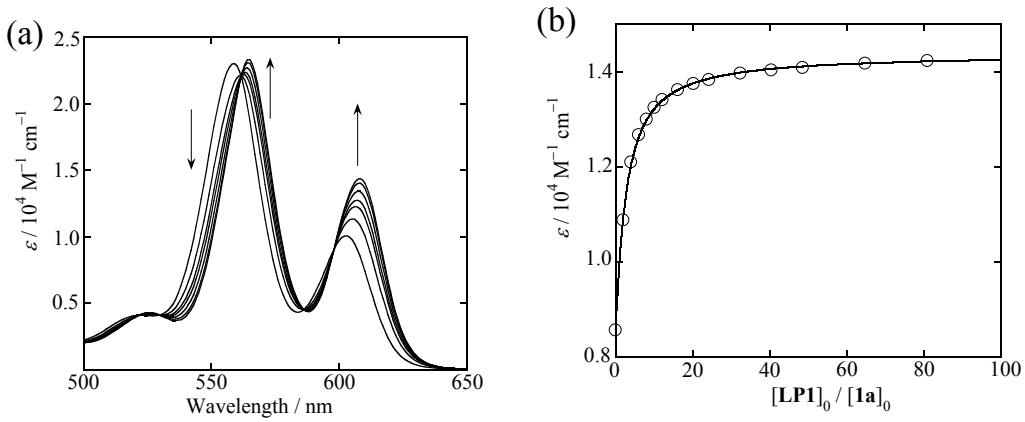

Figure 2-5. (a) UV−vis spectra change resulting from the titration of **1a** (5×10^{-5} M) with **LP1** in a toluene/acetonitrile (1/1 (v/v)) solution at 20 °C. (b) The change in the molar extinction coefficient at 608 nm. The solid line is a regression curve obtained by curve fitting. $[\mathbf{LP1}]_0$: The concentration of **LP1** when axial binding is ignored. $[\mathbf{1a}]_0$: The initial concentration of **1a**.

The binding constant of inactive allosteric receptor **1a·Fe** with an axial ligand ($K_{(\mathbf{1\cdot Fe})\cdot\mathbf{L}}$) was determined by a similar titration experiment. First, **1a·Fe** was prepared by adding 1.0 equiv of Fe(II) to a solution of **1a**. A solution of **LP1** (6×10^{-2} M) was added to a solution of **1a·Fe** (2×10^{-5} M). The porphyrin Q-band red-shifted because of the axial coordination of **LP1** to Zn porphyrin (Figure 2-6). The molar absorptivity of the MLCT band around 500 nm showed insignificant change during the titration, indicating that the dissociation of **1a·Fe** did not occur. The binding constant of inactive allosteric receptor **1a·Fe** with **LP1** ($K_{(\mathbf{1a\cdot Fe})\cdot\mathbf{LP1}}$) was determined to be 5.28 ± 0.05 × 10^3 M^{-1}.

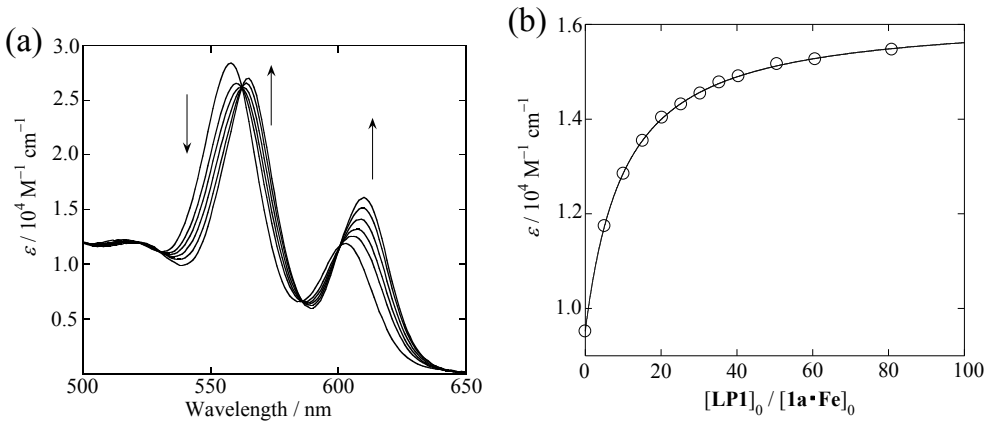

Figure 2-6. (a) UV–vis spectral change resulting from the titration of **1a•Fe** (2×10^{-5} M) with **LP1** (6×10^{-2} M) in a toluene/acetonitrile (1/1 (v/v)) solution at 20 °C. (b) The change in the molar extinction coefficient at 610 nm. The solid line is a regression curve obtained by curve fitting. $[\mathbf{LP1}]_0$: The concentration of **LP1** when axial binding is ignored. $[\mathbf{1a•Fe}]_0$: The initial concentration of **1a•Fe**.

The degree of allosteric inhibition on the ligand-binding ability of Zn porphyrin by Fe(II) ions was defined as the binding constant of the active form ($K_{\mathbf{1\cdot L}}$) divided by that of the inactive form ($K_{\mathbf{(1\cdot Fe)\cdot L}}$). The degree of allosteric inhibition ($K_{\mathbf{1\cdot L}}$/ $K_{\mathbf{(1\cdot Fe)\cdot L}}$) for **LP1** was calculated to be 1.64 ± 0.04, *i.e.*, the ligand-binding ability of the Zn porphyrin of receptor **1a** was inhibited by the addition of Fe(II) ions.

2-6. Conclusion

In conclusion, an artificial allosteric receptor **1a** with a Zn porphyrin as the axial ligand-binding site, flexible alkyl chains as the shielding units, and bipyridine terminals as the Fe ion-recognition site was designed and synthesized. Allosteric receptor **1a** formed a stable 1:1 complex with Fe ions as determined by UV–visible titration and ESI-MS spectrum. The binding constants of **1a** were determined by UV–visible spectroscopic titration before (active form) and after the Fe(II) complexation (inactive form). The addition of Fe ions significantly reduced the binding constant; the degree of allosteric inhibition was determined to be 1.64. Further structural optimization of the shielding unit may be required to increase the degree of allosteric inhibition.

2-7. Experimental section

2-7-1. Synthesis and characterization

General procedure.

Melting points were taken on a Yanako MP J-3 apparatus and are uncorrected. ^{1}H NMR and ^{13}C NMR spectra were recorded on Bruker Nanobay 300, JEOL Lambda 300WB, or JEOL Lambda 400 spectrometers. Chemical shifts were recorded in units of parts per million downfield from tetramethylsilane as an internal standard and all coupling constants are reported in Hz. IR spectra were obtained on a Shimadzu FTIR-8700 spectrometer. UV−vis spectra were obtained on a Shimadzu UV-2550PC spectrometer. The mass spectra were recorded on a JEOL JMS-700T and JMX-AX500 spectrometers. Elemental analyses were obtained from the Analytical Center in Osaka City University. TLC was carried out using 0.2 mm thick Merck silica gel (60 F_{254}) and 0.25 mm thick Merck aluminium oxide 60 precoated plates. Merck silica gel 60 (granulometry 0.063–0.200 mm) and Merck aluminium oxide 90 (granulometry 0.063–0.200 mm) were used for column chromatography. Recycling preparative GPC (gel permeation chromatography) was carried out using Japan Analytical Industry LC–908 with JAIGEL-1H and -2H GPC columns. 5-methy-2,2′-bipyridine (**4**)[2], 5,15-Bis(mesityl)-10,20-bis(4-iodophenyl)-porphyrinato zinc(II) (**8**)[4], 1,3-dibromo-2-ethynylbenzene (**9**)[5] and 5-ethynyl-2,2′-bipyridine (**10**)[2] were prepared according to the reported methods. Commercially available reagents and solvents were purified and dried when necessary.

4, 4, 5, 5-Tetramethyl-2-(4-(12-bromoundecyloxyphenyl))-1, 3, 2-dioxaborolane (3a)

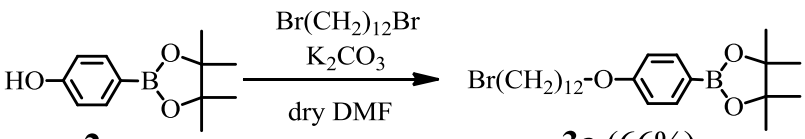

2 **3a** (66%)

To a mixture of **2** (330 mg, 1.5 mmol, 1.0 equiv.), 1,12-dibromododecane (2.46 g, 7.5 mmol, 5.0 equiv.) and potassium carbonate (355 mg, 3.0 mmol, 2.0 equiv.), dry DMF (40 mL) was added under a nitrogen atmosphere. The suspension was stirred overnight at 40 ^{o}C. After cooling to room temperature, the reaction mixture was poured into water. The mixture was extracted with diethyl ether. The extract was dried over sodium sulfate and filtered. The solvent was removed under reduced pressure and the residue was purified by column chromatography on silica gel (hexane/dichloromethane = 1/1 (v/v)) to give **3a** as a white solid (460 mg, 66%).

3a: $C_{24}H_{40}BBrO_3$. White solid; MW 467.3; mp 66 ^{o}C; ^{1}H NMR (300 MHz, $CDCl_3$): δ 7.73 (d, 2H, J = 8.6 Hz), 6.88 (d, 2H, J = 8.6 Hz), 3.97 (t, 2H, J = 6.6 Hz), 3.41 (t, 2H, J = 6.9 Hz), 1.90–1.73 (m,

4H), 1.44–1.27 (m, 28H); ^{13}C NMR (100 MHz, $CDCl_3$): δ 161.75, 136.47, 113.86, 83.49, 67.77, 34.02, 32.84, 29.51, 29.50, 29.41, 29.35, 29.19, 28.75, 28.16, 26.00, 24.85; MS (FAB+): *m/z* 468 [MH^+]; IR (KBr, cm^{-1}): 2924(s), 2849(m), 1734(w), 1716(w), 1699(w), 1684(w), 1636(w), 1605(s), 1570(w), 1558(w), 1508(w), 1472(w), 1458(w), 1396(m), 1362(s), 1323(m), 1306(w), 1244(s), 1213(w), 1175(m), 1142(s), 1092(m), 1028(m), 1009(w), 964(w), 860(m), 831(m), 820(m), 723(w), 671(w), 654(m), 625(m), 517(w); HRMS (FAB+): *m/z* Calcd for $C_{24}H_{40}B^{79}BrO_3$: 466.2254. Found: 466.2261.

5-(11-Bromoundecyl)-2,2´-bipyridine (5a)[3]

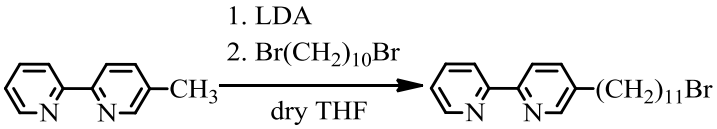

4 **5a** (56%)

To a solution of dry diisopropylamine (1.70 mL, 12 mmol, 2.4 equiv.) in dry THF (12 mL), *n*-butyllithium (1.63 M, in *n*-hexane, 6.13 mL, 10 mmol, 2.0 equiv.) was added dropwise at –78 °C under a nitrogen atmosphere. The solution was stirred for 1 h at –78 °C and 5-methyl-2,2´-bipyridine **4** (855 mg, 5.0 mmol, 1.0 equiv.) in dry THF (50 mL) was added at –78 °C. The temperature was allowed to raise gradually over 4 h to –40 °C. The solution was recooled to –78 °C and 1,10-dibromodecane (7.50 g, 25 mmol, 5.0 equiv.) in dry THF (25 mL) was added. The solution was allowed to warm up to room temperature and stirred overnight. After the addition of water, THF was evaporated under reduced pressure. Sodium hydrogen carbonate solution was added and the mixture was extracted with dichloromethane. The extract was washed with brine and dried over sodium sulfate. After filtration, the solvent was removed under reduced pressure. The crude product was purified by column chromatography on basic aluminium oxide (toluene) to give **5a** as a white powder (1.10 g, 56%). Analytically pure sample was obtained by recrystallization from hexane.

5a: $C_{21}H_{29}BrN_2$. White solid; MW 389.4; mp 48 °C; ^{1}H NMR (300 MHz, $CDCl_3$): δ 8.67 (d, 1H, J = 4.2 Hz), 8.50 (d, 1H, J = 1.8 Hz), 8.36 (d, 1H, J = 8.0 Hz), 8.31 (d, 1H, J = 8.1 Hz), 7.81 (td, 1H, J = 7.7, 1.8 Hz), 7.63 (dd, 1H, J = 8.1, 2.2 Hz), 7.31–7.29 (m, 1H), 3.40 (t, 2H, J = 6.9 Hz), 2.67 (t, 2H, J = 7.6 Hz), 1.85 (quintet, 2H, J = 7.1 Hz), 1.64–1.27 (m, 16H); ^{13}C NMR (100 MHz, $CDCl_3$) δ 156.35, 153.86, 149.35, 149.14, 138.26, 136.85, 136.79, 123.36, 120.79, 120.69, 34.02, 32.84, 32.83, 31.05, 29.47, 29.39, 29.10, 28.74, 28.16; MS (FAB+): *m/z* 389.1 [MH^+]; IR (KBr, cm^{-1}): 2926(s), 2852(s), 1716(w), 1684(w), 1587(m), 1574(s), 1558(s), 1541(w), 1508(w), 1458(s), 1435(m), 1423(w), 1394(w), 1223(w), 1090(w), 1026(w), 796(s), 775(w), 754(s), 729(m), 613(w), 548(w), 534(w), 517(w); HRMS (FAB+): *m/z* Calcd for $C_{19}H_{26}{}^{79}BrN_2$: 389.1592. Found: 389.1585.

Compound 6a

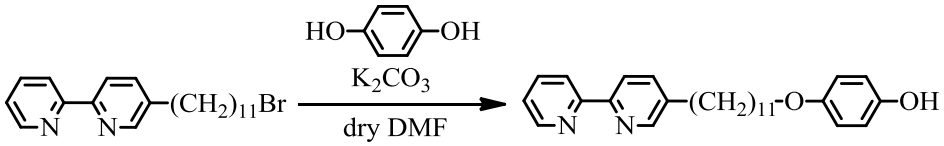

5a **6a** (64%)

To a mixture of **5a** (623 mg, 1.6 mmol, 1.0 equiv.), 1,4-dihydroxybenzene (880 mg, 8.0 mmol, 5.0 equiv.) and potassium carbonate (1.11 g, 8.0 mmol, 5.0 equiv.), dry DMF (70 mL) was added under a nitrogen atmosphere. The suspension was stirred overnight at 80 °C. After cooling to room temperature, the reaction mixture was poured into water. The mixture was extracted with diethyl ether. The extract was dried over sodium sulfate and filtered. The solvent was removed under reduced pressure and the residue was purified by column chromatography on basic aluminium oxide (dichloromethane/methanol = 49/1 (v/v)) to give **6a** as a light brown solid (430 mg, 64%).

6a: $C_{27}H_{34}N_2O_2$. light brown solid; MW 418.6; mp 83 °C; ^{1}H NMR (300 MHz, $CDCl_3$): δ 8.67 (d, 1H, J = 4.4 Hz), 8.50 (s like, 1H), 8.36 (d, 1H, J = 8.0 Hz), 8.29 (d, 1H, J = 8.0 Hz), 7.82 (td, 1H, J = 7.7, 1.5 Hz), 7.63 (dd, 1H, J = 8.1, 1.9 Hz), 7.32–7.28 (m, 1H), 6.77–6.70 (d like, 4H, J = 2.6 Hz), 5.63 (br, 1H), 3.88 (t, 2H, J = 6.5 Hz), 2.66 (t, 2H, J = 7.6 Hz), 1.76–1.28 (m, 18H); ^{13}C NMR (100 MHz, $CDCl_3$): δ 156.09, 153.59, 152.92, 150.11, 149.24, 149.05, 138.54, 137.19, 137.13, 123.56, 121.16, 121.08, 116.11, 115.63, 68.69, 32.84, 31.02, 29.43, 29.42, 29.39, 29.27, 29.19, 29.09, 25.96; MS (FAB+): *m/z* 419.2 [MH^+]; IR (KBr, cm^{-1}): 2918(s), 2851(s), 1734(w), 1716(w), 1699(w), 1684(w), 1591(w), 1576(w), 1558(w), 1541(w), 1514(s), 1458(m), 1446(w), 1394(w), 1340(w), 1296(w), 1238(s), 1097(w), 1043(w), 1018(w), 999(w), 820(m), 793(m), 772(m), 754(m), 719(w), 592(w), 517(w); HRMS (FAB+): *m/z* Calcd for $C_{27}H_{35}N_2O_2$: 419.2699. Found: 419.2695.

Compound 7a (Side chain)

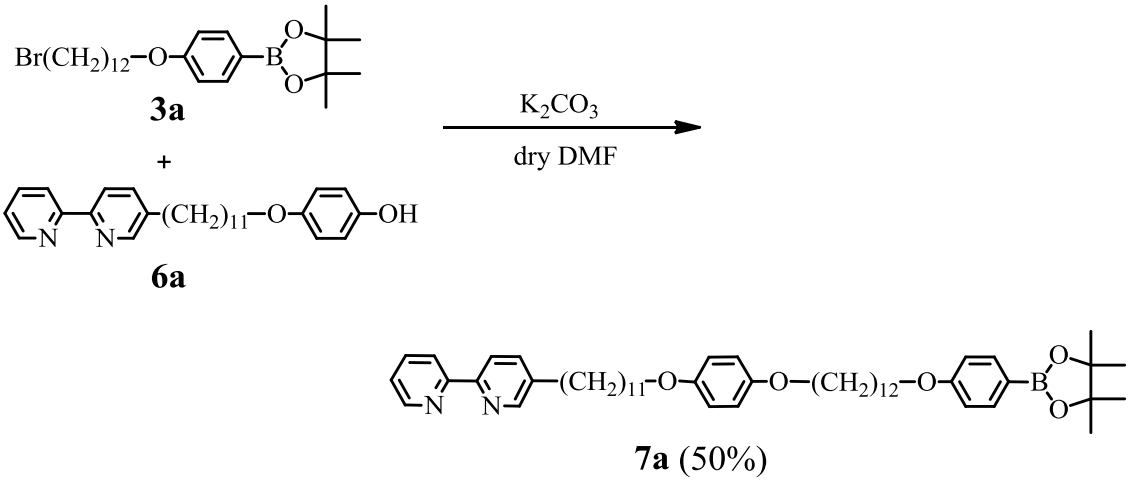

To a mixture of **3a** (234 mg, 0.50 mmol, 1.25 equiv.), **6a** (167 mg, 0.40 mmol, 1.0 equiv.) and potassium carbonate (276 mg, 2.0 mmol, 5.0 equiv.), dry DMF (20 mL) was added under a nitrogen atmosphere. The suspension was stirred overnight at 100 ^{o}C. After cooling to room temperature, the reaction mixture was poured into water. The mixture was extracted with diethyl ether. The extract was dried over sodium sulfate and filtered. The solvent was removed under reduced pressure and the residue was purified by column chromatography on basic aluminium oxide (dichloromethane/methanol = 19/1 (v/v)) to give **7a** as a white powder (161 mg, 50%).

7a: $C_{51}H_{73}BN_2O_5$. white solid; MW 805.0; mp 93 ^{o}C; ^{1}H NMR (400 MHz, $CDCl_3$): δ 8.66 (d like, 1H, J = 4.9 Hz), 8.50 (d, 1H, J = 2.0 Hz), 8.36 (d like, 1H, J = 7.8 Hz), 8.3 (d, 1H, J = 8.0 Hz), 7.80 (td, 1H, J = 7.7, 1.9 Hz), 7.73 (d like, 2H, J = 8.6 Hz), 7.63 (dd, 1H, J = 8.0, 2.2 Hz), 7.30–7.27 (m, 1H), 6.90–6.87 (d like, 4H, J = 8.5 Hz), 6.81 (s, 4H), 3.97 (t, 2H, J = 6.6 Hz), 3.89 (t, 2H, J = 6.6 Hz), 2.66 (t, 2H, J = 7.7 Hz), 1.81–1.57 (m, 8H), 1.48–1.28 (m, 42H); ^{13}C NMR (100 MHz, $CDCl_3$): δ 161.78, 156.36, 153.86, 153.23, 149.36, 149.14, 138.31, 136.86, 136.79, 136.49, 123.37, 120.82, 120.70, 115.42, 113.88, 83.51, 68.68, 67.81, 32.88, 31.09, 29.58, 29.54, 29.42, 29.22, 29.14, 26.07, 26.03, 24.87; MS (FAB+): *m/z* 805.5 [MH^+]; IR (KBr, cm^{-1}): 2920(s), 2851(s), 1607(s), 1589(w), 1558(w), 1510(s), 1474(s), 1458(m), 1396(m), 1364(s), 1317(w), 1279(w), 1232(s), 1177(w), 1144(m), 1092(w), 1042(m), 1009(w), 964(w), 864(w), 810(w), 793(w), 773(w), 750(w), 721(w), 654(w), 613(w), 542(w), 517(w), 502(w); HRMS (FAB+): *m/z* Calcd for $C_{51}H_{74}BN_2O_5$: 805.5691. Found: 805.5717.

Compound 11 (Main chain)[6]

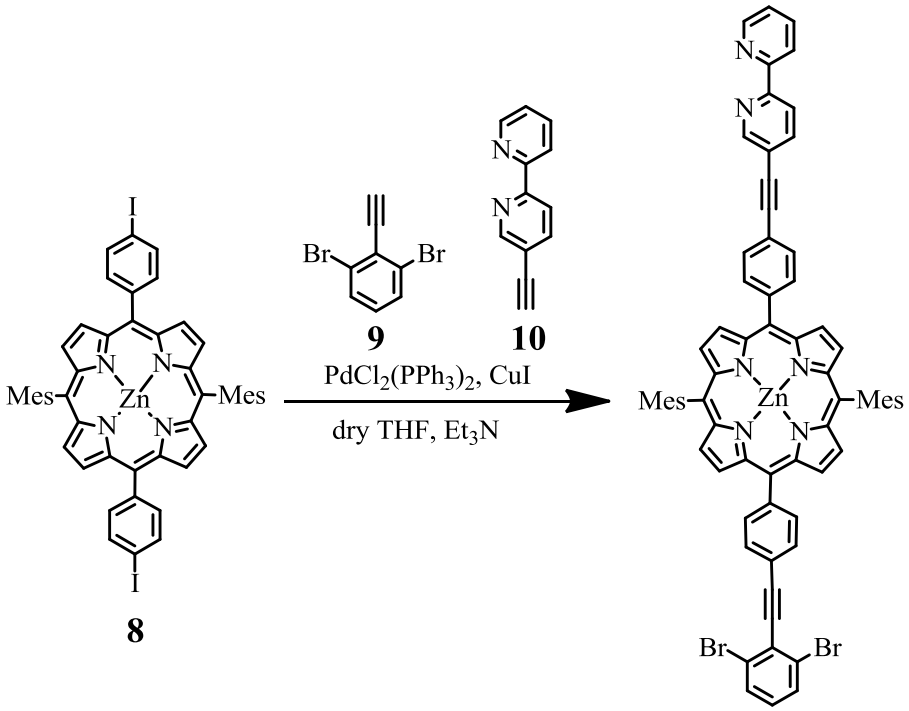

11 (41%)

A solution of **8** (507 mg, 0.50 mmol, 1.0 equiv.), **9** (143 mg, 0.55 mmol, 1.1 equiv.), **10** (100 mg, 0.55 mmol, 1.1 equiv.), bis(triphenylphosphine)palladium dichloride (35 mg, 50 μmol, 0.1 equiv.) and copper(I) iodide (9.5 mg, 0.50 μmol, 0.1 equiv.) in dry triethylamine (8 mL) and dry THF (40 mL) was stirred under a nitrogen atmosphere for a 1 day at 40 ^{o}C. The reaction mixture was filtered and the solvent was evaporated under reduced pressure. The residue was purified by column chromatography on silica gel (hexane/ethyl acetate = 5/1 (v/v)) to give **11** as a purple powder (248 mg, 41%).

11: $C_{70}H_{48}Br_2N_6Zn$. purple solid; MW 1194.4; mp > 300 ^{o}C; ^{1}H NMR (400 MHz, $CDCl_3$): δ 8.97–8.96 (m, 1H), 8.91–8.90 (m, 4H), 8.81–8.0 (m, 4H), 8.73–8.72 (m, 1H), 8.51–8.47 (m, 2H), 8.28–8.26 (m, 4H), 8.10–8.08 (m, 1H), 8.02 (d, 2H, J = 8.0 Hz), 7.97 (d, 2H, J = 8.0 Hz), 7.89–7.85 (m, 1H), 7.66 (d, 2H, J = 8.0 Hz), 7.37–7.34 (m, 1H), 7.29 (s, 4H), 7.09 (t, 1H, J = 8.0 Hz), 2.64 (s, 6H), 1.84 (s, 12H); ^{13}C NMR (100 MHz, $CDCl_3$): δ 151.79, 150.07, 149.79, 149.76, 149.35, 143.74, 143.53, 139.50, 139.23, 138.88, 137.59, 137.02, 134.56, 134.52, 132.19, 132.12, 131.42, 131.07, 130.5, 130.00, 129.96, 129.75, 127.72, 127.34, 126.52, 123.98, 121.79, 121.76, 121.42, 120.48, 120.43, 119.65, 119.45, 119.39, 98.73, 88.46, 21.74, 21.48; MS (FAB+): m/z 1198 [M^+]; IR (KBr, cm^{-1}): 2916(w), 2216(w), 1572(w), 1543(w), 1524(w), 1489(m), 1456(s), 1435(m), 1423(w), 1375(w), 1337(m), 1204(m), 1190(w), 1065(m), 999(s), 852(m), 831(m), 796(s), 768(m), 727(m), 552(w), 542(w), 517(w); HRMS (FAB+): m/z Calcd for $C_{70}H_{48}{}^{79}Br_2N_6{}^{64}Zn$: 1194.1599. Found: 1194.1599.

Compound 1a

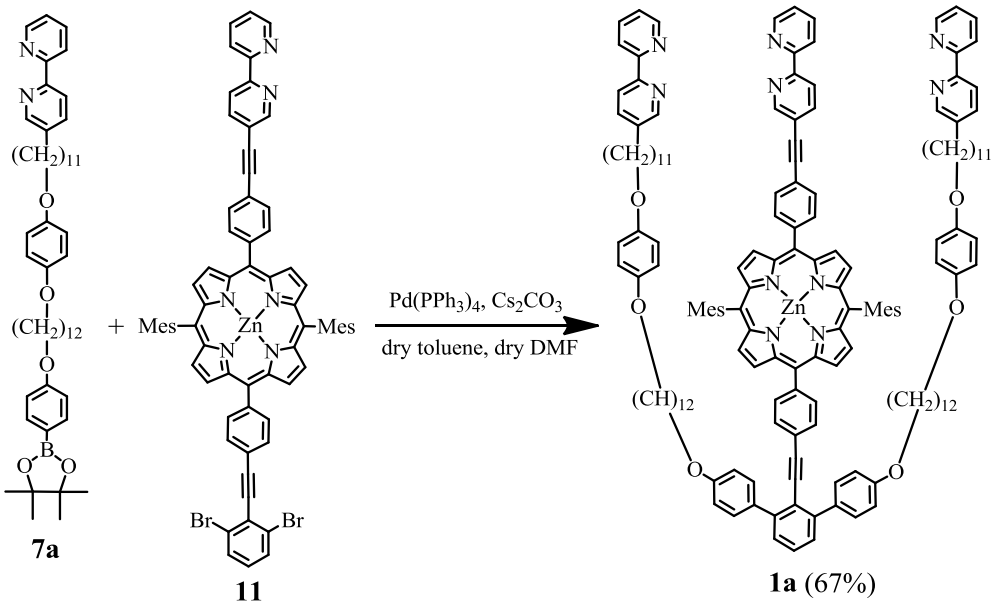

A solution of **11** (48.0 mg, 40 μmol, 1.0 equiv.), **7a** (74.3 mg, 92 μmol, 2.3 equiv.), cesium carbonate (23.2 mg, 71 μmol, 1.8 equiv.), and tetrakis(triphenylphosphine)palladium(0) (9.3 mg, 8.0 μmol, 0.2 equiv.) in dry DMF (4 mL) and dry toluene (4 mL) was heated at 80 °C under a nitrogen atmosphere and stirred for 2 days. After cooling to room temperature, the reaction mixture was filtered. A diethyl ether was added to the solution and the solution was washed with distilled water. The solution was dried over sodium sulfate and filtered. The solvent was removed under reduced pressure and the residue was purified by column chromatography on hydroscopic (6wt%) basic aluminium oxide (dichloromethane) to give **1a** as a purple powder (65 mg, 67%).

1a: $C_{160}H_{170}N_{10}O_6Zn$; MW 2394.5; purple solid; mp 80 °C; ^{1}H NMR (400 MHz, $CDCl_3$): δ 8.96 (m, 1H), 8.90–8.72 (m, 9H), 8.65–8.64 (m, 2H), 8.51–8.47 (m, 4H), 8.33 (d, 2H, J = 8.0 Hz), 8.27 (d, 2H, J = 8.0 Hz), 8.23 (d, 2H, J = 8.0 Hz), 8.10–8.07 (m, 3H), 7.94 (d, 2H, J = 8.0 Hz), 7.89–7.85 (m, 1H), 7.80–7.75 (m, 6H), 7.62–7.60 (m, 2H), 7.54–7.41 (m, 7H), 7.37–7.34 (m, 1H), 7.28 (s, 4H), 7.09 (d, 4H, J = 8.8 Hz), 6.71–6.69 (m, 4H), 6.61–6.58 (m, 4H), 4.04 (t, 4H, J = 6.5 Hz), 3.89 (t, 4H, J = 6.5 Hz), 3.60 (t, 4H, J = 6.6 Hz), 2.66–2.63 (m, 10H), 1.88–1.12 (m, 88H); ^{13}C NMR (100 MHz, $CDCl_3$): δ 158.78, 156.24, 155.46, 154.90, 153.74, 153.08, 152.82, 151.72, 149.95, 149.91, 149.80, 149.68, 149.27, 149.05, 144.83, 143.61, 142.52, 139.43, 139.18, 138.99, 138.24, 137.48, 136.95, 136.80, 136.75, 134.58, 134.26, 133.52, 132.15, 132.01, 130.91, 130.84, 129.87, 129.21, 128.22, 128.07, 127.67, 123.91, 123.30, 122.88, 121.66, 121.37, 120.76, 120.66, 120.43, 120.39, 120.10, 119.66, 119.41, 119.19, 115.41, 115.26, 113.90, 95.68, 93.71, 90.57, 87.34, 68.59, 68.57, 68.11, 32.81, 31.04, 29.68, 29.51, 29.50, 29.43, 29.41, 29.37, 29.32, 29.31, 29.27, 29.20, 29.10, 26.00, 25.81, 21.64, 21.45; MS (FAB+): *m/z* 2393 [MH^+]; IR (KBr, cm^{-1}): 2926(s), 2852(s), 1716(w), 1608(m), 1587(m), 1573(m), 1558(m), 1543(w), 1508(s), 1458(s), 1435(m), 1389(w), 1337(w),

1290(w), 1229(s), 1204(m), 1175(w), 1107(w), 1063(w), 995(s), 953(w), 852(w), 831(m), 796(s), 746(m), 721(w), 696(w), 650(w), 567(w), 542(w), 523(w); HRMS (FAB+): *m/z* Calcd for $C_{160}H_{170}N_{10}O_6{}^{64}Zn$: 2391.2596. Found: 2391.2593.

2-7-2. UV–vis titration

General procedure

UV-vis spectra were measured by a Shimadzu UV-2550 spectrophotometer using 1 cm quartz cuvettes. The temperature of the solution was regulated at 20 ^{o}C by using an EYELA NCB-1200 water bath. A spectrochemical analysis grade of solvent was purchased from Wako pure chemical industries, Ltd. The curve fittings were calculated by using KaleidaGraph 4.1J.

Method

A solution of **1a** in toluene-acetonitrile (1/1 (v/v)) was prepared by careful weighting using an analytical balance. Solution of **1a** (3 mL) was added in a quartz cell by using a whole pipette. The solution of **1a**·**Fe** was prepared by adding the solution of $Fe(BF_4)_2$ (1.0 equiv.) to the solution of **1a** (3.0 mL). A guest solution was added to the solution by using a micropipette. A solution of $Fe(BF_4)_2$ and **LP1** were used as the guest solution for the determination of the complex formation constant and the axial binding constants, respectively. After each addition of the guest solution, the quartz cell was placed in the cell compartment of a spectrometer and allowed to come to thermal equilibrium. UV–vis spectra were measured with a spectrophotometer equipped with a temperature controller to keep the temperature at 20 °C. This procedure was repeated until no change was recorded within the spectra. The association constants were determined by the curve fitting of the change of the apparent molar extinction coefficient ε (app) by eq 2n or 2q (see section 2-7-3) as a regression expression. The conditions of each titration were summarized in Table 2-1.

Table 2-1. Conditions of titration experiments.

Host	$[Host]_0$	Guest	[Guest]	wavelength
1a	2×10^{-5} M	$Fe(BF_4)_2$•$6H_2O$	3×10^{-4} M	500 nm
1a	5×10^{-5} M	**LP1**	6×10^{-2} M	608 nm
1a•Fe[a]	2×10^{-5} M	**LP1**	6×10^{-2} M	611 nm

(a) solution of $Fe(BF_4)_2$•$6H_2O$ (1.5×10^{-3} M, 40 μmol, 1 equiv.) was added.

2-7-3. Determination of association constants

The association constants (complex formation constant and axial binding constant) were determined by UV–visible spectroscopic titration and curve fitting calculations. The complexation of **1** with Fe(II) ions and the axial coordination of the axial ligand to the porphyrin Zn centre were one-to-one association. The Association constants were determined by the curve fitting of the titration data with the regression expressions of the one-to-one association model.

Herein, only three components were considered, *i.e.* host **H** (allosteric receptor **1**), guest **G** (Fe ion or axial ligand), and aggregate **A** (complex **1·Fe** or **1·L**). According to Lambert–Beer law, the observed absorbance of a solution *Abs*(obs) is

$$Abs(\text{obs}) = (\varepsilon_H C_H + \varepsilon_G C_G + \varepsilon_A C_A)\, l \qquad (2a)$$

ε_i: molar extinction coefficient of component i (M^{-1} cm^{-1}),

C_i: concentration of component i (M), l: light path length (cm)

Association constant K can be expressed as follows:

$$K = C_A / C_H C_G \qquad (2b)$$

The correction coefficient a is defined as follows:

$$a = V/(V + \Delta V) \qquad (2c)$$

a: corrective coefficient for dilution, V: volume of the solution just before the titration,

ΔV: the total volume of added solutions

Concentrations of **H** and **G** in the titration can be calculated from

$$C_H = aC_{H0} - C_A \qquad (2d)$$

$$C_G = aC_{G0} - C_A \qquad (2e)$$

C_{H0}: concentration of **H** before the addition of a solution of **G**

C_{G0}: concentration of **G** when the volume increase due to the addition of **G** solution is ignored

If $\varepsilon_G = 0$, *Abs*(obs) can be calculated from

$$Abs(\text{obs}) = [\varepsilon_H (aC_{H0} - C_A) + \varepsilon_A C_A]\, l$$

$$Abs(\text{obs}) = [a\varepsilon_H C_{H0} + (\varepsilon_A - \varepsilon_H) C_A]\, l \qquad (2f)$$

The apparent molar extinction coefficient ε (app) is defined as follows:

$$\varepsilon\,(\text{app}) = Abs(\text{obs})/(C_{\text{H}} + C_{\text{A}})\, l \qquad (2g)$$

Using Eq 2d, Abs(obs) can be calculated from

$$Abs(\text{obs}) = a\varepsilon\,(\text{app})C_{\text{H0}}l \qquad (2h)$$

According to Eqs. 2h and 2f, ε (app) can be calculated from

$$\varepsilon\,(\text{app}) = Abs(\text{obs})/aC_{\text{H0}}l = \varepsilon_{\text{H}} + (\varepsilon_{\text{A}} - \varepsilon_{\text{H}})\, C_{\text{A}}/aC_{\text{H0}} \qquad (2i)$$

Using Eqs. 2d and 2e, K is

$$K = C_{\text{A}}/(aC_{\text{H0}} - C_{\text{A}})(aC_{\text{G0}} - C_{\text{A}})$$

$$(K/a)C_{\text{A}}^{\,2} - (KC_{\text{H0}} + KC_{\text{G0}} + 1/a)C_{\text{A}} + aKC_{\text{H0}}C_{\text{G0}} = 0$$

If $0 \le C_{\text{A}} < aC_{\text{H0}}$, C_{A} can be calculated from

$$C_{\text{A}} = a\,\frac{\left(KC_{\text{H0}}+KC_{\text{G0}}+\frac{1}{a}\right) - \sqrt{\left(KC_{\text{H0}}+KC_{\text{G0}}+\frac{1}{a}\right)^2 - 4K^2C_{\text{H0}}C_{\text{G0}}}}{2K} \qquad (2j)$$

ε (app) is

$$\varepsilon\,(\text{app}) = \varepsilon_{\text{H}} + (\varepsilon_{\text{A}} - \varepsilon_{\text{H}})\,\frac{\left(KC_{\text{H0}}+KC_{\text{G0}}+\frac{1}{a}\right) - \sqrt{\left(KC_{\text{H0}}+KC_{\text{G0}}+\frac{1}{a}\right)^2 - 4K^2C_{\text{H0}}C_{\text{G0}}}}{2KC_{\text{H0}}} \qquad (2k)$$

When the concentration of the ligand solution C_{G}' is constant, the total volume of the solution V is

$$V = \Delta V_{\text{G}}\, C_{\text{G}}'/C_{\text{G0}} \qquad (2l)$$

ΔV_{G}: the total volume of added guest solutions

The correction coefficient a is defined by Eq 2c

$$a = V/(V + \Delta V) \qquad (2c)$$

Now, the total volume of the added solution ΔV is equal to ΔV_G

$$a = V/(V + \Delta V_G)$$

$$1/a = (V + \Delta V_G)/V = 1 + C_{G0} / C_G' \qquad (2m)$$

Using Eq. 2k, ε (app) is

$$\varepsilon(\text{app}) = \varepsilon_H + (\varepsilon_A - \varepsilon_H) \frac{\left(KC_{H0} + KC_{G0} + \frac{C_{G0}}{C_{G'}} + 1\right) - \sqrt{\left(KC_{H0} + KC_{G0} + \frac{C_{G0}}{C_{G'}} + 1\right)^2 - 4K^2 C_{H0} C_{G0}}}{2KC_{H0}} \qquad (2n)$$

Eq. 2n was used as the regression expression for curve fitting for the determination of association constants of both **1**·**Fe** and **1**·**L**.

In the titration experiment for the formation of **1**•**Fe**•**L**, C_{H0} is the concentration of **1** before the addition of a Fe solution. Complex **1**·**Fe** was prepared by adding a Fe(II) solution (volume: V') to the solution of **1** (volume: V) just before the titration. We assumed that the formation of **1**·**Fe** is quantitative and ignored the equilibrium of the formation of **1**·**Fe**.
Now, the total volume of the added solution ΔV is

$$\Delta V = \Delta V_G + V' \qquad (2o)$$

The correction coefficient a is defined by Eq. 2c

$$a = V / (V + \Delta V) \qquad (2c)$$

$$1/a = (V + \Delta V_G + V') / V = (V + V') / V + C_{G0} / C_G' \qquad (2p)$$

Using Eq. 2k, ε (app) is

$$\varepsilon(\text{app}) = \varepsilon_H + (\varepsilon_A - \varepsilon_H) \frac{\left(KC_{H0} + KC_{G0} + \frac{C_{G0}}{C_{G'}} + \frac{V+V'}{V}\right) - \sqrt{\left(KC_{H0} + KC_{G0} + \frac{C_{G0}}{C_{G'}} + \frac{V+V'}{V}\right)^2 - 4K^2 C_{H0} C_{G0}}}{2KC_{H0}} \qquad (2q)$$

Eq. 2q was used as the regression expression for curve fitting for the determination of the association constants of **1**·**Fe**·**L**.

2-8. References

(1) *Spartan'08*, Wavefunction, Inc., Irvine, CA.

(2) Kato, M.; Hashimoto, E.; Kozaki, M.; Suzuki S.; Okada, K. *Tetrahedron Lett.* **2012**, *53*, 309–312.

(3) Fletcher, N. C.; Nieuwenhuyzen, M.; Rainey *J. Chem. Soc., Dalton Trans.* **2001**, 2641–2648.

(4) Lee, C.-H.; Lindsey, J. S. *Tetrahedron* **1994**, *50*, 11427−11440.

(5) Mao, G.; Orita, A.; Matsuo, D.; Hirate, T.; Iwanaga, T.; Toyota, S.; Otera, J. *Tetrahedron Lett.* **2009**, *50*, 2860–2864.

(6) (a) Sonogashira, K.; Tohda, Y.; Hagihara, N. *Tetrahedron Lett*. **1975**, *16*, 4467–4470; (b) Chinchilla, R.; Nájera, C. *Chem. Rev.* **2007**, *107*, 874–922; (c) Kozaki, M.; Okada, K. *Org. Lett.* **2004**, *6*, 485–488.

(7) (a) Miyaura, N.; Suzuki, A. *Chem. Rev.* **1995**, *95*, 2457–2483; (b) Uetomo, A.; Kozaki, M.; Suzuki, S.; Yamanaka, K.; Ito, O.; Okada, K. *J. Am. Chem. Soc.* **2011**, *133*, 13276−13279.

(8) (a) Nabeshima, T.; Yoshihira, Y.; Saiki, T.; Akine, S.; Horn, E. *J. Am. Chem. Soc.* **2003**, *125*, 28−29. (b) Nabeshima, T.; Tanaka, Y.; Saiki, T.; Akine, S.; Ikeda, C.; Sato, S. *Tetrahedron Lett.* **2006**, *47*, 3541−3544.

(9) (a) Miller, J. R.; Dorough, G. D. *J. Am. Chem. Soc.* **1952**, *74*, 3977–3981. (b) Sanders, J. K. M.; Bampos, N.; C.-Watson, Z.; Darling, S. L.; Hawley, J. C.; Kim, H.-J.; Mak, C. C.; Webb, S. J. In *Porphyrin Handbook*, Kadaish, K. M.; Smith, K. M.; Guliard, R. Eds; Academic Press, **2000**,; Vol. 3, pp 1–48.

~Chapter 3~
Development of allosteric receptors with alkyl chains of different lengths

3-1. Introduction

In **chapter 2**, allosteric receptor **1a** was developed; it significantly decreased the ligand-binding ability of the Zn porphyrin in **1a** by Fe complexation. However, the degree of allosteric inhibition ($K_{\mathbf{1a}\cdot\mathbf{L}}/K_{(\mathbf{1a}\cdot\mathbf{Fe})\cdot\mathbf{L}}$) was moderate (1.64). Additional structural modification of the receptor is required to improve the degree of allosteric inhibition. In this chapter, we describe the design, synthesis, and properties of allosteric receptors with improved properties based on the results obtained in **chapter 2**. The length of the alkyl chain is significant in this system, as it affects both the stability of the [M(bpy)$_3$]-type complexes and the degree of shielding at the axial ligand-binding site in the Zn porphyrin unit (*vide infra*). In the Fe complex of receptor **1**, the accessibility of an axial ligand to the Zn porphyrin is regulated by the alkyl chains. When the chains are closer to the Zn porphyrin, more effective shielding of the Zn porphyrin should be achieved. Therefore, an allosteric receptor with a shorter alkyl chain was investigated to achieve more effective shielding of the Zn porphyrin (Figure 3-1).

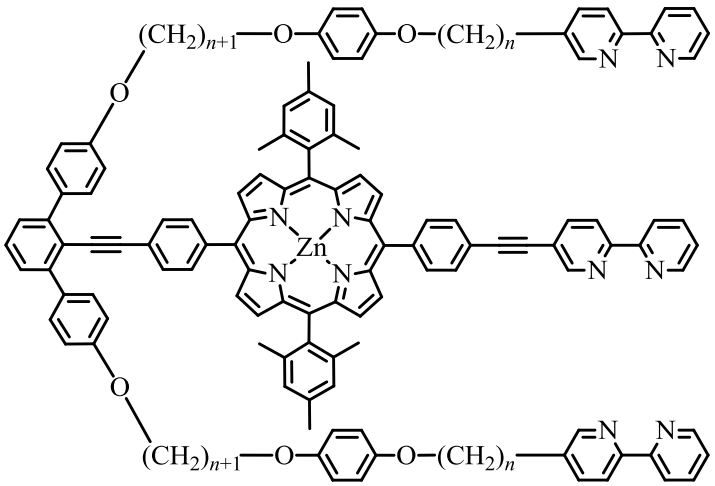

1a (n = 11), **1b** (n = 9), **1c** (n = 7), **1d** (n = 5)

Figure 3-1. Chemical structure of receptor **1**.

3-2. Molecular mechanics force field (MMFF) calculations[1]

Before the synthesis, MMFF calculations were carried out for **1** containing alkyl chains of different lengths (n = 5–11). The shorter alkyl chains are advantageous for more effective shielding of the Zn porphyrin in the Fe complex of receptor **1**. When the alkyl chains were too short, receptor **1** could not form a stable 1: 1 complex with Fe ions. The steric energies (E_{Fe}) of iron complex **1·Fe** were calculated. The steric energies (E_{cut}) were also calculated for the corresponding model complex where the carbon–carbon bonds C_A–C_B shown in Figure 3-2 were disconnected, and the hydrogen atoms were connected to both carbons A and B. The strain energies in **1·Fe** were estimated by subtracting E_{cut} from E_{Fe}. The results are summarized in Table 3-1.

Table 3-1. The steric energies of complex **1·Fe** and model complexes and strain energies.

receptor	E_{Fe} / kJ mol^{-1}	E_{cut} / kJ mol^{-1}	($E_{Fe} - E_{cut}$) / kJ mol^{-1}
1a (n = 11)	71.01	8.88	62.13
1b (n = 9)	50.52	–7.29	57.81
1c (n = 7)	37.71	–32.18	69.89
1d (n = 5)	357.03	–0.60	357.63

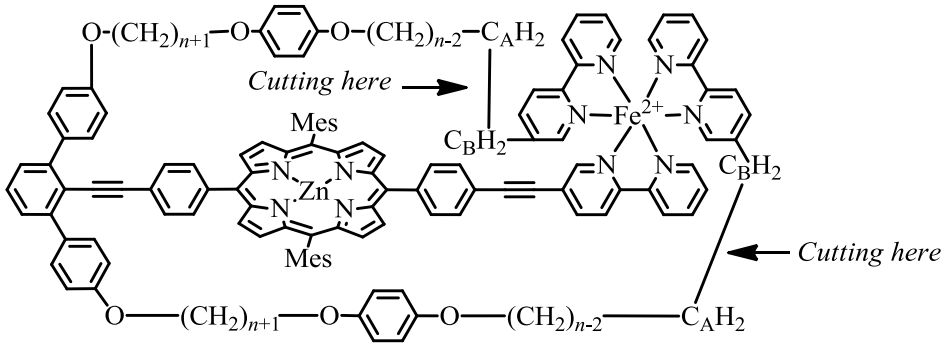

Fe complex (Fe)

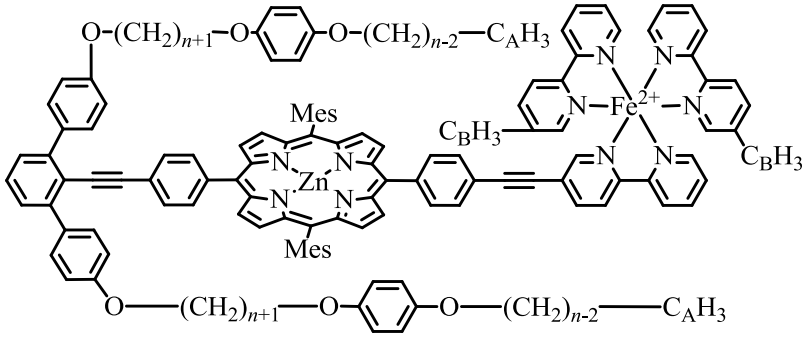

Severed form (Cut)

Figure 3-2. Chemical structure of calculated complexes.

Complexes **1b·Fe** (57.81 kJ mol^{-1}) and **1c·Fe** (69.89 kJ mol^{-1}) showed comparable strain energies with **1a·Fe** (62.13 kJ mol^{-1}), indicating that both **1b** and **1c** afforded stable Fe complexes. In contrast, **1d·Fe** showed a distinctly larger strain energy (357.63 kJ mol^{-1}) than **1a·Fe**. Therefore, the formation of Fe complex **1d·Fe** is probably not possible. Based on these results, **1b** and **1c** were selected as the allosteric receptors.

3-3. Synthesis of receptor 1

Allosteric receptors **1b** and **1c** were synthesized following a method similar to that described for **1a** (see sections 2-2 and 2-3). Bromoalkanes **3** and **5** were prepared using suitable dibromoalkanes from pinacol borate **2** and bipyridine **4**, respectively. Bromoalkanes **3** and **5** were attached to hydroquinone stepwise by Williamson ether synthesis reaction, affording side chains **7b** and **7c** in 30% and 25% yields (two steps), respectively (Scheme 3-1). The Suzuki–Miyaura cross-coupling reaction between side chain **7** and main chain **11** afforded **1b** and **1c** as purple solids in 85% and 86% yields, respectively (Scheme 3-2).

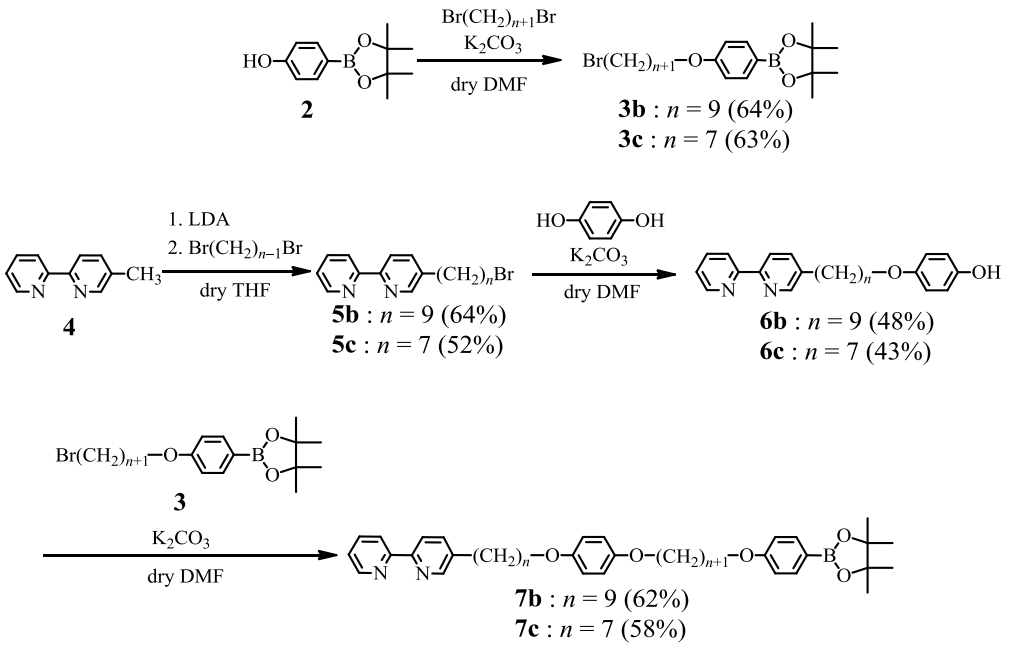

Scheme 3-1. Synthesis of side chain **7**.

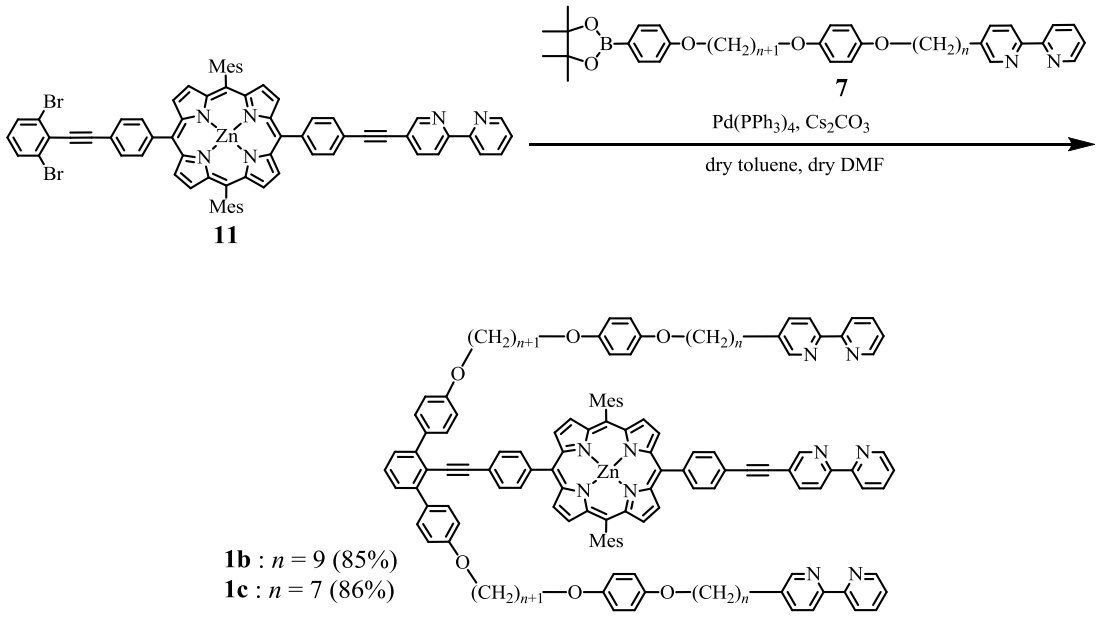

Scheme 3-2. Synthesis of receptor **1**.

3-4. Iron complexation

It was conformed that allosteric receptor 1a formed a stable 1:1 complex with Fe(II) ions in a mixture of toluene/acetonitrile (1:1 v/v) by UV–visible titration, same as receptor **1a** (see section 2-5). As shown in Figures 3-3a and 3-4a, when Fe(II) ions were added to a solution of **1** (2×10^{-5} M), the characteristic MLCT absorption band of the Fe(II)$(bpy)_3$-type complex appeared at ~500 nm.[2] The absorption due to the MLCT band at 500 nm linearly increased in proportion to the amount of Fe(II) ions until the concentration of Fe(II) ions became the same as that of **1** (Figures 3-3b and 3-4b). These results indicate the almost quantitative formation ($K_{1\cdot Fe} > 10^6$ M^{-1}) of Fe(II)$(bpy)_3$-type complexes **1b·Fe** and **1c·Fe**. The formation of 1:1 complexes **1b·Fe** and **1c·Fe** was confirmed by their ESI-MS spectra (Figures 3-5 and 3-6). Intense molecular ion peaks and reasonable isotope patterns were observed for both $[(\mathbf{1b{\cdot}Fe}){\cdot}\mathbf{BF_4}]^+$ and $[(\mathbf{1c{\cdot}Fe}){\cdot}\mathbf{BF_4}]^+$.

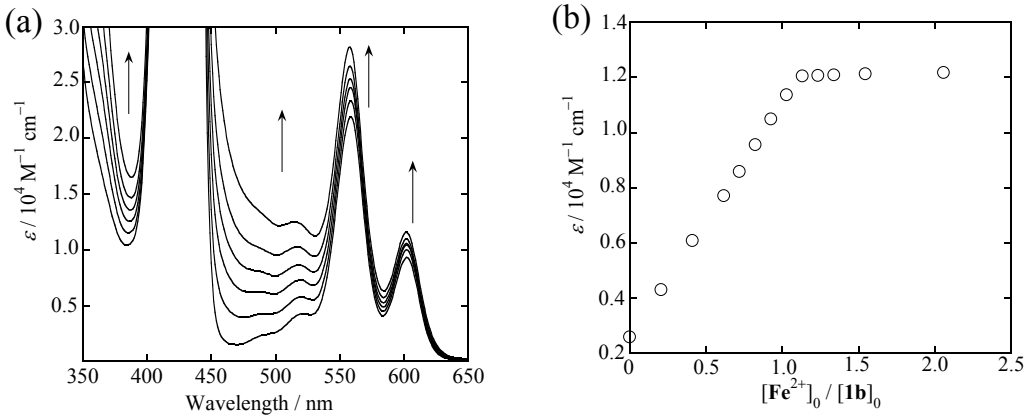

Figure 3-3. (a) UV–vis spectral change resulting from the titration of **1b** (2×10^{-5} M) with $Fe(BF_4)_2{\bullet}6H_2O$ (1.2×10^{-3} M) in a toluene/acetonitrile (1/1 (v/v)) solution at 20 °C. (b) The change in the molar extinction coefficient at 500 nm. $[Fe^{2+}]_0$: The concentration of Fe^{2+} when complexation is ignored. $[\mathbf{1b}]_0$: The initial concentration of **1b**.

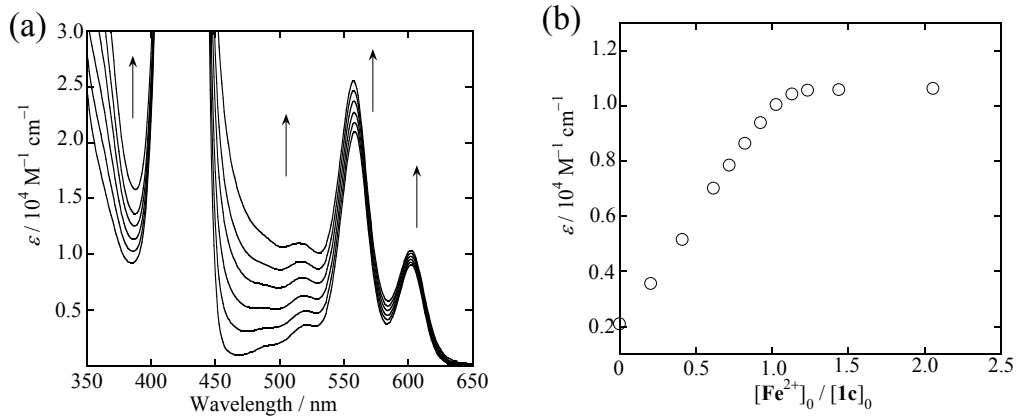

Figure 3-4. (a) UV−vis spectral change resulting from the titration of **1c** (2×10^{-5} M) with $Fe(BF_4)_2 \bullet 6H_2O$ (6×10^{-4} M) in a toluene/acetonitrile (1/1 (v/v)) solution at 20 °C. (b) The change in the molar extinction coefficient at 500 nm. $[Fe^{2+}]_0$: The concentration of Fe^{2+} when complexation is ignored. $[\mathbf{1c}]_0$: The initial concentration of **1c**.

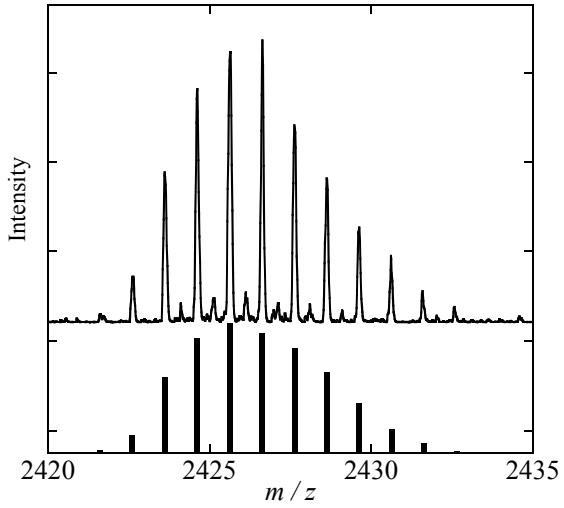

Figure 3-5. ESI-Mass spectrum of **1b** with $Fe(BF_4)_2 \bullet 6H_2O$ in a toluene/acetonitrile (1/1 (v/v)) solution. Line is observed spectrum. The block height is calculated isotope pattern of $[(\mathbf{1b \bullet Fe}) \bullet \mathbf{BF_4}]^+$, calcd for $C_{152}H_{154}BF_4FeN_{10}O_6Zn$: 2422.

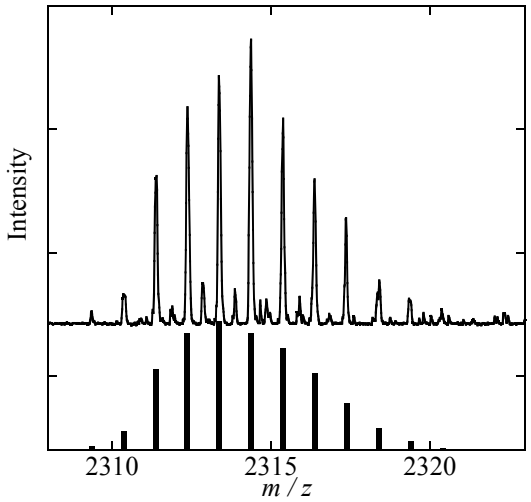

Figure 3-6. ESI-Mass spectrum of **1c** with $Fe(BF_4)_2$•$6H_2O$ in a toluene/acetonitrile (1/1 (v/v)) solution. Line is observed spectrum. The block height is calculated isotope pattern of $[$(**1c•Fe)•BF**$_4]^+$, calcd for $C_{144}H_{138}BF_4FeN_{10}O_6Zn$: 2310.

3-5. Axial binding and allosteric inhibition with LP1

The binding constants of active receptors **1b** and **1c** with an axial ligand ($K_{\mathbf{1}\cdot\mathbf{L}}$) were determined by UV–visible spectroscopic titrations in a mixture of toluene/acetonitrile (1:1 v/v), same as receptor **1a** (see section 2-6). When a solution of **LP1** (6×10^{-2} M) was added to a solution of **1b** and **1c**, the porphyrin Q-bands red-shifted because of the axial coordination of **LP1** to the porphyrin Zn centre (Figures 3-7 and 3-8). The binding constants of allosteric receptors **1b** and **1c** with **LP1** were determined to be $7.83 \pm 0.12 \times 10^3$ M^{-1} ($K_{\mathbf{1b}\cdot\mathbf{LP1}}$) and $8.45 \pm 0.23 \times 10^3$ M^{-1} ($K_{\mathbf{1c}\cdot\mathbf{LP1}}$), respectively, by the curve fitting of experimental data (see section 2-7-2).

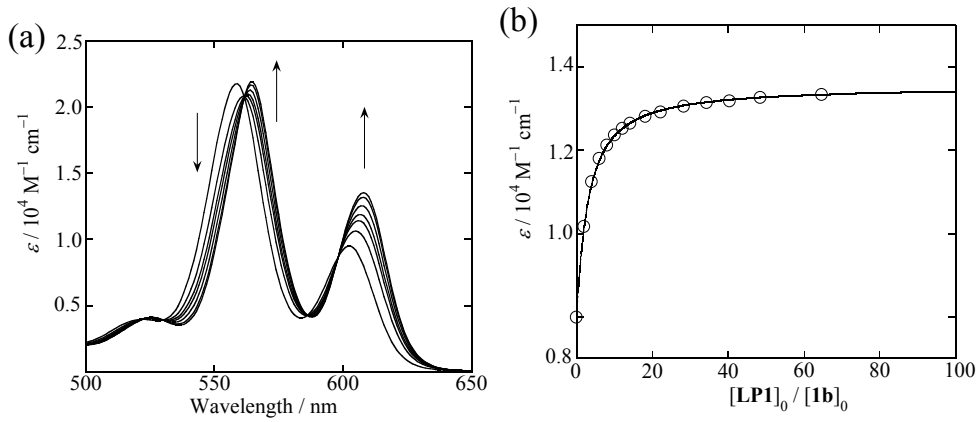

Figure 3-7. (a) UV–vis spectral change resulting from the titration of **1b** (5×10^{-5} M) with **LP1** (6×10^{-2} M) in a toluene/acetonitrile (1/1 (v/v)) solution at 20 °C. (b) The change in the molar extinction coefficient at 608 nm. The solid line is a regression curve obtained by curve fitting. $[\mathbf{LP1}]_0$: The concentration of **LP1** when axial binding is ignored. $[\mathbf{1b}]_0$: The initial concentration of **1b**.

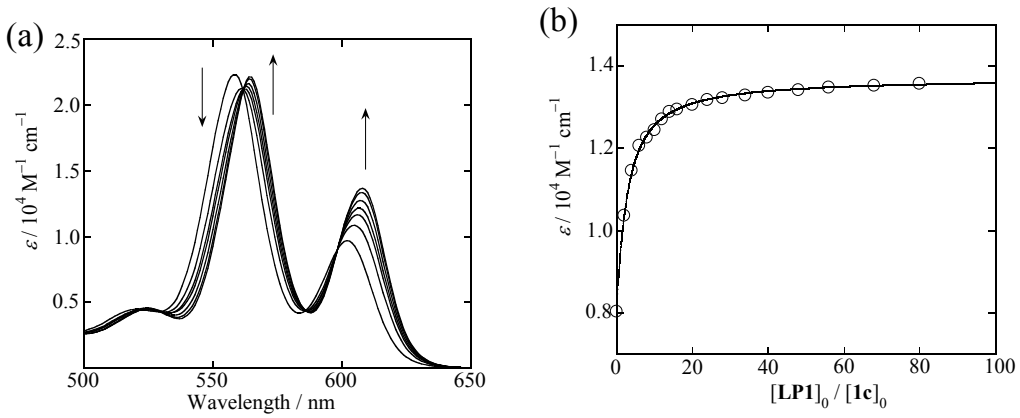

Figure 3-8. (a) UV–vis spectral change resulting from the titration of **1c** (5×10^{-5} M) with **LP1** (6×10^{-2} M) in a toluene/acetonitrile (1/1 (v/v)) solution at 20 °C. (b) The change in the molar extinction coefficient at 608 nm. The solid line is a regression curve obtained by curve fitting. $[\mathbf{LP1}]_0$: The concentration of **LP1** when axial binding is ignored. $[\mathbf{1c}]_0$: The initial concentration of **1c**.

The binding constants of inactive allosteric receptors **1b·Fe** and **1c·Fe** with an axial ligand ($K_{(\mathbf{1\cdot Fe})\cdot\mathbf{L}}$) were determined by similar titration experiments. First, **1b·Fe** and **1c·Fe** were prepared by adding 1.0 equiv of Fe(II) to solutions of **1b·Fe** and **1c·Fe**, respectively. A solution of **LP1** was added to a solution of **1·Fe**; the axial coordination of **LP1** to the Zn porphyrin was indicated by the red shift of the porphyrin Q-band (Figures 3-9 and 3-10). Insignificant changes in the molar absorptivity of the MLCT band were observed during the titration of **1b·Fe**, indicating that the dissociation of **1b·Fe** did not occur under the experimental conditions. The binding constants of inactive allosteric receptor **1b·Fe** and **1c·Fe** with **LP1** were determined to be $3.72 \pm 0.03 \times 10^3$ M^{-1} ($K_{(\mathbf{1b\cdot Fe})\cdot\mathbf{LP1}}$) and $5.39 \pm 0.15 \times 10^3$ M^{-1} ($K_{(\mathbf{1c\cdot Fe})\cdot\mathbf{LP1}}$), respectively.

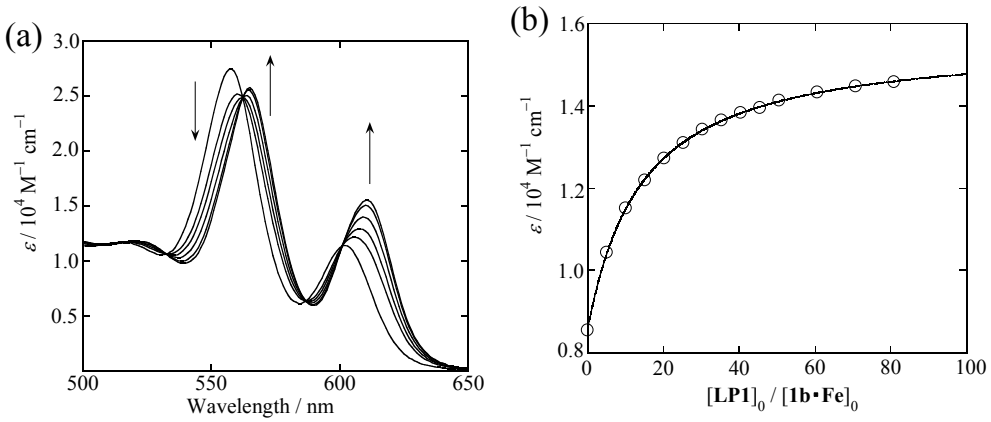

Figure 3-9. (a) UV–vis spectral change resulting from the titration of **1b•Fe** (2×10^{-5} M) with **LP1** (6×10^{-2} M) in a toluene/acetonitrile (1/1 (v/v)) solution at 20 °C. (b) The change in the molar extinction coefficient at 610 nm. The solid line is a regression curve obtained by curve fitting. $[\mathbf{LP1}]_0$: The concentration of **LP1** when axial binding is ignored. $[\mathbf{1b{\bullet}Fe}]_0$: The initial concentration of **1b•Fe**.

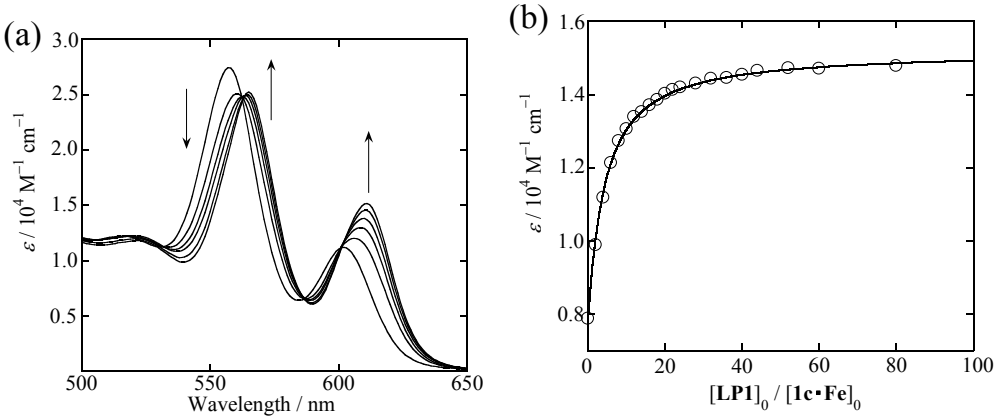

Figure 3-10. (a) UV–vis spectral change resulting from the titration of **1c•Fe** (5×10^{-5} M) with **LP1** (6×10^{-2} M) in a toluene/acetonitrile (1/1 (v/v)) solution at 20 °C. (b) The change in the molar extinction coefficient at 611 nm. The solid line is a regression curve obtained by curve fitting. $[\mathbf{LP1}]_0$: The concentration of **LP1** when axial binding is ignored. $[\mathbf{1c{\bullet}Fe}]_0$: The initial concentration of **1c•Fe**.

The degrees of allosteric inhibition ($K_{\mathbf{1{\cdot}L}}/ K_{\mathbf{(1{\cdot}Fe){\cdot}L}}$) in **1b** and **1c** for **LP1** were calculated to be 2.10 ± 0.05 and 1.57 ± 0.09, respectively. These results indicate that the ligand-binding abilities of the Zn porphyrins in **1b** (n = 9) and **1c** (n = 7) were significantly inhibited by the addition of Fe ions. Allosteric receptor **1b** showed a stronger allosteric inhibition ($K_{\mathbf{1{\cdot}L}}/ K_{\mathbf{(1{\cdot}Fe){\cdot}L}}$ = 2.1) than **1a** (1.6, n = 11). Although the strongest allosteric inhibition of **1c** was expected to arise from the shortest alkyl chains, **1c** showed a comparable degree of allosteric inhibition to **1a**. In other words, no correlation was observed between the degree of allosteric inhibition and the length of alkyl chains. Shorter alkyl chains may be advantageous to increase the steric shielding. However, **LP1** may be too small to

cause significant steric repulsion among the alkyl chains.

3-6. Effect of ligand size and geometry

A series of axial ligands shown in Figure 3-11 were prepared to evaluate the effect of the steric bulkiness of an axial ligand and a type of heterocyclic unit in axial ligands for allosteric inhibition. **LIm1** was obtained commercially and used as received without further purification. **LIm2**,[3] **LIm3**,[3] and **LP2**[4] were prepared following reported methods. The synthesis of **LP3** is shown in Scheme 3-3. 1-Bromo-3,5-di-*t*-butylbenzene (**13**) was synthesized following the literature.[5] 3,5-Di-*tert*-butylphenylboronic acid (**14**) was synthesized from compound **13** by using *n*-butyllithium and boric acid triisopropyl ester.[6] The Suzuki–Miyaura cross-coupling of 3,5-dibromopyridine with boronic acid **14** afforded **LP3** in 93% yield.[4]

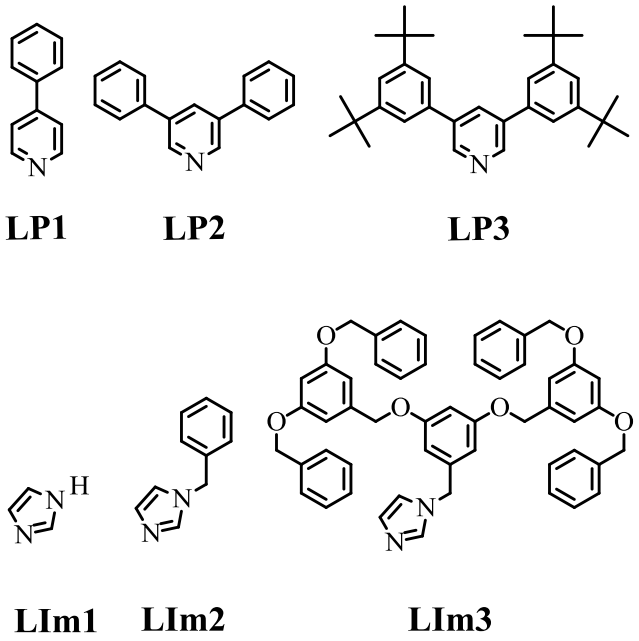

Figure 3-11. Chemical structure of axial ligands.

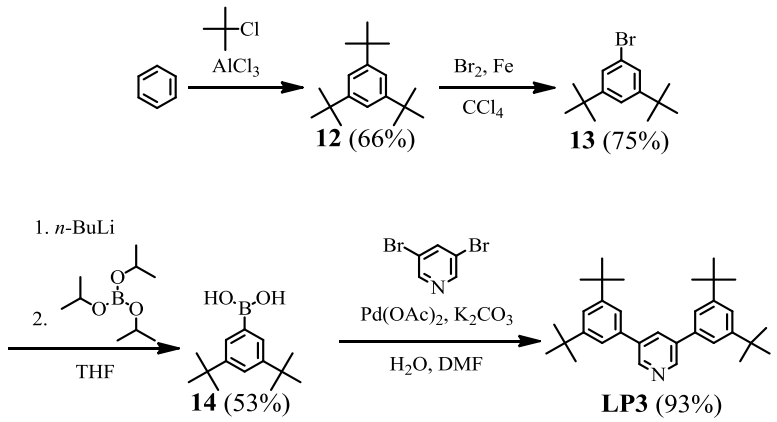

Scheme 3-3. Synthesis of axial ligand **LP3**.

The binding constants of active receptor **1** ($K_{1\bullet L}$) and inactive receptor **1•Fe** ($K_{(1\bullet Fe)\bullet L}$) with axial ligands were determined by UV–visible spectroscopic titrations in a mixture of toluene/acetonitrile (1:1 v/v) at 20 °C. When the solution of a ligand (1.2×10^{-2} M, 2.4×10^{-2} M or 3.0×10^{-2} M) was added to a solution of **1** (2×10^{-5} M or 5×10^{-5} M), the porphyrin Q-band red-shifted because of the coordination of the axial ligand to the porphyrin Zn centre (Figures 3-12 to 3-41). The binding constants of allosteric receptor **1** with ligands were determined by the curve fitting of the experimental data. The titration results are summarized in Figures 3-12 to 3-41. The binding constants and degree of allosteric effect ($K_{\mathbf{1\bullet L}}/K_{\mathbf{(1\bullet Fe)\bullet L}}$) are summarized in Table 3-2. Insignificant changes in the molar absorptivity of the MLCT band were observed during the titration of **1e•Fe**, indicating that the dissociation of **1e•Fe** did not occur under the experimental conditions.

Table 3-2. The summary of binding constants of allosteric receptors **1** and degree of allosteric inhibition.

Ligand	Receptor	$K_{1\bullet L}$ / 10^{-4} M^{-1}	$K_{(1\bullet Fe)\bullet L}$ / 10^{-4} M^{-1}	$K_{1\bullet L}$ / $K_{(1\bullet Fe)\bullet L}$
LIm1	**1a**	3.48 ± 0.06	2.97 ± 0.03	1.17 ± 0.03
LIm1	**1b**	3.65 ± 0.10	2.06 ± 0.04	1.77 ± 0.08
LIm1	**1c**	3.51 ± 0.13	2.50 ± 0.09	1.40 ± 0.10
LIm2	**1a**	4.31 ± 0.07	3.40 ± 0.04	1.27 ± 0.04
LIm2	**1b**	4.27 ± 0.12	2.46 ± 0.10	1.74 ± 0.10
LIm2	**1c**	4.15 ± 0.20	2.58 ± 0.03	1.61 ± 0.10
LIm3	**1a**	4.73 ± 0.12	3.40 ± 0.10	1.39 ± 0.08
LIm3	**1b**	4.60 ± 0.14	2.83 ± 0.07	1.63 ± 0.09
LIm3	**1c**	4.12 ± 0.16	2.85 ± 0.08	1.44 ± 0.10
LP1	**1a**	0.867 ± 0.014	0.528 ± 0.005	1.64 ± 0.04
LP1	**1b**	0.783 ± 0.012	0.372 ± 0.003	2.10 ± 0.05
LP1	**1c**	0.845 ± 0.023	0.539 ± 0.015	1.57 ± 0.09
LP2	**1a**	0.707 ± 0.005	0.465 ± 0.006	1.52 ± 0.03
LP2	**1b**	0.660 ± 0.006	0.390 ± 0.004	1.69 ± 0.03
LP2	**1c**	0.563 ± 0.010	0.422 ± 0.006	1.33 ± 0.04
LP3	**1a**	3.34 ± 0.08	1.73 ± 0.02	1.93 ± 0.07
LP3	**1b**	3.68 ± 0.07	0.882 ± 0.008	4.18 ± 0.11
LP3	**1c**	2.94 ± 0.07	0.649 ± 0.012	4.53 ± 0.19

in toluene/acetonitrile (1:1 v/v) at 20 ^{o}C

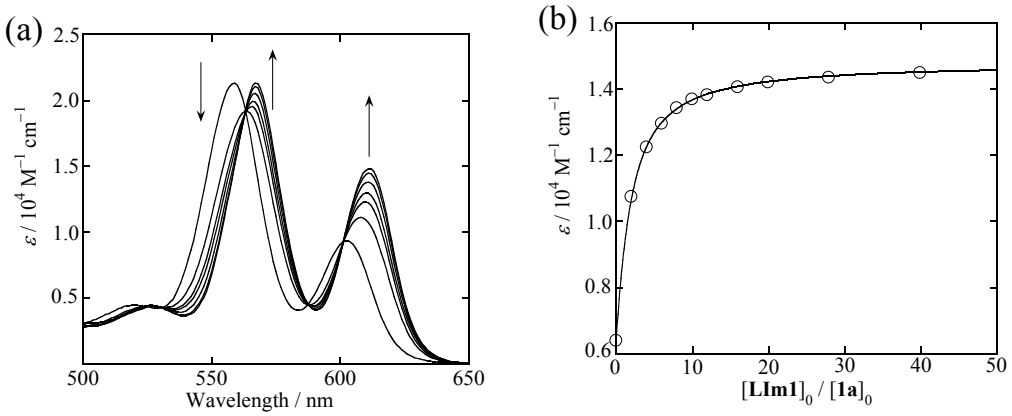

Figure 3-12. (a) UV–vis spectral change resulting from the titration of **1a** (2×10^{-5} M) with **LIm1** (2.4×10^{-2} M) in a toluene/acetonitrile (1/1 (v/v)) solution at 20 °C. (b) The change in the molar extinction coefficient at 611 nm. The solid line is a regression curve obtained by curve fitting. $[\mathbf{LIm1}]_0$: The concentration of **LIm1** when axial binding is ignored. $[\mathbf{1a}]_0$: The initial concentration of **1a**.

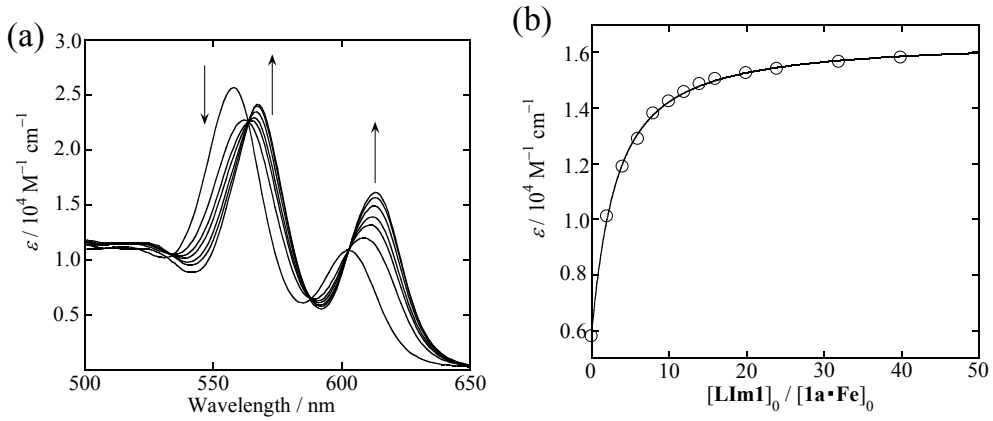

Figure 3-13. (a) UV–vis spectral change resulting from the titration of **1a•Fe** (2×10^{-5} M) with **LIm1** (2.4×10^{-2} M) in a toluene/acetonitrile (1/1 (v/v)) solution at 20 °C. (b) The change in the molar extinction coefficient at 614 nm. The solid line is a regression curve obtained by curve fitting. $[\mathbf{LIm1}]_0$: The concentration of **LIm1** when axial binding is ignored. $[\mathbf{1a•Fe}]_0$: The initial concentration of **1a•Fe**.

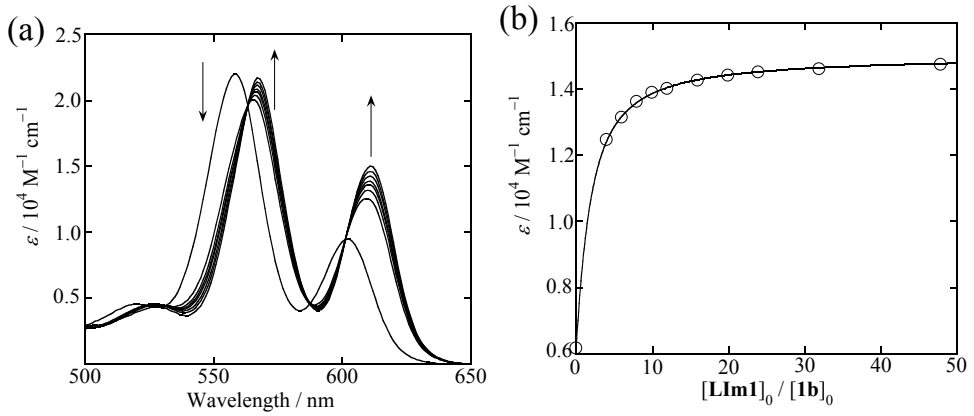

Figure 3-14. (a) UV–vis spectral change resulting from the titration of **1b** (2×10^{-5} M) with **LIm1** (2.4×10^{-2} M) in a toluene/acetonitrile (1/1 (v/v)) solution at 20 °C. (b) The change in the molar extinction coefficient at 611 nm. The solid line is a regression curve obtained by curve fitting. $[\mathbf{LIm1}]_0$: The concentration of **LIm1** when axial binding is ignored. $[\mathbf{1b}]_0$: The initial concentration of **1b**.

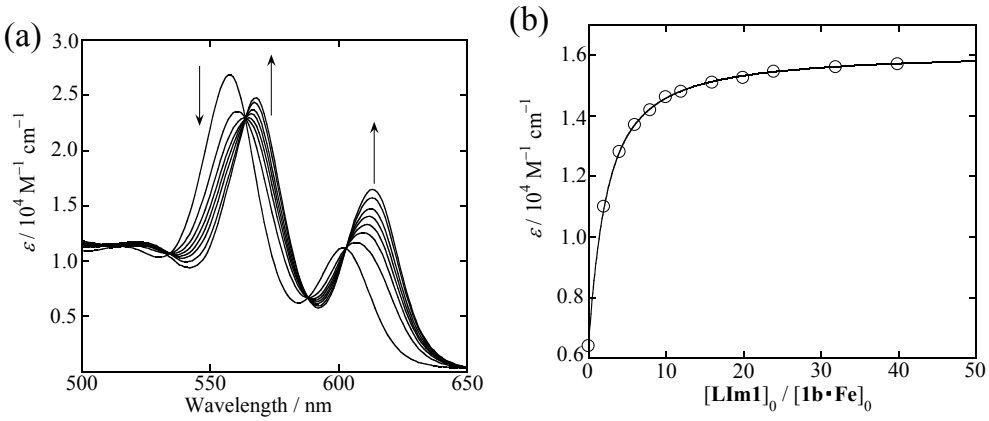

Figure 3-15. (a) UV–vis spectral change resulting from the titration of **1b•Fe** (2×10^{-5} M) with **LIm1** (2.4×10^{-2} M) in a toluene/acetonitrile (1/1 (v/v)) solution at 20 °C. (b) The change in the molar extinction coefficient at 614 nm. The solid line is a regression curve obtained by curve fitting. $[\mathbf{LIm1}]_0$: The concentration of **LIm1** when axial binding is ignored. $[\mathbf{1b{\bullet}Fe}]_0$: The initial concentration of **1b•Fe**.

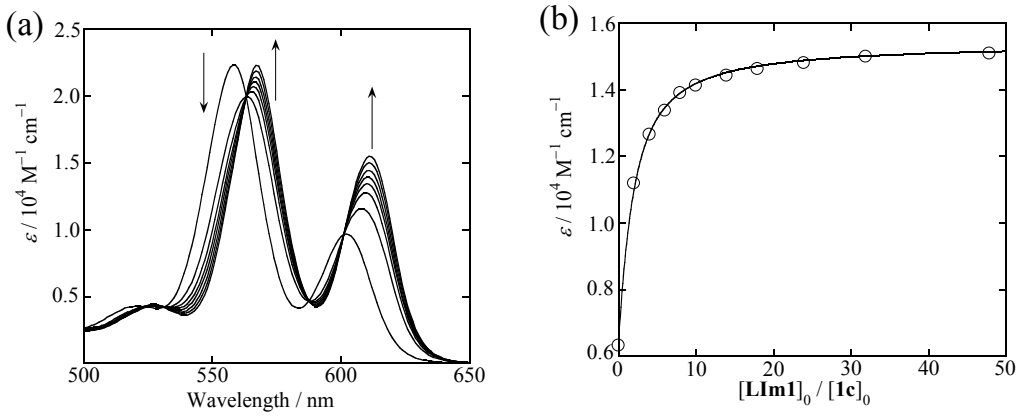

Figure 3-16. (a) UV–vis spectral change resulting from the titration of **1c** (2×10^{-5} M) with **LIm1** (2.4×10^{-2} M) in a toluene/acetonitrile (1/1 (v/v)) solution at 20 °C. (b) The change in the molar extinction coefficient at 611 nm. The solid line is a regression curve obtained by curve fitting. $[\mathbf{LIm1}]_0$: The concentration of **LIm1** when axial binding is ignored. $[\mathbf{1c}]_0$: The initial concentration of **1c**.

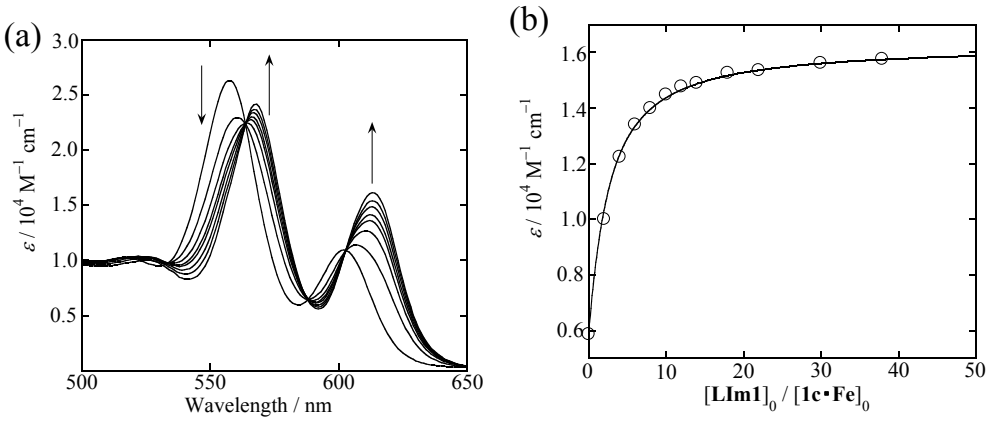

Figure 3-17. (a) UV–vis spectral change resulting from the titration of **1c•Fe** (2×10^{-5} M) with **LIm1** (2.4×10^{-2} M) in a toluene/acetonitrile (1/1 (v/v)) solution at 20 °C. (b) The change in the molar extinction coefficient at 614 nm. The solid line is a regression curve obtained by curve fitting. $[\mathbf{LIm1}]_0$: The concentration of **LIm1** when axial binding is ignored. $[\mathbf{1c{\bullet}Fe}]_0$: The initial concentration of **1c•Fe**.

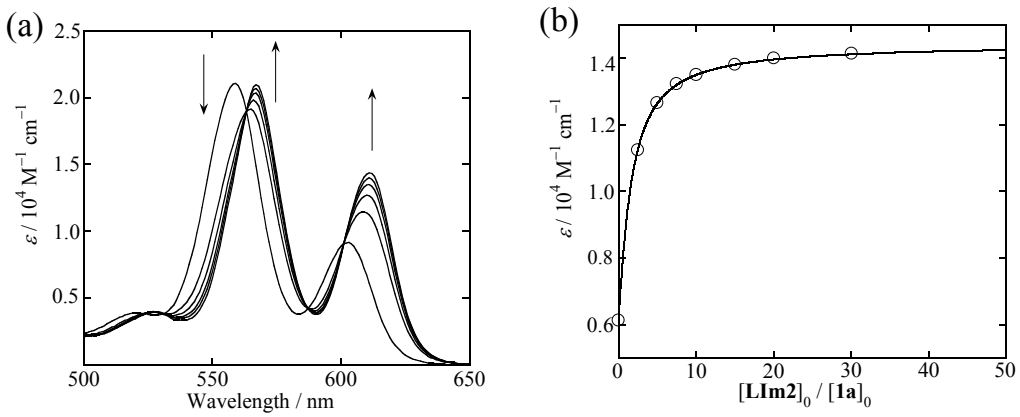

Figure 3-18. (a) UV–vis spectral change resulting from the titration of **1a** (2×10^{-5} M) with **LIm2** (3×10^{-2} M) in a toluene/acetonitrile (1/1 (v/v)) solution at 20 °C. (b) The change in the molar extinction coefficient at 611 nm. The solid line is a regression curve obtained by curve fitting. $[\mathbf{LIm2}]_0$: The concentration of **LIm2** when axial binding is ignored. $[\mathbf{1a}]_0$: The initial concentration of **1a**.

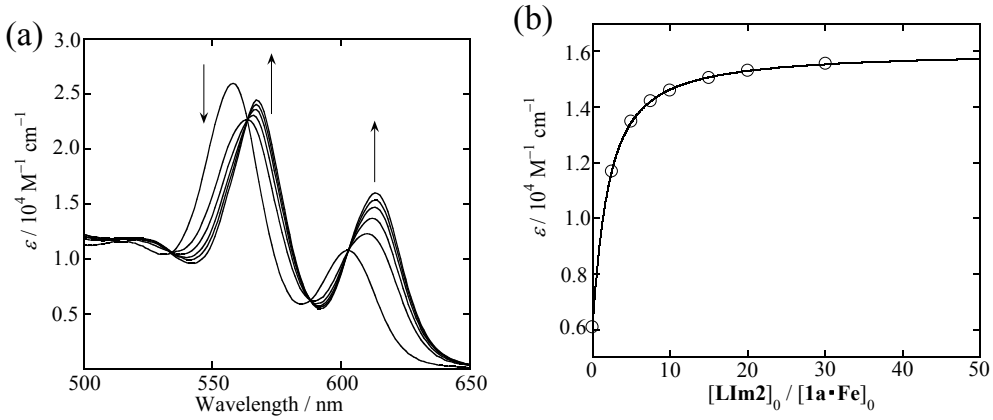

Figure 3-19. (a) UV–vis spectral change resulting from the titration of **1a•Fe** (2×10^{-5} M) with **LIm2** (3×10^{-2} M) in a toluene/acetonitrile (1/1 (v/v)) solution at 20 °C. (b) The change in the molar extinction coefficient at 614 nm. The solid line is a regression curve obtained by curve fitting. $[\mathbf{LIm2}]_0$: The concentration of **LIm2** when axial binding is ignored. $[\mathbf{1a•Fe}]_0$: The initial concentration of **1a•Fe**.

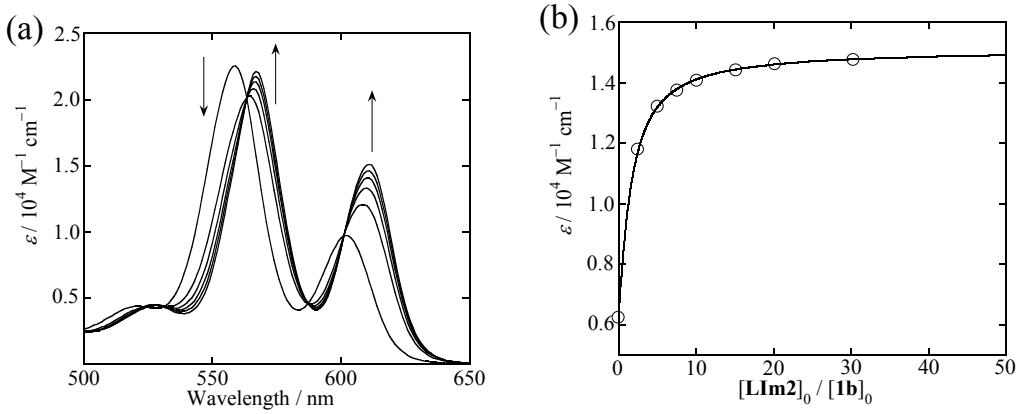

Figure 3-20. (a) UV–vis spectral change resulting from the titration of **1b** (2×10^{-5} M) with **LIm2** (3×10^{-2} M) in a toluene/acetonitrile (1/1 (v/v)) solution at 20 °C. (b) The change in the molar extinction coefficient at 611 nm. The solid line is a regression curve obtained by curve fitting. $[\mathbf{LIm2}]_0$: The concentration of **LIm2** when axial binding is ignored. $[\mathbf{1b}]_0$: The initial concentration of **1b**.

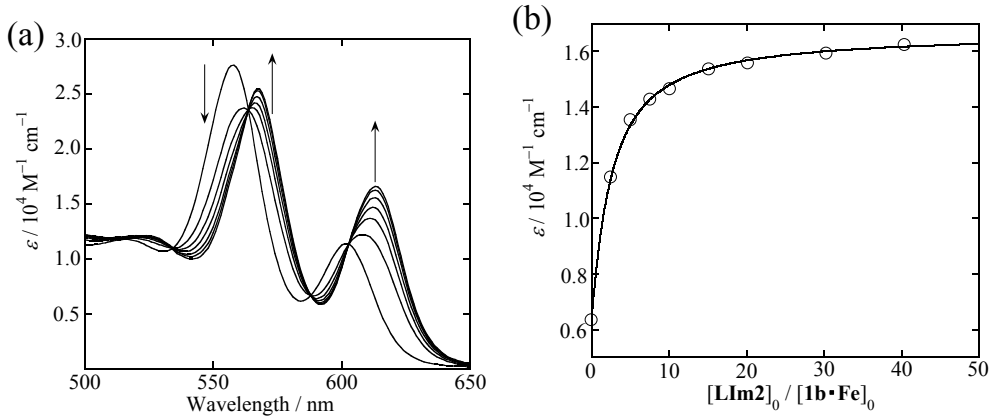

Figure 3-21. (a) UV–vis spectral change resulting from the titration of **1b•Fe** (2×10^{-5} M) with **LIm2** (3×10^{-2} M) in a toluene/acetonitrile (1/1 (v/v)) solution at 20 °C. (b) The change in the molar extinction coefficient at 614 nm. The solid line is a regression curve obtained by curve fitting. $[\mathbf{LIm2}]_0$: The concentration of **LIm2** when axial binding is ignored. $[\mathbf{1b{\bullet}Fe}]_0$: The initial concentration of **1b•Fe**.

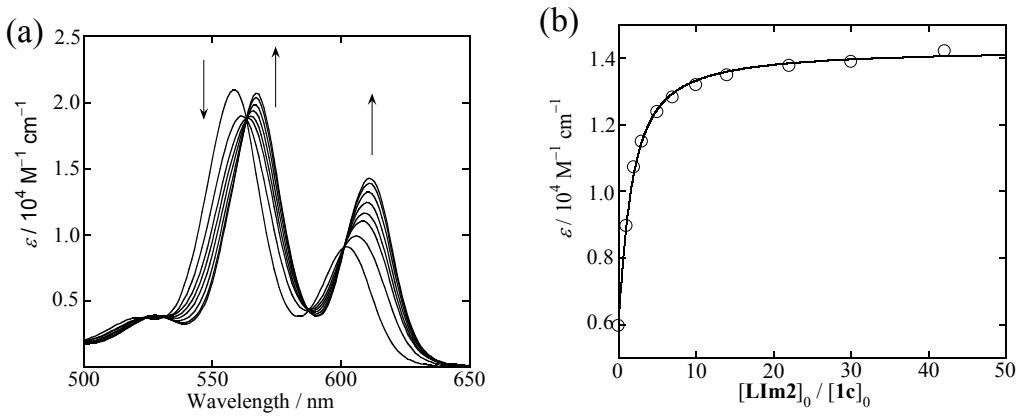

Figure 3-22. (a) UV−vis spectral change resulting from the titration of **1c** (2×10^{-5} M) with **LIm2** (1.2×10^{-2} M) in a toluene/acetonitrile (1/1 (v/v)) solution at 20 °C. (b) The change in the molar extinction coefficient at 611 nm. The solid line is a regression curve obtained by curve fitting. $[\mathbf{LIm2}]_0$: The concentration of **LIm2** when axial binding is ignored. $[\mathbf{1c}]_0$: The initial concentration of **1c**.

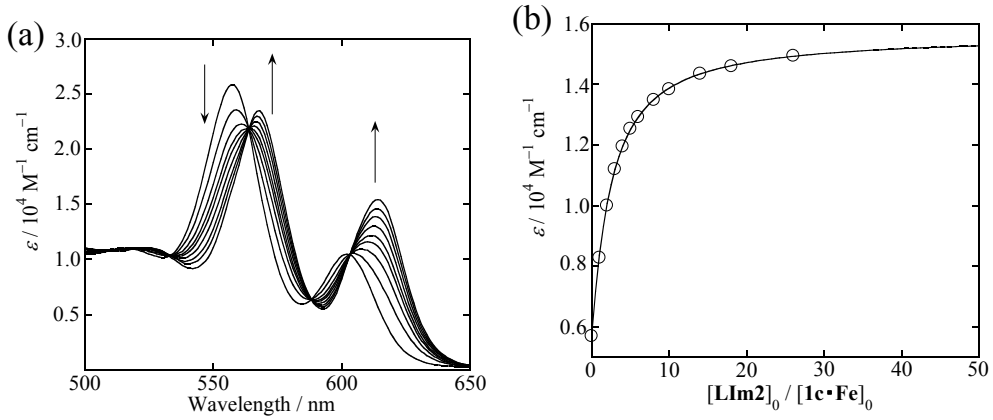

Figure 3-23. (a) UV−vis spectral change resulting from the titration of **1c•Fe** (2×10^{-5} M) with **LIm2** (1.2×10^{-2} M) in a toluene/acetonitrile (1/1 (v/v)) solution at 20 °C. (b) The change in the molar extinction coefficient at 614 nm. The solid line is a regression curve obtained by curve fitting. $[\mathbf{LIm2}]_0$: The concentration of **LIm2** when axial binding is ignored. $[\mathbf{1c{\bullet}Fe}]_0$: The initial concentration of **1c•Fe**.

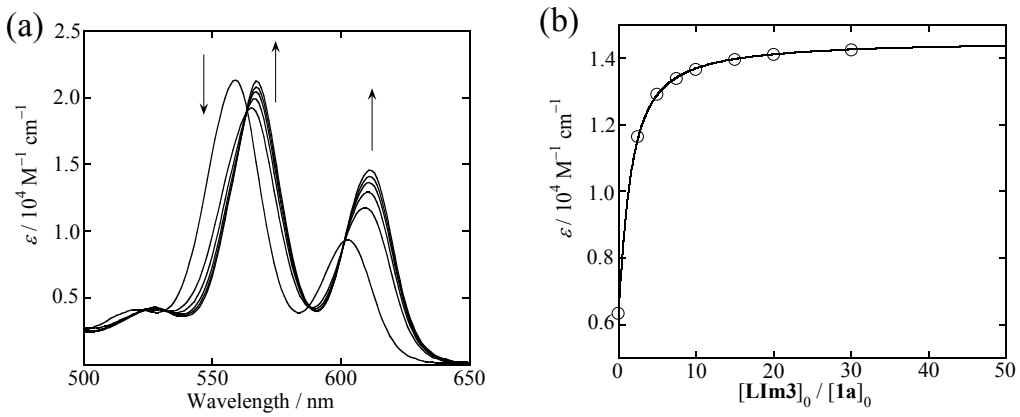

Figure 3-24. (a) UV–vis spectral change resulting from the titration of **1a** (2×10^{-5} M) with **LIm3** (3×10^{-2} M) in a toluene/acetonitrile (1/1 (v/v)) solution at 20 °C. (b) The change in the molar extinction coefficient at 611 nm. The solid line is a regression curve obtained by curve fitting. $[\mathbf{LIm3}]_0$: The concentration of **LIm3** when axial binding is ignored. $[\mathbf{1a}]_0$: The initial concentration of **1a**.

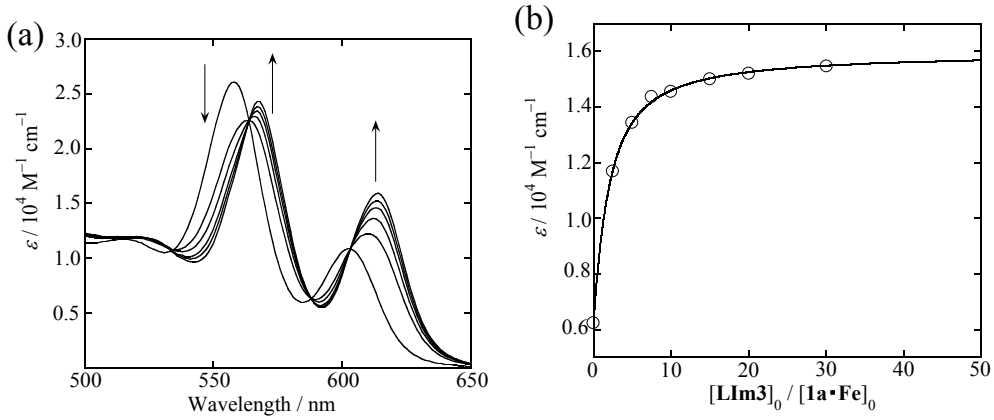

Figure 3-25. (a) UV–vis spectral change resulting from the titration of **1a•Fe** (2×10^{-5} M) with **LIm3** (3×10^{-2} M) in a toluene/acetonitrile (1/1 (v/v)) solution at 20 °C. (b) The change in the molar extinction coefficient at 614 nm. The solid line is a regression curve obtained by curve fitting. $[\mathbf{LIm3}]_0$: The concentration of **LIm3** when axial binding is ignored. $[\mathbf{1a•Fe}]_0$: The initial concentration of **1a•Fe**.

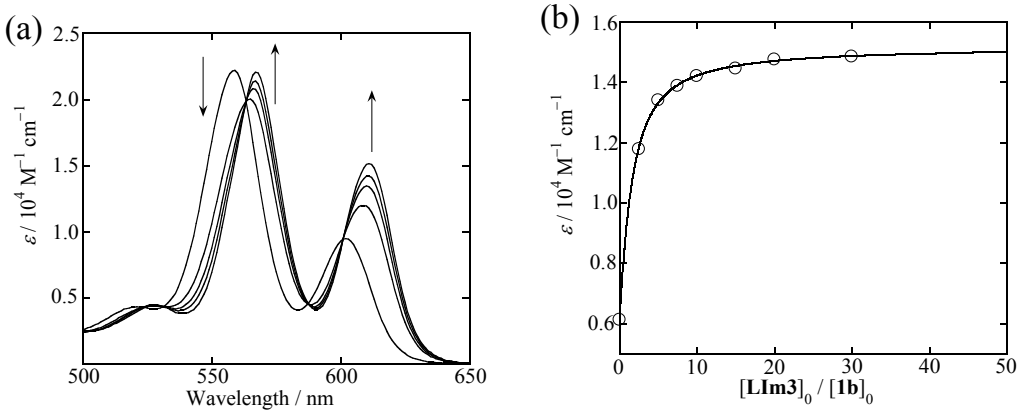

Figure 3-26. (a) UV−vis spectral change resulting from the titration of **1b** (2×10^{-5} M) with **LIm3** (3×10^{-2} M) in a toluene/acetonitrile (1/1 (v/v)) solution at 20 °C. (b) The change in the molar extinction coefficient at 611 nm. The solid line is a regression curve obtained by curve fitting. $[\mathbf{LIm3}]_0$: The concentration of **LIm3** when axial binding is ignored. $[\mathbf{1b}]_0$: The initial concentration of **1b**.

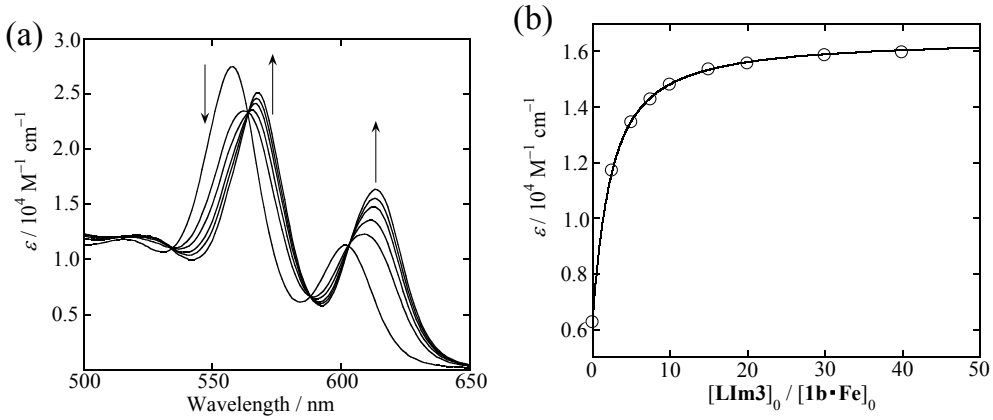

Figure 3-27. (a) UV−vis spectral change resulting from the titration of **1b•Fe** (2×10^{-5} M) with **LIm3** (3×10^{-2} M) in a toluene/acetonitrile (1/1 (v/v)) solution at 20 °C. (b) The change in the molar extinction coefficient at 613 nm. The solid line is a regression curve obtained by curve fitting. $[\mathbf{LIm3}]_0$: The concentration of **LIm3** when axial binding is ignored. $[\mathbf{1b{\bullet}Fe}]_0$: The initial concentration of **1b•Fe**.

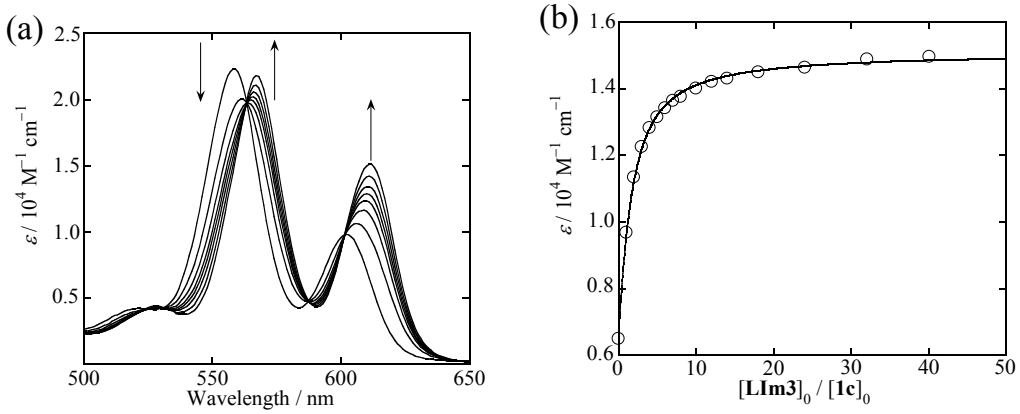

Figure 3-28. (a) UV–vis spectral change resulting from the titration of **1c** (2×10^{-5} M) with **LIm3** (1.2×10^{-2} M) in a toluene/acetonitrile (1/1 (v/v)) solution at 20 °C. (b) The change in the molar extinction coefficient at 611 nm. The solid line is a regression curve obtained by curve fitting. $[\mathbf{LIm3}]_0$: The concentration of **LIm3** when axial binding is ignored. $[\mathbf{1c}]_0$: The initial concentration of **1c**.

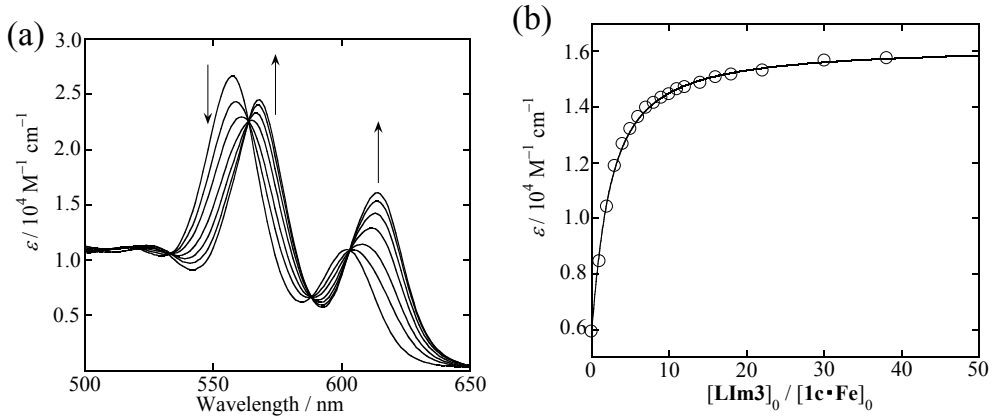

Figure 3-29. (a) UV–vis spectral change resulting from the titration of **1c•Fe** (2×10^{-5} M) with **LIm3** (1.2×10^{-2} M) in a toluene/acetonitrile (1/1 (v/v)) solution at 20 °C. (b) The change in the molar extinction coefficient at 614 nm. The solid line is a regression curve obtained by curve fitting. $[\mathbf{LIm3}]_0$: The concentration of **LIm3** when axial binding is ignored. $[\mathbf{1c•Fe}]_0$: The initial concentration of **1c•Fe**.

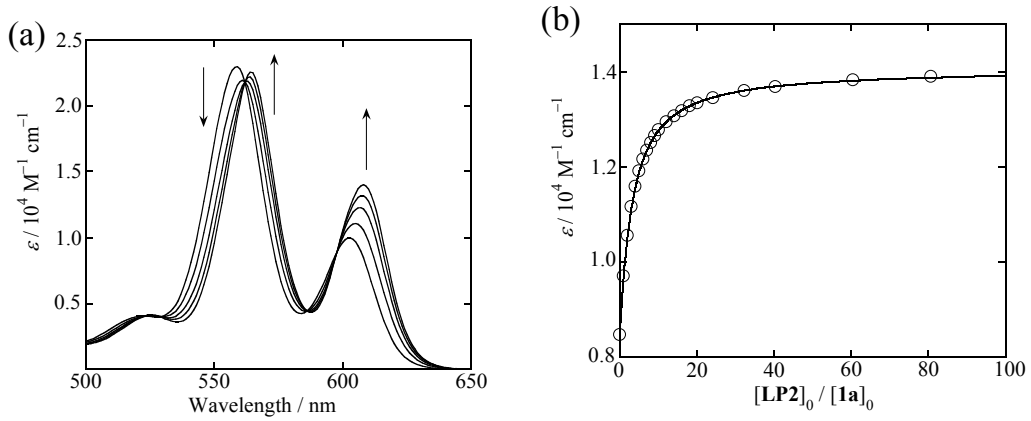

Figure 3-30. (a) UV–vis spectral change resulting from the titration of **1a** (5×10^{-5} M) with **LP2** (3×10^{-2} M) in a toluene/acetonitrile (1/1 (v/v)) solution at 20 °C. (b) The change in the molar extinction coefficient at 608 nm. The solid line is a regression curve obtained by curve fitting. $[\mathbf{LP2}]_0$: The concentration of **LP2** when axial binding is ignored. $[\mathbf{1a}]_0$: The initial concentration of **1a**.

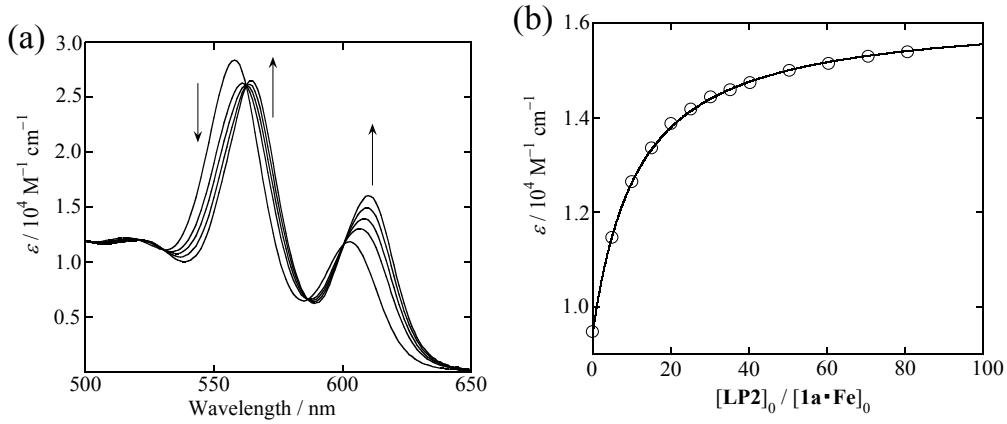

Figure 3-31. (a) UV–vis spectral change resulting from the titration of **1a•Fe** (2×10^{-5} M) with **LP2** (3×10^{-2} M) in a toluene/acetonitrile (1/1 (v/v)) solution at 20 °C. (b) The change in the molar extinction coefficient at 610 nm. The solid line is a regression curve obtained by curve fitting. $[\mathbf{LP2}]_0$: The concentration of **LP2** when axial binding is ignored. $[\mathbf{1a{\bullet}Fe}]_0$: The initial concentration of **1a•Fe**.

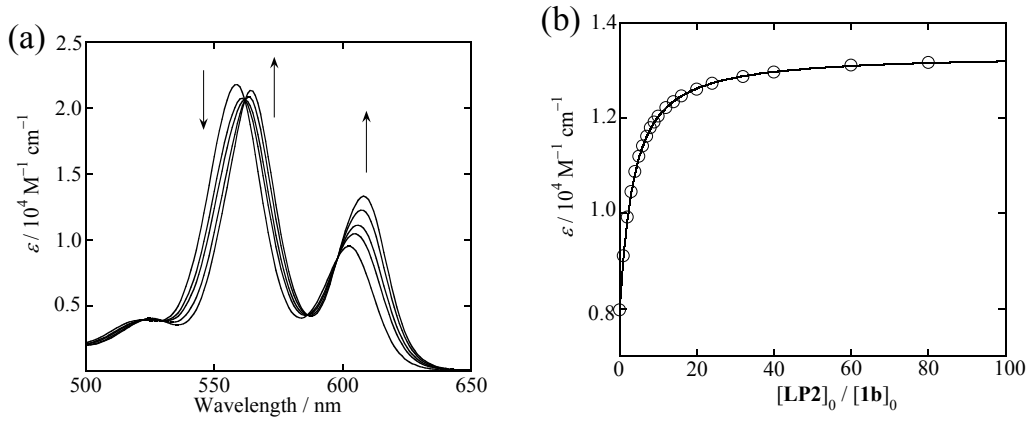

Figure 3-32. (a) UV–vis spectral change resulting from the titration of **1b** (5×10^{-5} M) with **LP2** (3×10^{-2} M) in a toluene/acetonitrile (1/1 (v/v)) solution at 20 °C. (b) The change in the molar extinction coefficient at 608 nm. The solid line is a regression curve obtained by curve fitting. $[\mathbf{LP2}]_0$: The concentration of **LP2** when axial binding is ignored. $[\mathbf{1b}]_0$: The initial concentration of **1b**.

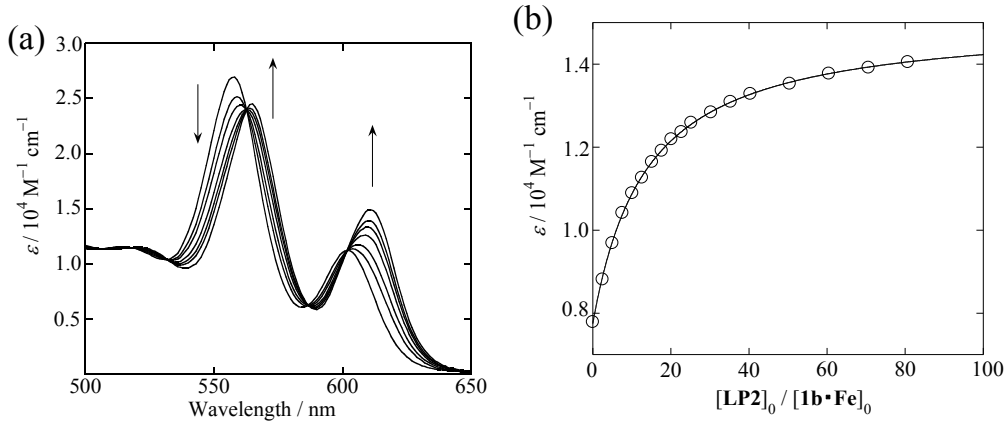

Figure 3-33. (a) UV–vis spectral change resulting from the titration of **1b•Fe** (2×10^{-5} M) with **LP2** (3×10^{-2} M) in a toluene/acetonitrile (1/1 (v/v)) solution at 20 °C. (b) The change in the molar extinction coefficient at 611 nm. The solid line is a regression curve obtained by curve fitting. $[\mathbf{LP2}]_0$: The concentration of **LP2** when axial binding is ignored. $[\mathbf{1b{\bullet}Fe}]_0$: The initial concentration of **1b•Fe**.

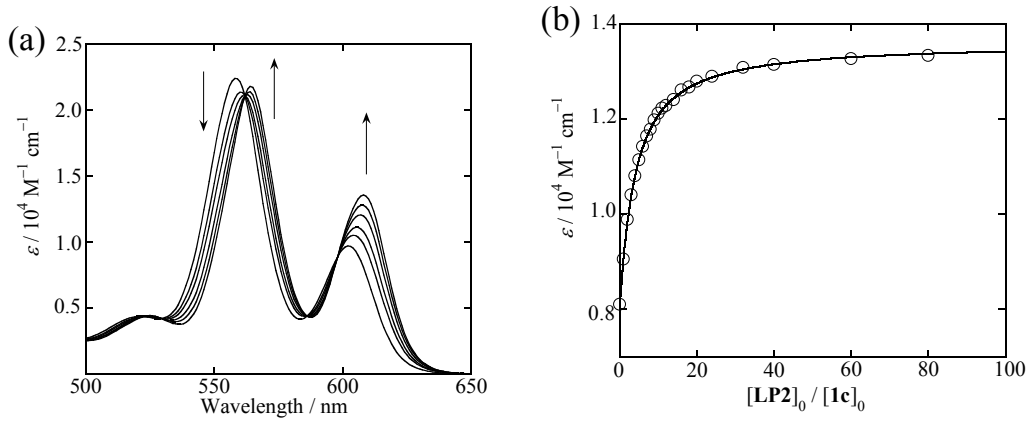

Figure 3-34. (a) UV–vis spectral change resulting from the titration of **1c** (5×10^{-5} M) with **LP2** (3×10^{-2} M) in a toluene/acetonitrile (1/1 (v/v)) solution at 20 °C. (b) The change in the molar extinction coefficient at 608 nm. The solid line is a regression curve obtained by curve fitting. $[\mathbf{LP2}]_0$: The concentration of **LP2** when axial binding is ignored. $[\mathbf{1c}]_0$: The initial concentration of **1c**.

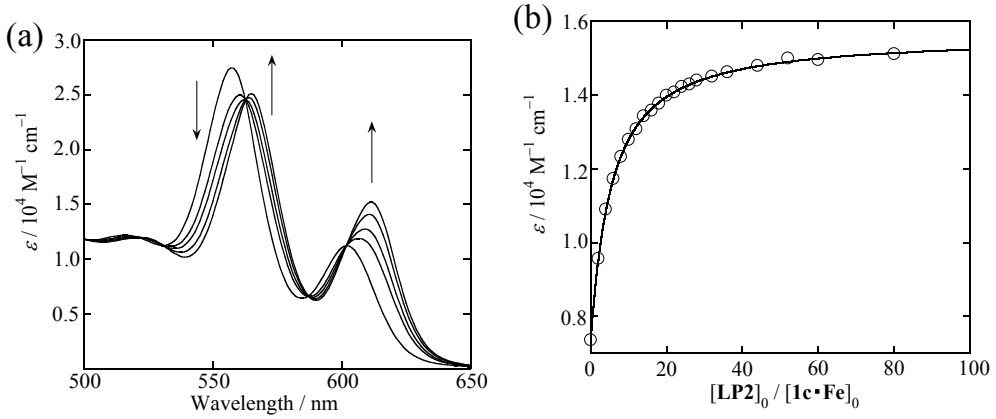

Figure 3-35. (a) UV–vis spectral change resulting from the titration of **1c•Fe** (5×10^{-5} M) with **LP2** (3×10^{-2} M) in a toluene/acetonitrile (1/1 (v/v)) solution at 20 °C. (b) The change in the molar extinction coefficient at 612 nm. The solid line is a regression curve obtained by curve fitting. $[\mathbf{LP2}]_0$: The concentration of **LP2** when axial binding is ignored. $[\mathbf{1c{\bullet}Fe}]_0$: The initial concentration of **1c•Fe**.

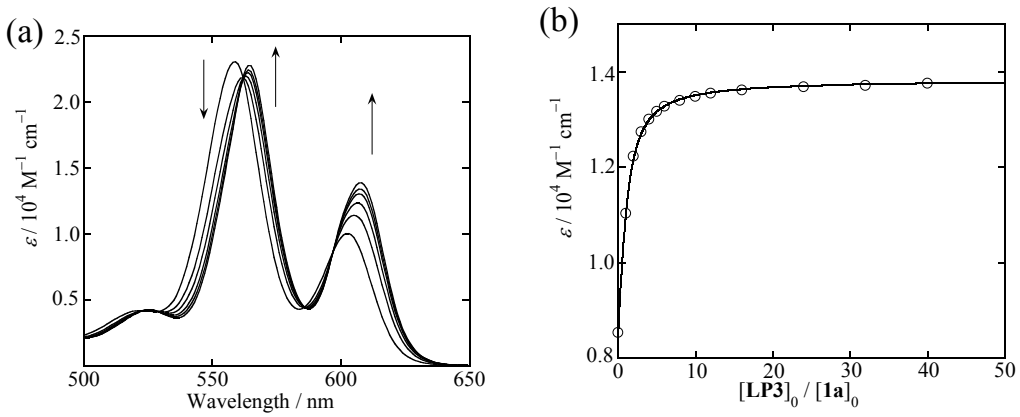

Figure 3-36. (a) UV−vis spectral change resulting from the titration of **1a** (5×10^{-5} M) with **LP3** (3×10^{-2} M) in a toluene/acetonitrile (1/1 (v/v)) solution at 20 °C. (b) The change in the molar extinction coefficient at 608 nm. The solid line is a regression curve obtained by curve fitting. $[\mathbf{LP3}]_0$: The concentration of **LP3** when axial binding is ignored. $[\mathbf{1a}]_0$: The initial concentration of **1a**.

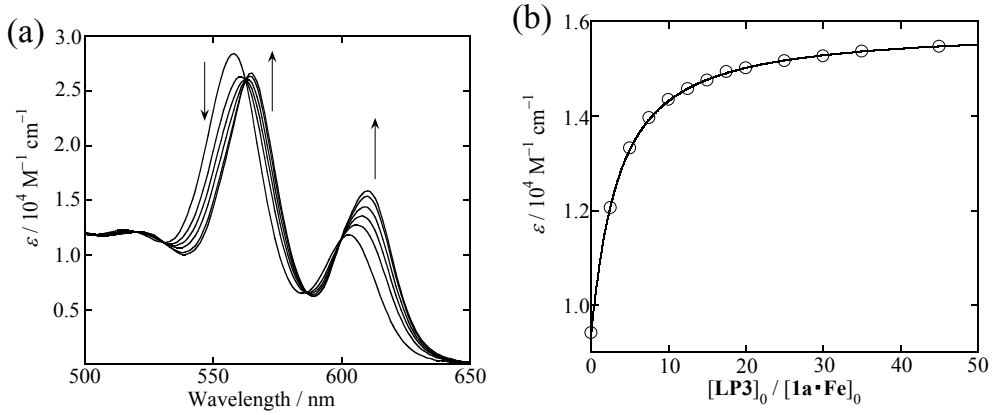

Figure 3-37. (a) UV−vis spectral change resulting from the titration of **1a•Fe** (2×10^{-5} M) with **LP3** (3×10^{-2} M) in a toluene/acetonitrile (1/1 (v/v)) solution at 20 °C. (b) The change in the molar extinction coefficient at 610 nm. The solid line is a regression curve obtained by curve fitting. $[\mathbf{LP3}]_0$: The concentration of **LP3** when axial binding is ignored. $[\mathbf{1a{\bullet}Fe}]_0$: The initial concentration of **1a•Fe**.

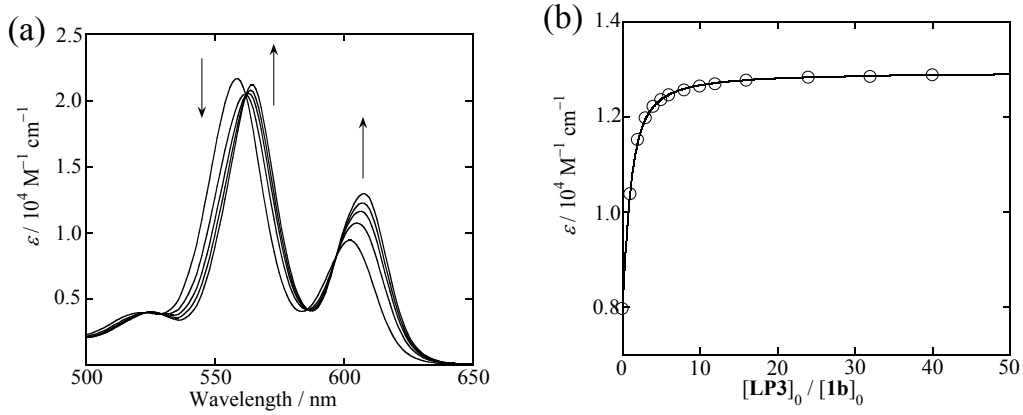

Figure 3-38. (a) UV−vis spectral change resulting from the titration of **1b** (5×10^{-5} M) with **LP3** (3×10^{-2} M) in a toluene/acetonitrile (1/1 (v/v)) solution at 20 °C. (b) The change in the molar extinction coefficient at 608 nm. The solid line is a regression curve obtained by curve fitting. $[\mathbf{LP3}]_0$: The concentration of **LP3** when axial binding is ignored. $[\mathbf{1b}]_0$: The initial concentration of **1b**.

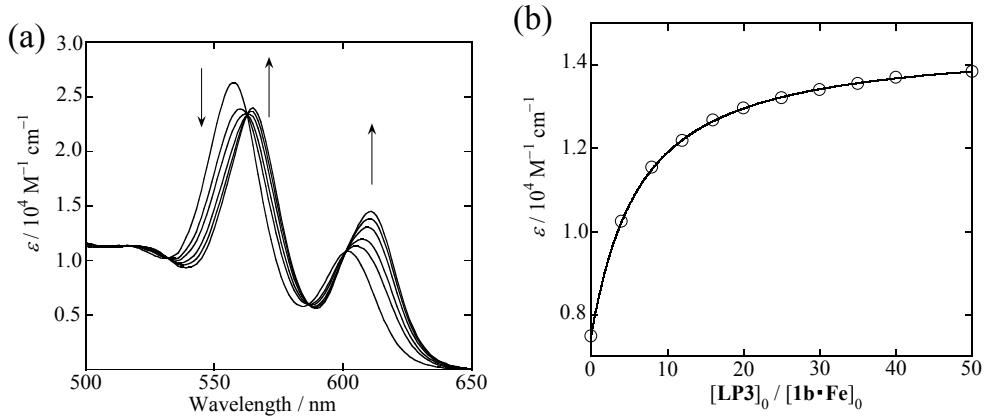

Figure 3-39. (a) UV−vis spectral change resulting from the titration of **1b•Fe** (2×10^{-5} M) with **LP3** (3×10^{-2} M) in a toluene/acetonitrile (1/1 (v/v)) solution at 20 °C. (b) The change in the molar extinction coefficient at 611 nm. The solid line is a regression curve obtained by curve fitting. $[\mathbf{LP3}]_0$: The concentration of **LP3** when axial binding is ignored. $[\mathbf{1b{\bullet}Fe}]_0$: The initial concentration of **1b•Fe**.

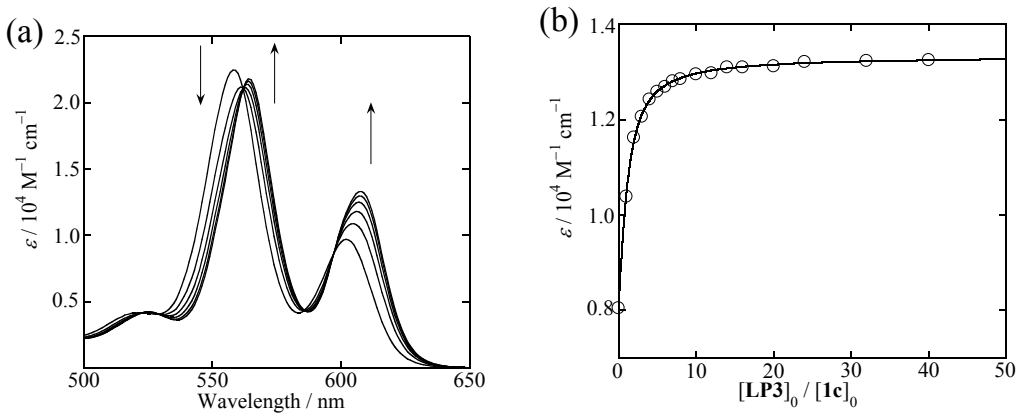

Figure 3-40. (a) UV–vis spectral change resulting from the titration of **1c** (5×10^{-5} M) with **LP3** (3×10^{-2} M) in a toluene/acetonitrile (1/1 (v/v)) solution at 20 °C. (b) The change in the molar extinction coefficient at 608 nm. The solid line is a regression curve obtained by curve fitting. $[\mathbf{LP3}]_0$: The concentration of **LP3** when axial binding is ignored. $[\mathbf{1c}]_0$: The initial concentration of **1c**.

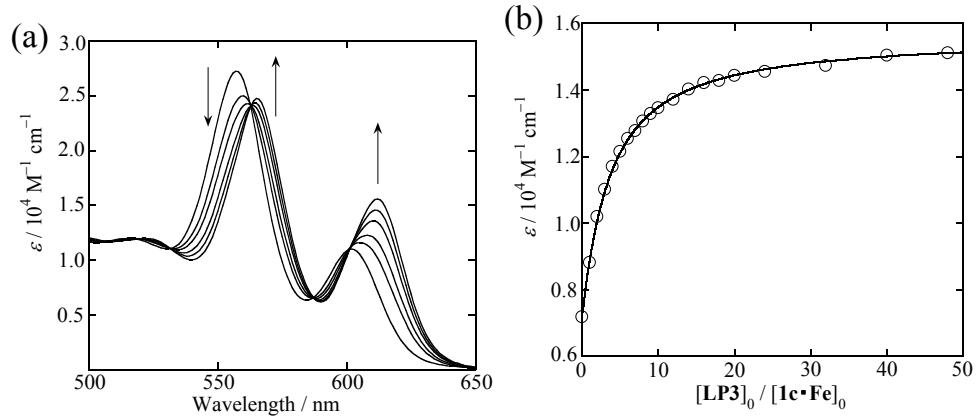

Figure 3-41. (a) UV–vis spectral change resulting from the titration of **1c•Fe** (5×10^{-5} M) with **LIm3** (3×10^{-2} M) in a toluene/acetonitrile (1/1 (v/v)) solution at 20 °C. (b) The change in the molar extinction coefficient at 612 nm. The solid line is a regression curve obtained by curve fitting. $[\mathbf{LP3}]_0$: The concentration of **LP3** when axial binding is ignored. $[\mathbf{1c{\bullet}Fe}]_0$: The initial concentration of **1c•Fe**.

In all the combinations of allosteric receptor **1** and axial ligands, the ligand-binding abilities of the Zn porphyrin in receptors **1** were suppressed by adding Fe ions. The strongest degree of allosteric inhibition (4.5 ± 0.2) was obtained when the receptor with the shortest alkyl chain and the most sterically bulky ligand with a pyridine unit was used, namely, receptors **1c** and **LP3**. Ligands containing imidazole units generally have a small degree of allosteric inhibition (1.2–1.7) compared to pyridine-type ligands (1.3–4.5). Moreover, the effect of the steric bulkiness of ligands on the degree of allosteric inhibition is limited in imidazole-type ligands. Even **LIm3** with bulky dendritic units showed allosteric inhibition of 1.39, 1.63, and 1.44 for **1a**, **1b**, and **1c**, respectively. Almost the same values were observed for **Lim1** and **LIm2**. The imidazole unit is connected to the carbon atom at the benzyl position in **LIm2** and **LIm3**. The MMFF-optimized structure indicates that the benzyl unit in **LIm2** and **LIm3** may avoid severe steric repulsion among the alkyl chains (Figure 3-42). The dendritic unit can be located apart from the porphyrin unit owing to the free rotation of **Zn**–**N**(imidazole) and **C**(benzyl)–**N**(imidazole) single bonds. Consequently, the dendritic unit of **LIm3** slightly increases the steric congestion. On the other hand, the degrees of allosteric inhibition observed in pyridyl ligands **LP1** and **LP2** are ~2. These results indicate that the steric demand of both **LP1** and **LP2** is too small to produce significant steric repulsion among the alkyl chains. The most sterically bulky pyridyl ligand **LP3** showed allosteric inhibition of 1.93, 4.18, and 4.53 for **1a**, **1b**, and **1c**, respectively. Receptors **1b** and **1c** with shorter alkyl chains showed considerable allosteric inhibition for the coordination of **LP3** with the Zn porphyrin unit. These results indicate that the effective allosteric inhibition is insufficient when the receptor with short alkyl chains is used. Moreover, it is essential to use sterically demanding pyridyl ligands.

3-7. Conclusion

In conclusion, artificial allosteric receptors **1b** and **1c** with shorter alkyl chains than **1a** were designed and synthesized. The new allosteric receptors **1b** and **1c** formed a stable 1:1 complex with Fe ions as confirmed by the UV–visible titration results and ESI-MS spectra. The binding constants of **1** with various types of axial ligand were determined by UV–visible spectroscopic titration before (active form) and after the Fe(II) complexation (inactive form). These binding constants were distinctly different and showed that the binding ability of the Zn porphyrin in **1** with axial ligands were suppressed by adding Fe ions. When receptor **1c** with the shortest alkyl chains and **LP3** with the most sterically bulky ligand were combined, the largest degree of allosteric inhibition (4.5) was observed.

(a)

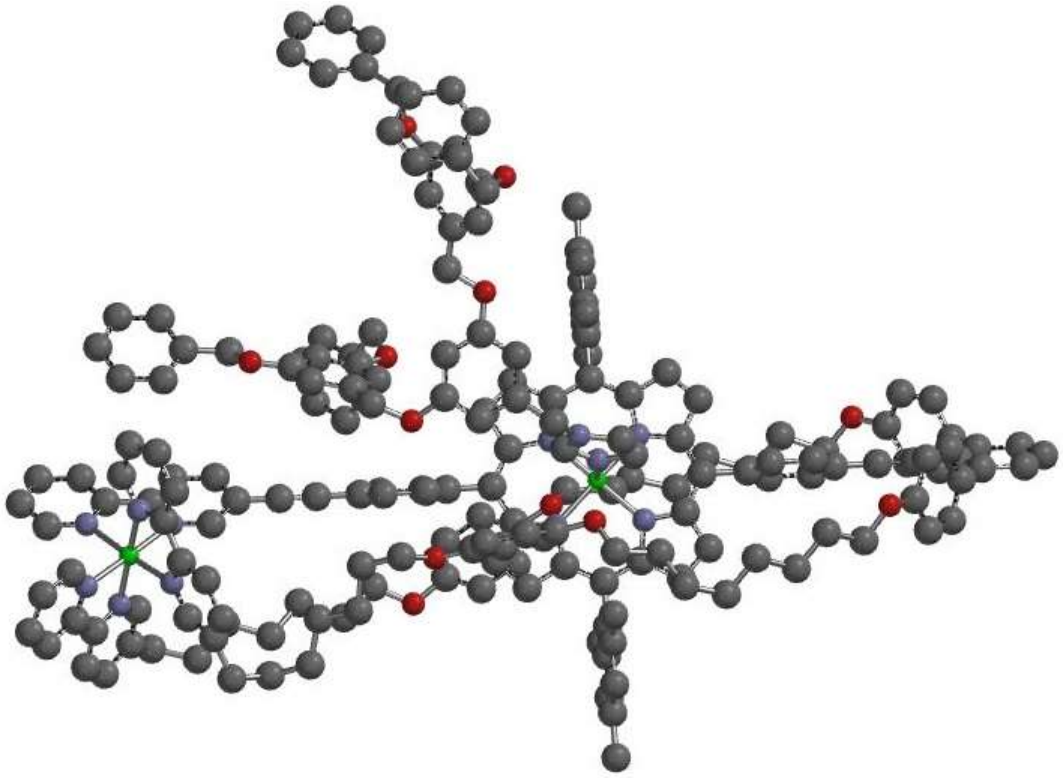

(b)

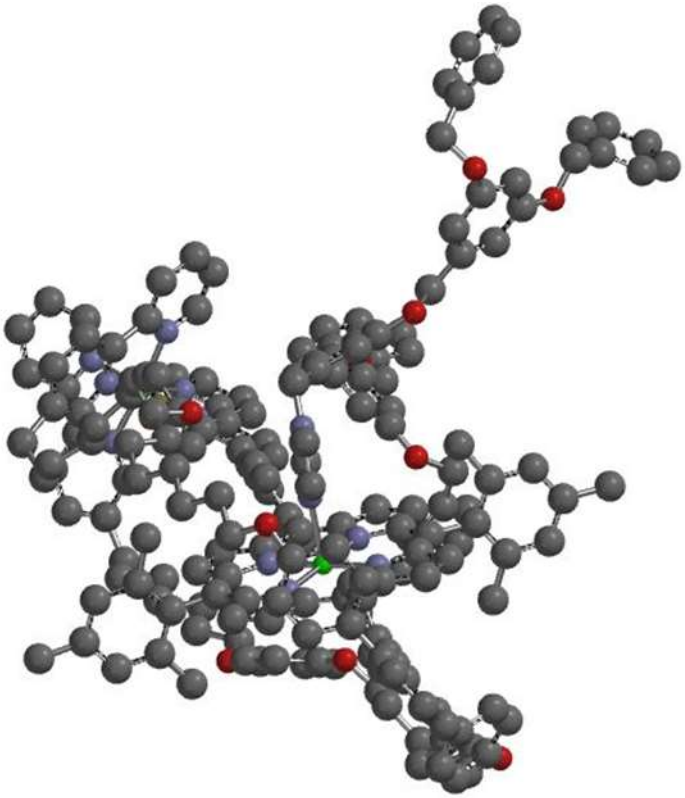

Figure 3-42. MMFF optimized structure of aggregate **1c•Fe•LIm3**. (a) top view. (b) side view. Hydrogen atoms are omitted for clarity.

3-8. Experimental section

3-8-1. Synthesis and characterization

General procedure.

Melting points were taken on a Yanako MP J-3 apparatus and are uncorrected. ^{1}H NMR and ^{13}C NMR spectra were recorded on Bruker Nanobay 300, JEOL Lambda 300WB, or JEOL Lambda 400 spectrometers. Chemical shifts were recorded in units of parts per million downfield from tetramethylsilane as an internal standard and all coupling constants are reported in Hz. IR spectra were obtained on a Shimadzu FTIR-8700 spectrometer. UV−vis spectra were obtained on a Shimadzu UV-2550PC spectrometer. The mass spectra were recorded on a JEOL JMS-700T and JMX-AX500 spectrometers. Elemental analyses were obtained from the Analytical Center in Osaka City University. TLC was carried out using 0.2 mm thick Merck silica gel (60 F_{254}) and 0.25 mm thick Merck aluminium oxide 60 precoated plates. Merck silica gel 60 (granulometry 0.063–0.200 mm) and Merck aluminium oxide 90 (granulometry 0.063–0.200 mm) were used for column chromatography. Recycling preparative GPC (gel permeation chromatography) was carried out using Japan Analytical Industry LC–908 with JAIGEL-1H and -2H GPC columns. 5-Methy-2,2′-bipyridine (**4**)[3] was prepared according to the reported methods. Commercially available reagents and solvents were purified and dried when necessary.

4, 4, 5, 5-Tetramethyl-2-(4-(10-bromodecyloxyphenyl)-1, 3, 2-dioxaborolane (3b)

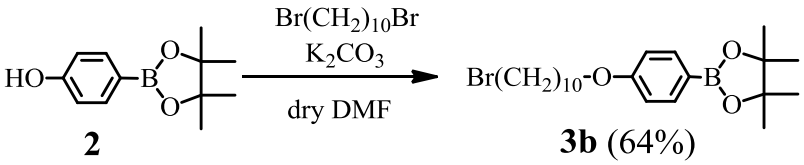

2 **3b** (64%)

To a mixture of **2** (220 mg, 1.0 mmol, 1.0 equiv.), 1,10-dibromodecane (900 mg, 3.0 mmol, 3.0 equiv.) and potassium carbonate (207 mg, 1.5 mmol, 1.5 equiv.), dry DMF (25 mL) was added under a nitrogen atmosphere. The suspension was stirred overnight at 40 ^{o}C. After cooling to room temperature, the reaction mixture was poured into water. The mixture was extracted with diethyl ether. The extract was dried over sodium sulfate and filtered. The solvent was removed under reduced pressure and the residue was purified by column chromatography on silica gel (hexane/dichloromethane = 1/1 (v/v)) to give **3b** as a white solid (280 mg, 64%).

3b: $C_{22}H_{36}BBrO_3$. White solid; MW 439.2; mp 72 ^{o}C; ^{1}H NMR (400 MHz, $CDCl_3$): δ 7.73 (d, 2H, J = 8.5 Hz), 6.88 (d, 2H, J = 8.5 Hz), 3.97 (t, 2H, J = 6.5 Hz), 3.41 (t, 2H, J = 6.8 Hz), 1.89–1.76 (m, 4H), 1.43–1.31 (m, 24H); ^{13}C NMR (100 MHz, $CDCl_3$): δ 161.73, 136.47, 113.86, 83.50, 67.74, 34.01, 32.81, 29.41, 29.33, 29.30, 29.18, 28.72, 28.15, 25.98, 24.85; MS (FAB+): m/z 440 [MH^+]; IR (KBr, cm^{-1}): 2982(m), 2924(s), 2851(m), 1605(s), 1568(w), 1468(w), 1458(w), 1396(m), 1362(s), 1325(m), 1313(w), 1277(w), 1242(s), 1219(w), 1175(m), 1142(s), 1094(m), 1038(m), 1013(m), 964(w), 860(m), 831(m), 820(m), 737(w), 723(w), 671(w), 654(m), 623(m), 519(w); HRMS (FAB+): m/z Calcd for $C_{22}H_{36}B^{79}BrO_3$: 438.1941. Found: 438.1936.

4, 4, 5, 5-Tetramethyl-2-(4-(8-bromooctyloxyphenyl)-1, 3, 2-dioxaborolane (3c)

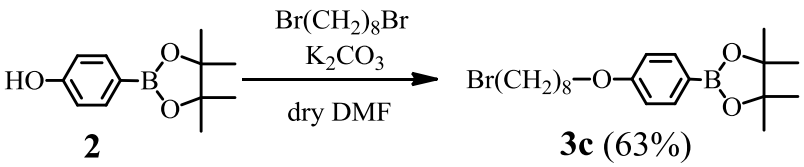

2 **3c** (63%)

This compound was prepared as same as **3b** by using **2** (880 mg, 4.0 mmol, 1.0 equiv.), 1,8-dibromooctane (3.26 g, 12.0 mmol, 3.0 equiv.), potassium carbonate (709 mg, 6.0 mmol, 1.5 equiv.) and dry DMF (100 mL). The crude product was purified by column chromatography on silica gel (hexane/dichloromethane = 1/1 (v/v)) to give **3c** as a white solid (1.04 g, 63%).

3c: $C_{20}H_{32}BBrO_3$. White solid; MW 411.2; mp 70 ^{o}C; ^{1}H NMR (300 MHz, $CDCl_3$): δ 7.73 (d, 2H, J = 7.9 Hz), 6.88 (d, 2H, J = 8.0 Hz), 3.98 (t, 2H, J = 6.4 Hz), 3.41 (t, 2H, J = 6.9 Hz), 1.88–1.73 (m, 4H), 1.44–1.33 (m, 20H); ^{13}C NMR (100 MHz, $CDCl_3$): δ 161.70, 136.47, 113.85, 83.50, 67.78, 33.95, 32.77, 29.15, 28.67, 28.08, 25.92, 24.85; MS (FAB+): m/z 412 [MH^+]; IR (KBr, cm^{-1}): 2982(m), 2939(s), 2926(s), 2854(m), 1605(s), 1568(w), 1508(w), 1472(m), 1458(w), 1396(m),

1362(s), 1327(m), 1308(w), 1277(w), 1248(s), 1213(w), 1176(m), 1142(s), 1094(m), 1065(w), 1020(s), 984(w), 964(m), 860(m), 833(s), 820(m), 737(w), 721(w), 669(w), 654(s), 623(m), 577(w), 519(w); HRMS (FAB+): *m/z* Calcd for $C_{20}H_{32}B^{79}BrO_3$: 410.1628. Found: 410.1619.

5-(9-Bromononyl)-2,2′-bipyridine (5b)[7]

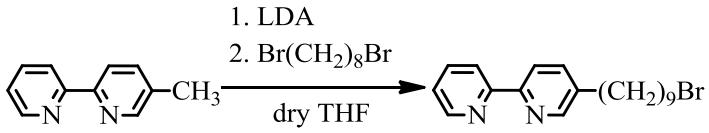

4 **5b** (64%)

To a solution of dry diisopropylamine (2.5 mL, 18 mmol, 1.8 equiv.) in dry THF (90 mL), *n*-butyllithium (1.6 M, in *n*-hexane, 9.6 mL, 15 mmol, 1.5 equiv.) was added dropwise at −78 °C under a nitrogen atmosphere. The solution was stirred for 1 h at −78 °C and 5-methyl-2,2′-bipyridine **4** (1.7 g, 10 mmol, 1.0 equiv.) in dry THF (30 mL) was added at −78 °C. The temperature was allowed to raise gradually over 4 h to −40 °C. The solution was recooled to −78 °C and 1,8-dibromooctane (13.6 g, 50 mmol, 5.0 equiv.) in dry THF (30 mL) was added. The solution was allowed to warm up to room temperature and stirred overnight. After the addition of water, THF was evaporated under reduced pressure. Sodium hydrogen carbonate solution was added and the mixture was extracted with dichloromethane. The extract was washed with brine and dried over sodium sulfate. After filtration, the solvent was removed under reduced pressure. The crude product was purified by column chromatography on basic aluminium oxide (toluene) to give **5b** as a white solid (2.33 g, 64%).

5b: $C_{19}H_{25}BrN_2$. White solid; MW 361.3; mp 45 °C; ^{1}H NMR (300 MHz, $CDCl_3$): δ 8.67 (d, 1H, J = 4.8 Hz), 8.50 (d, 1H, J = 2.0 Hz), 8.36 (d, 1H, J = 8.1 Hz), 8.30 (d, 1H, J = 8.1 Hz), 7.86 (td, 1H, J = 7.7, 1.8 Hz), 7.63 (dd, 1H, J = 8.1, 2.2 Hz), 7.31–7.28 (m, 1H), 3.40 (t, 2H, J = 6.8 Hz), 2.67 (t, 2H, J = 7.7 Hz), 1.85 (quintet, 2H, J = 7.1 Hz), 1.66–1.30 (m, 12H); ^{13}C NMR (100 MHz, $CDCl_3$): δ 156.31, 153.85, 149.32, 149.13, 138.21, 136.86, 136.79, 123.37, 120.80, 120.69, 33.99, 32.82, 32.79, 31.03, 29.31, 29.27, 29.04, 28.70, 28.12; MS (FAB+): *m/z* 361.2 [MH^+]; IR (KBr, cm^{-1}): 2934(s), 2854(s), 1587(m), 1574(s), 1558(s), 1541(w), 1458(s), 1433(m), 1362(w), 1232(m), 1182(m), 1146(m), 1090(m), 1026(s), 864(m), 798(s), 773(s), 752(m), 731(s), 652(w), 613(m), 556(m); HRMS (FAB+): *m/z* Calcd for $C_{19}H_{26}{}^{79}BrN_2$: 361.1279. Found: 361.1257.

5-(7-Bromoheptyl)-2,2′-bipyridine (5c)[7]

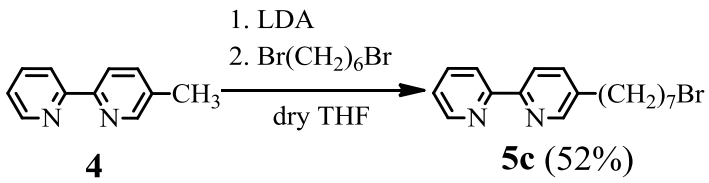

4 **5c** (52%)

This compound was prepared as same as **5b** by using dry diisopropylamine (1.3 mL, 9.3 mmol, 1.9 equiv.), *n*-butyllithium (1.6 M, in *n*-hexane, 4.7 mL, 7.5 mmol, 1.5 equiv.), 5-methyl-2,2′-bipyridine **4** (851 mg, 5.0 mmol, 1.0 equiv.), 1,6-dibromohexane (6.1 g, 25 mmol, 5.0 equiv.) and dry THF (90 mL). The crude product was purified by column chromatography on basic aluminium oxide (toluene) to give **5c** as a white solid (868 mg, 52%).

5c: $C_{17}H_{21}BrN_2$. White solid; MW 333.3; mp 42 °C; ^{1}H NMR (300 MHz, $CDCl_3$): δ 8.67 (d, 1H, J = 5.0 Hz), 8.50 (d, 1H, J = 2.0 Hz), 8.36 (d, 1H, J = 8.1 Hz), 8.30 (d, 1H, J = 8.2 Hz), 7.81 (td, 1H, J = 7.7 Hz, 1.8 Hz), 7.63 (dd, 1H, J = 8.1, 2.3 Hz), 7.31 (m, 1H), 3.40 (t, 2H, J = 6.8 Hz), 2.67 (t, 2H, J = 7.6 Hz), 1.86 (quintet, 2H, J = 7.1 Hz), 1.68–1.30 (m, 8H); ^{13}C NMR (100 MHz, $CDCl_3$): δ 156.28, 153.91, 149.30, 149.12, 138.05, 136.85, 136.77, 123.38, 120.79, 120.70, 33.87, 32.77, 32.71, 30.92, 28.89, 28.53, 28.02; MS (FAB+): *m/z* 333.2 [M^+]; IR (KBr, cm^{-1}): 2924(s), 2856(s), 1587(m), 1576(s), 1558(s), 1541(w), 1460(s), 1435(m), 1396(w), 1248(m), 1186(m), 1148(m), 1090(m), 1026(s), 991(m), 957(w), 876(w), 849(w), 796(s), 772(m), 748(s), 727(m), 652(m), 613(s), 556(m), 507(w); HRMS (FAB+): *m/z* Calcd for $C_{19}H_{26}{}^{79}BrN_2$: 333.0966. Found: 333.0958.

Compound 6b

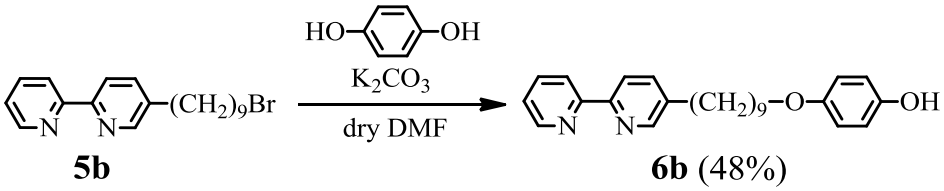

5b **6b** (48%)

To a mixture of **5b** (723 mg, 2.0 mmol, 1.0 equiv.), 1,4-dihydroxybenzene (1.10 g, 10 mmol, 5.0 equiv.) and potassium carbonate (1.38 g, 10 mmol, 5.0 equiv.), dry DMF (20 mL) was added under a nitrogen atmosphere. The suspension was stirred overnight at 80 °C. After cooling to room temperature, the reaction mixture was poured into water. The mixture was extracted with diethyl ether. The extract was dried over sodium sulfate and filtered. The solvent was removed under reduced pressure and the residue was purified by column chromatography on basic aluminium oxide (dichloromethane/methanol = 49/1 (v/v)) to give **6b** as a light brown solid (374 mg, 48%).

6b: $C_{25}H_{30}N_2O_2$. light brown solid; MW 390.5; mp 76 °C; ^{1}H NMR (400 MHz, $CDCl_3$): δ 8.67 (m,

1H), 8.49 (d, 1H, J = 1.9 Hz), 8.36 (d, 1H, J = 8.0 Hz), 8.29 (d, 1H, J = 8.3 Hz), 7.81 (td, 1H, J = 7.8, 1.8 Hz), 7.62 (dd, 1H, J = 8.0, 2.3 Hz), 7.31–7.28 (m, 1H), 6.81–6.71 (d like, 4H, J = 6.1 Hz), 5.16 (br, 1H), 3.89 (t, 2H, J = 6.5 Hz), 2.66 (t, 2H, J = 7.6 Hz), 1.74–1.32 (m, 14H); ^{13}C NMR (100 MHz, $CDCl_3$) δ 156.14, 153.63, 152.96, 149.91, 149.25, 149.04, 138.42, 137.12, 137.03, 123.49, 121.07, 120.97, 116.09, 115.67, 68.65, 32.80, 30.98, 29.32, 29.25, 29.18, 29.00, 25.88; MS (FAB+): *m/z* 391.3 [MH^+]; IR (KBr, cm^{-1}): 2922(s), 2899(m), 2852(s), 1591(m), 1574(m), 1558(m), 1514(s), 1475(m), 1460(s), 1443(m), 1394(m), 1342(m), 1296(w), 1236(s), 1209(m), 1184(m), 1097(m), 1043(w), 1043(s), 1020(m), 999(w), 847(m), 820(s), 798(m), 770(s), 752(m), 737(m), 719(w), 652(w), 617(w), 511(w); HRMS (FAB+): *m/z* Calcd for $C_{25}H_{31}N_2O_2$: 391.2386. Found: 391.2387.

Compound 6c

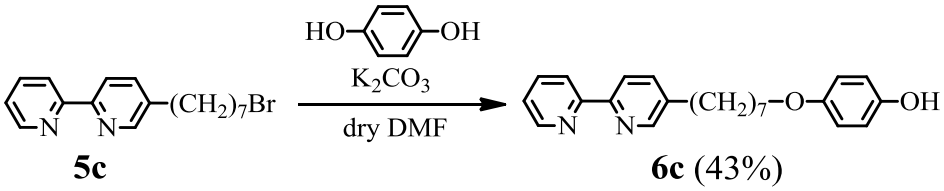

5c **6c** (43%)

This compound was prepared as same as **6b** by using **5c** (333 mg, 1.0 mmol, 1.0 equiv.), 1,4-dihydroxybenzene (1.10 g, 10 mmol, 10 equiv.), potassium carbonate (691 mg, 5.0 mmol, 5.0 equiv.) and DMF (25 mL). The crude product was purified by column chromatography on basic aluminium oxide (dichloromethane/methanol = 49/1 (v/v)) and recrystallized from hexane to give **6c** as a light brown solid (157 mg, 43%).

6c: $C_{23}H_{26}N_2O_2$. light brown solid; MW 362.5; mp 93 ^{o}C; ^{1}H NMR (400 MHz, $CDCl_3$): δ 8.67 (d, 1H, J = 4.9 Hz), 8.49 (s like, 1H), 8.36 (d, 1H, J = 8.3 Hz), 8.28 (d, 1H, J = 8.3 Hz), 7.81 (t like, 1H, J = 7.7 Hz), 7.60 (d like, 1H, J = 9.8 Hz), 7.32–7.28 (m, 1H), 6.76–6.70 (d like, 4H, J = 5.1 Hz), 5.12 (br, 1H), 3.89 (t, 2H, J = 6.5 Hz), 2.66 (t, 2H, J = 7.6 Hz), 1.75–1.36 (m, 10H); ^{13}C NMR (100 MHz, $CDCl_3$): δ 156.22, 153.69, 153.05, 149.62, 149.28, 149.05, 138.24, 137.04, 136.93, 123.46, 121.02, 120.88, 116.09, 115.72, 68.55, 32.80, 30.90 29.09, 29.01, 28.86, 25.79; MS (FAB+): *m/z* 363.3 [MH^+]; IR (KBr, cm^{-1}): 3346(br), 2926(s), 2852(m), 1734(w), 1716(w), 1701(w), 1684(w), 1653(w), 1636(w), 1597(w), 1576(m), 1558(m), 1541(w), 1507(s), 1458(s), 1429(m), 1394(m), 1364(w), 1340(w), 1296(w), 1230(s), 1182(w), 1151(w), 1105(w), 1053(w), 1034(m), 991(w), 858(w), 827(m), 795(s), 766(s), 746(s), 725(m), 621(w), 554(w), 502(w); HRMS (FAB+): *m/z* Calcd for $C_{23}H_{27}N_2O_2$: 363.2073 Found: 363.2072.

Compound 7b (Side chain)

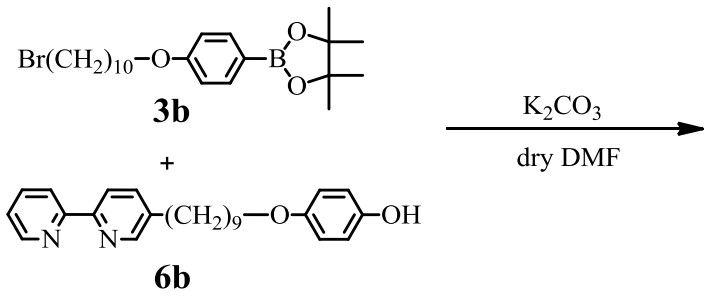

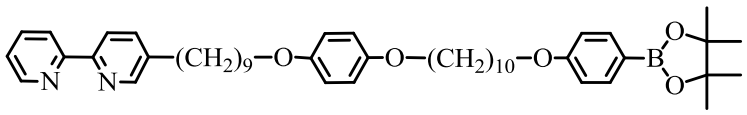

7b (62%)

To a mixture of **3b** (329 mg, 0.75 mmol, 1.5 equiv.), **6b** (190 mg, 0.50 mmol, 1.0 equiv.) and potassium carbonate (346 mg, 2.5 mmol, 5.0 equiv.), dry DMF (25 mL) was added under a nitrogen atmosphere. The suspension was stirred overnight at 100 ^{o}C. After cooling to room temperature, the reaction mixture was poured into water. The mixture was extracted with diethyl ether. The extract was dried over sodium sulfate and filtered. The solvent was removed under reduced pressure and the residue was purified by column chromatography on basic aluminium oxide (dichloromethane/methanol = 19/1 (v/v)) to give **7b** as a white powder (231 mg, 62%).

7b: $C_{47}H_{65}BN_2O_5$. white solid; MW 748.8; mp 96 ^{o}C; ^{1}H NMR (400 MHz, $CDCl_3$): δ 8.67 (d like, 1H, J = 4.4 Hz), 8.50 (s like, 1H), 8.36 (d, 1H, J = 8.0 Hz), 8.30 (d, 1H, J = 8.0 Hz), 7.80 (td, 1H, J = 7.7, 1.7 Hz), 7.73 (d like, 2H, J = 8.8 Hz), 7.63 (dd, 1H, J = 8.2, 2.3 Hz), 7.30–7.27 (m, 1H), 6.88 (d like, 4H, J = 8.5 Hz), 6.81 (s, 4H), 3.97 (t, 2H, J = 6.5 Hz), 3.89 (t, 2H, J = 6.6 Hz), 2.66 (t, 2H, J = 7.7 Hz), 1.81–1.62 (m, 8H), 1.43–1.26 (m, 34H); ^{13}C NMR (100 MHz, $CDCl_3$): δ 161.74, 156.29, 153.81, 153.17, 149.31, 149.11, 138.27, 136.85, 136.79, 136.46, 123.36, 120.80, 120.69, 115.39, 113.85, 83.48, 68.62, 67.76, 32.83, 31.04, 29.46, 29.45, 29.37, 29.34, 29.18, 29.09, 26.02, 25.99, 24.84; MS (FAB+): *m/z* 749.7 [MH^+]; IR (KBr, cm^{-1}): 2922(s), 2851(s), 1718(w), 1701(w), 1655(w), 1605(s), 1589(w), 1558(m), 1508(s), 1474(s), 1458(s), 1437(w), 1396(m), 1362(s), 1319(w), 1277(w), 1230(s), 1175(w), 1142(m), 1109(w), 1092(w), 1045(m), 1020(m), 962(w), 860(w), 815(w), 772(w), 723(w), 654(w), 615(w); HRMS (FAB+): *m/z* Calcd for $C_{47}H_{66}BN_2O_5$: 749.5056. Found: 749.5081.

Compound 7c (Side chain)

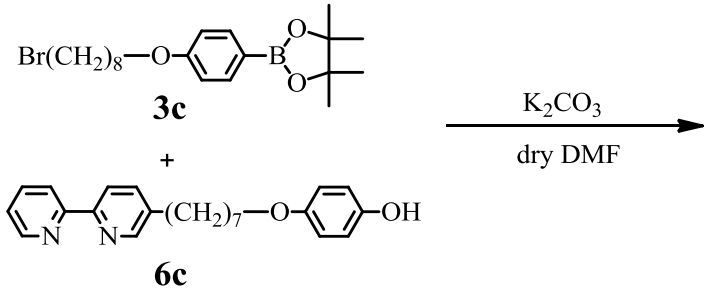

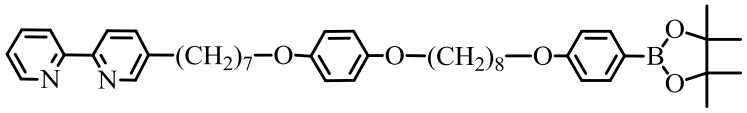

7c (58%)

This compound was prepared as same as **7b** by using **3c** (164 mg, 0.40 mmol, 1.25 equiv.), **6c** (116 mg, 0.32 mmol, 1.0 equiv.), potassium carbonate (221 mg, 1.6 mmol, 5.0 equiv.) and dry DMF (20 mL). The crude product was purified by column chromatography on basic aluminium oxide (dichloromethane/methanol = 19/1 (v/v)) to give **7c** as a white powder (126 mg, 58%).

7c: $C_{43}H_{57}BN_2O_5$. white solid; MW 692.7; mp 97 ^{o}C; ^{1}H NMR (400 MHz, $CDCl_3$): δ 8.67 (d like, 1H, J = 4.6 Hz), 8.50 (d, 1H, J = 1.7 Hz), 8.36 (d, 1H, J = 8.1 Hz), 8.30 (d, 1H, J = 8.3 Hz), 7.80 (td, 1H, J = 7.7, 1.7 Hz), 7.73 (d like, 2H, J = 8.8 Hz), 7.63 (dd, 1H, J = 8.0, 2.2 Hz), 7.30–7.28 (m, 1H), 6.88 (d like, 4H, J = 8.5 Hz), 6.81 (s, 4H), 3.97 (t, 2H, J = 6.6 Hz), 3.89 (t, 2H, J = 6.6 Hz), 2.67 (t, 2H, J = 7.6 Hz), 1.81–1.65 (m, 8H), 1.45–1.38 (m, 14H), 1.33 (s, 12H); ^{13}C NMR (100 MHz, $CDCl_3$): δ 161.75, 156.31, 153.86, 153.22, 153.19, 149.33, 149.13, 138.22, 136.89, 136.83, 136.49, 123.40, 120.85, 120.74, 115.43, 113.88, 83.52, 68.63, 68.57, 67.75, 32.84, 31.00, 29.39, 29.36, 29.20, 29.06, 26.01, 25.99, 25.97, 24.86; MS (FAB+): *m/z* 693.5 [MH^+]; IR (KBr, cm^{-1}): 3649(w), 2939(s), 2852(s), 1716(w), 1699(w), 1653(w), 1607(s), 1558(w), 1541(w), 1508(s), 1474(m), 1458(m), 1437(w), 1396(m), 1364(s), 1321(w), 1281(w), 1230(s), 1176(w), 1142(m), 1107(w), 1092(w), 1042(s), 994(m), 964(w), 862(w), 831(w), 813(w), 795(w), 773(w), 723(w) 654(w), 623(w), 517(w), 507(w); HRMS (FAB+): *m/z* Calcd for $C_{43}H_{58}BN_2O_5$: 693.4439. Found: 693.4440.

Compound 1b

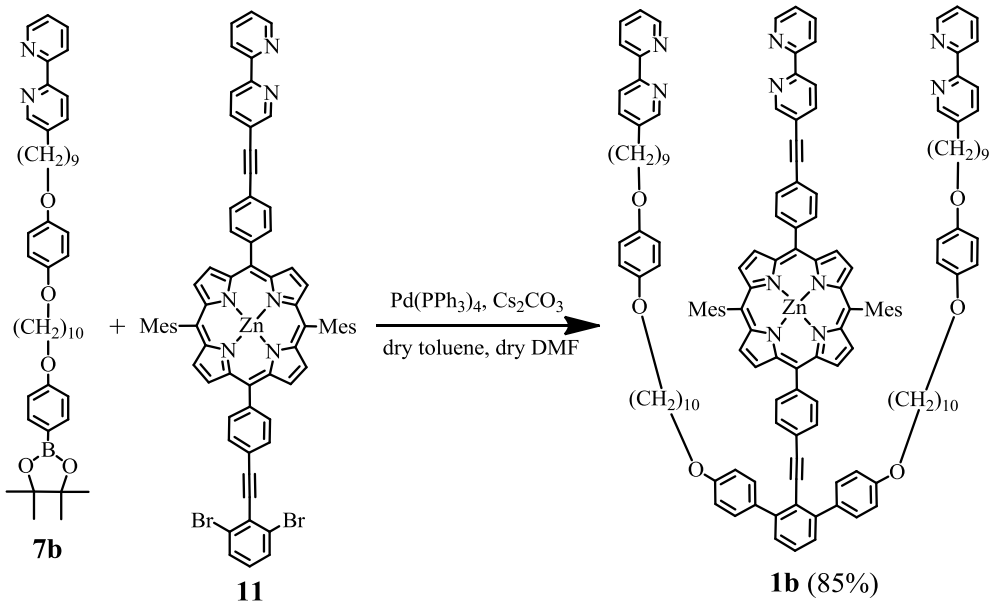

A solution of **11** (59.9 mg, 50 μmol, 1.0 equiv.), **7b** (86.1 mg, 115 μmol, 2.3 equiv.), cesium carbonate (48.9 mg, 150 μmol, 3.0 equiv.) and tetrakis(triphenylphosphine)palladium(0) (11.5 mg, 10 μmol, 0.2 equiv.) in dry DMF (4 mL) and dry toluene (4 mL) was heated at 80 ^{o}C under a nitrogen atmosphere and stirred for 3 days. After cooling to room temperature, the reaction mixture was filtered. A diethyl ether was added to the solution and the solution was washed with distilled water. The solution was dried over sodium sulfate and filtered. The solvent was removed under reduced pressure and the residue was purified by column chromatography on hydroscopic (6wt%) basic aluminium oxide (hexane/dichloromethane = 1/1 (v/v)) to give **1b** as a purple powder (99 mg, 85%).

1b: $C_{152}H_{154}N_{10}O_6Zn$; MW 2282.3; purple solid; mp 85 ^{o}C; ^{1}H NMR (400 MHz, $CDCl_3$): δ 8.96 (m, 1H), 8.94–8.71 (m, 9H), 8.65–8.63 (m, 2H), 8.51–8.47 (m, 4H), 8.33 (d, 2H, J = 8.0 Hz), 8.27 (d, 2H, J = 8.0 Hz), 8.19 (d, 2H, J = 7.8 Hz), 8.09–8.07 (m, 3H), 7.93 (d, 2H, J = 7.8 Hz), 7.87–7.75 (m, 9H), 7.60 (dd, 2H, J = 8.1, 2.0 Hz), 7.47–7.41 (m, 5H), 7.37–7.34 (m, 1H), 7.28 (s, 4H), 7.09 (d, 4H, J = 8.6 Hz), 6.61 (d, 4H, J = 9.0 Hz), 6.36 (d, 4H, J = 9.0 Hz), 4.05 (t, 4H, J = 6.5 Hz), 3.78 (t, 4H, J = 6.5 Hz), 3.32 (t, 4H, J = 6.5 Hz), 2.66–2.63 (m, 10H) , 1.83–1.10 (m, 72H); ^{13}C NMR (100 MHz, $CDCl_3$): δ 158.78, 156.28, 154.94, 153.81, 153.10, 152.40, 151.75, 149.93, 149.87, 149.78, 149.68, 149.30, 149.09, 144.85, 143.62, 142.56, 139.44, 139.18, 139.02, 138.22, 137.48, 136.98, 136.82, 136.75, 134.60, 134.24, 133.53, 132.11, 132.01, 130.93, 130.88, 130.83, 129.83, 129.21, 128.04, 127.67, 123.33, 122.87, 121.62, 121.39, 120.77, 120.67, 120.44, 120.41, 120.17, 119.59, 119.37, 119.18, 115.54, 115.37, 115.10, 113.91, 95.65, 93.72, 90.57, 87.32, 68.59, 68.52, 68.07, 32.81, 31.04, 29.44, 29.36, 29.33, 29.26, 29.22, 29.16, 29.09, 28.87, 25.98, 25.70, 21.66, 21.46; MS (FAB+) : *m/z* 2282 [MH^+]; IR (KBr, cm^{-1}): 2920(s), 2852(s), 1734(w), 1716(w), 1701(w), 1653(w), 1636(w),

1558(m), 1541(m), 1508(s), 1491(w), 1458(s), 1437(w), 1364(w), 1229(s), 1204(m), 1175(w), 995(s), 795(s), 507(w); HRMS (FAB+): *m/z* Calcd for $C_{152}H_{154}N_{10}O_6{}^{64}Zn$: 2279.1344. Found: 2279.1335.

Compound 1c

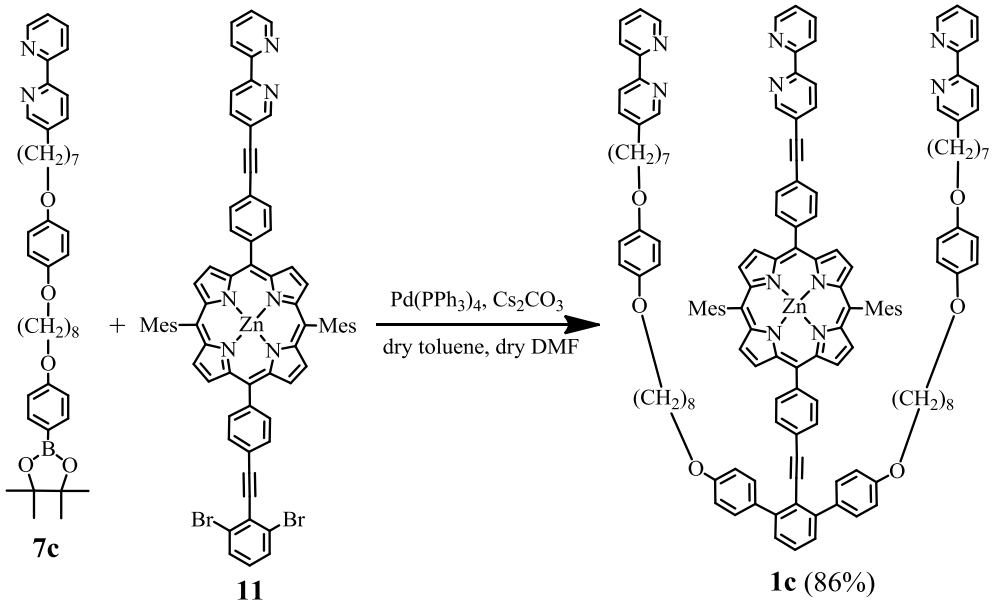

7c + **11** → **1c** (86%)

This compound was prepared as same as **1b** by using **11** (59.9 mg, 50 μmol, 1.0 equiv.), **7c** (78.7 mg, 115 μmol, 2.3 equiv.), tetrakis(triphenylphosphine)palladium(0) (11.6 mg, 10 μmol, 0.2 equiv.), cesium carbonate (48.9 mg, 150 μmol, 3.0 equiv.), dry DMF (5 mL) and dry toluene (5 mL). The mixture was stirred at 70 ^{o}C for 4 days. The crude product was purified by column chromatography on hydroscopic (6wt%) basic aluminium oxide (toluene) to give **1c** as a purple powder (93 mg, 86%).

1c: $C_{144}H_{138}N_{10}O_6Zn$; MW 2170.1; purple solid; mp 98 ^{o}C; ^{1}H NMR (400 MHz, $CDCl_3$): δ 8.96 (m, 1H), 8.82–8.72 (m, 9H), 8.65–8.64 (s like, 2H, J = 4.9 Hz), 8.51–8.47 (m, 4H), 8.33 (d, 2H, J = 7.8 Hz), 8.27 (d, 2H, J = 8.3 Hz), 8.17 (d, 2H, J = 7.8 Hz), 8.09–8.05 (m, 3H), 7.93 (d, 2H, J = 8.0 Hz), 7.88–7.85 (m, 1H), 7.80–7.74 (m, 6H), 7.60 (dd, 2H, J = 8.1, 2.2 Hz), 7.58–7.51 (m, 1H), 7.47–7.42 (m, 5H), 7.37–7.34 (m, 1H), 7.28 (s, 4H), 7.09 (d, 4H, J = 8.6 Hz), 6.49 (d, 4H, J = 9.0 Hz), 6.19 (d, 4H, J = 9.0 Hz), 4.05 (t, 4H, J = 6.5 Hz), 3.78 (t, 4H, J = 6.6 Hz), 3.17 (t, 4H, J = 6.6 Hz), 2.66–2.63 (m, 10H), 1.84–1.75 (m, 16H), 1.63–1.09 (m 40H); ^{13}C NMR (100 MHz, $CDCl_3$): δ 158.74, 156.28, 154.97, 153.84, 153.01, 152.19, 151.76, 149.91, 149.85, 149.74, 149.67, 149.31, 149.10, 144.87, 143.71, 142.63, 139.44, 139.19, 139.10, 138.14, 137.45, 136.99, 136.83, 136.75, 134.61, 134.23, 133.59, 132.07, 131.96, 131.77, 131.67, 130.94, 130.84, 130.79, 129.80, 129.21, 129.03, 128.38, 128.26, 128.01, 127.66, 123.34, 122.82, 121.57, 121.40, 120.78, 120.68, 120.46, 120.34, 119.52,

119.31, 119.11, 115.60, 115.03, 113.95, 95.80, 93.73, 90.63, 87.32, 68.62, 68.40, 68.02, 32.80, 30.97, 29.22, 29.18, 29.13, 29.03, 28.79, 25.94, 25.90, 25.66, 21.69, 21.47; MS (FAB+): *m/z* 2170 [MH^+]; IR (KBr, cm^{-1}): 2928(s), 2854(s), 1734(w), 1716(w), 1699(w), 1607(m), 1558(w), 1541(w), 1508(s), 1489(w), 1474(m), 1458(s), 1435(m), 1396(w), 1364(m), 1338(w), 1230(s), 1204(m), 1175(m), 1144(w), 995(s), 797(s), 748(m), 710(m), 590(w), 538(w), 517(w); HRMS (FAB+): *m/z* Calcd for $C_{144}H_{38}N_{10}O_6{}^{64}Zn$: 2167.0092. Found: 2167.0085.

LP3

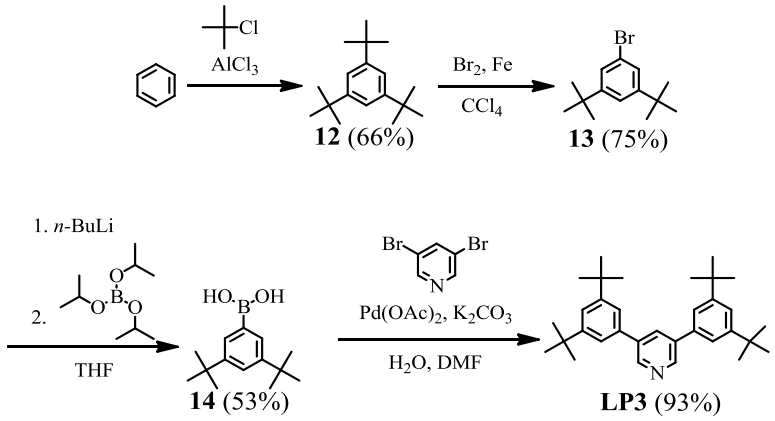

1,3,5-Tri-*tert*-butylbenzene (12)[5].

To mixture of benzene (17.7 mL, 15.6 g, 200 mmol, 1.0 equiv.) and 2-chloro-2-methylpropane (224 mL, 190 g, 10.5 equiv.), aluminium chloride (13.2 g, 100 mmol, 0.5 equiv) was added little by little for 30 min at –40 °C. After stirring at –15 °C for 2 h, the reaction mixture was poured into ice–water. The mixture was extracted with diethyl ether. The solution was dried over sodium sulfate and filtered. The solvent was removed under reduced pressure, and the residue was washed with hot methanol to give **12** as a white solid (32.7 g, 66%)

12: $C_{18}H_{30}$; MW 246.4; White solid; ^{1}H NMR (300 MHz, DMSO-d_6): δ 7.18 (s, 3H), 1.27 (s, 27H).

1-Bromo-3,5-di-*tert*-butylbenzene (13)[5].

To a suspension of **12** (24.6 g, 100 mmol, 1.0 equiv.) and Fe powder (6.70 g, 120 mmol, 1.2 equiv.) in carbon tetrachloride (50 mL), bromine (10.8 mL, 33.6 g, 210 mmol, 2.1 equiv.) in carbon tetrachloride (20 mL) was added dropwise at 0 °C. The solution was allowed to warm up to room temperature and stirred overnight. The mixture was filtered and the filtrate was washed with aqueous sodium disulfite solution until the organic layer became transparent. The solution was dried over sodium sulfate and filtered. The solvent was removed under reduced pressure and the residue was washed with hot ethanol. The crude product was purified by column chromatography on silica gel (hexane) to give **13** as a white solid (20.3 g, 75%).

13: $C_{14}H_{21}Br$; MW 269.2; White solid; ^{1}H NMR (400 MHz, $CDCl_3$): δ 7.32 (s, 3H), 1.30 (s, 18H).

3,5-di-*tert*-butylphenylboronic acid (14)[6].

To a solution of **13** (13.5 g, 50 mmol, 1.0 equiv.) in dry THF (90 mL), *n*-butyllithium (1.6 M, *n*-hexane solution, 35.7 mL, 60 mmol, 1.2 equiv.) was added dropwise at −78 °C under a nitrogen atmosphere. The solution was stirred for 1.5 h and triisopropyl borate (34.6 mL, 28.2 g, 150 mmol, 3.0 equiv.) was added at −70 °C. The solution was allowed to warm up to room temperature and stirred overnight. After the addition of a 5% HCl solution (50 mL), the solution was stirred for 4 h. The mixture was extracted with diethyl ether. The solution was dried over sodium sulfate and filtered. The solvent was removed under reduced pressure to give crud product (11.4 g). The crude product was dissolved in diethyl ether and the solution was extracted with sodium hydroxide solution. The extract was acidified by hydrochloric acid and filtered to give **14** as a white solid (6.2 g, 53%).

14: $C_{14}H_{23}BO_2$; MW 234.1; White solid; ^{1}H NMR (300 MHz, DMSO-d_6): δ 7.92 (br, 2H), 7.64 (d, J = 1.8 Hz, 2H), 7.40 (t, J = 1.8 Hz, 1H), 1.27 (s, 18H).

LP3[4]

A solution of 3,5-dibromopyridine (711 mg, 3.0 mmol, 1.0 equiv.), **14** (2.46 g, 10.5 mmol, 3.5 equiv.), potassium carbonate (2.49 g, 18 mmol, 6.0 equiv.) and palladium(II) acetate (33.7 mg, 150 μmol, 0.05 equiv.) in a mixed solvent (DMF/water = 7/6, v/v, 60 mL) was heated at 110 °C under an argon atmosphere overnight. After cooling to room temperature, the reaction mixture was poured into water (200 mL). The mixture was filtered and the solid was washed with water. The solid was dissolved with dichloromethane and an insoluble solid was filtered off. The filtrate was dried over sodium sulfate and filtered. The solvent was removed under reduced pressure and the residue was purified by chromatography on silica gel (dichloromethane) to give **LP3** as a white solid (1.27 g, 93%).

LP3: $C_{33}H_{45}N$; MW 455.7; white solid; mp 200 °C; ^{1}H NMR (300 MHz, $CDCl_3$): δ 8.79 (d, 2H, J = 2.0 Hz), 8.02 (t, 1H, J = 2.1 Hz), 7.52 (t, 2H, J = 1.6 Hz), 7.45 (d, 4H, J = 1.6 Hz), 1.39 (s, 18H); ^{13}C NMR (100 MHz, $CDCl_3$): δ 151.69, 147.13, 137.82, 137.49, 133.66, 122.35, 121.86, 35.05, 31.50; MS (FAB+): *m/z* 456 [MH^+]; IR (KBr, cm^{-1}): 3032(m), 2964(s), 2903(s), 2866(s), 1763(w), 1595(s), 1533(w), 1475(s), 1462(s), 1400(s), 1364(s), 1298(m), 1248(s), 1229(m), 1204(m), 1165(m), 1140(w), 1024(m), 926(m), 891(m), 872(s), 845(m), 818(m), 768(m), 714(s), 671(s), 629(w), 530(w); Anal. Calcd for $C_{33}H_{45}N$: C, 86.97; H, 9.95; N, 3.07. Found: C, 86.84; H, 10.08; N, 3.10.

3-8-2. UV–vis titration

General procedure

UV-vis spectra were measured by a Shimadzu UV-2550 spectrophotometer using 1 cm quartz cuvettes and EYELA NCB-1200 Low Temperature Bath at 20 ^{o}C. A spectrochemical analysis grade of solvent was purchased from Wako pure chemical industries, Ltd. The curve fittings were calculated by using KaleidaGraph 4.1J.

Method

A solution of **1** in toluene-acetonitrile (1/1 (v/v)) was prepared by careful weighting using an analytical balance. Solution of **1** (3 mL) was added in a quartz cell by using a whole pipette. The solution of **1**·**Fe** was prepared by adding the solution of $Fe(BF_4)_2$ (1.0 equiv.) to the solution of **1** (3.0 mL). A guest solution was added to the solution by using a micropipette. A solution of $Fe(BF_4)_2$ and axial ligands shown in Figure 3-11 were used as the guest solution for the determination of the complex formation constant and the axial binding constants, respectively. After each addition of the guest solution, the quartz cell was placed in the cell compartment of a spectrometer and allowed to come to thermal equilibrium. UV–vis spectra were measured with a spectrophotometer equipped with a temperature controller to keep the temperature at 20 °C. This procedure was repeated until no change was recorded within the spectra. The association constants were determined by the curve fitting using expression 2n or 2q (see section 2-7-3) as a regression expression for the change of the apparent molar extinction coefficient ε(app) at appropriate wavelength. The conditions of each titration were summarized in Table 3-3 and 3-4.

Table 3-3. Conditions of each titration in section 3-4 and 3-5.

Host[a]	Guest	[Guest]	wavelength	Figure No.
1b	$Fe(BF_4)_2$•$6H_2O$	1.2×10^{-3} M	500 nm	3-3
1c	$Fe(BF_4)_2$•$6H_2O$	6×10^{-4} M	500 nm	3-4
1b[b]	**LP1**	6×10^{-2} M	608 nm	3-7
1c[b]	**LP1**	6×10^{-2} M	608 nm	3-8
1b•Fe[c]	**LP1**	6×10^{-2} M	610 nm	3-9
1c•Fe[b,d]	**LP1**	6×10^{-2} M	611 nm	3-10

(a): $[\mathbf{1}]_0 = 2 \times 10^{-5}$ M, (b): $[\mathbf{1}]_0 = 5 \times 10^{-5}$ M, (c): $Fe(BF_4)_2$•$6H_2O$ (1.5×10^{-3} M, 40 μmol, 1 equiv.) was added. (d): $Fe(BF_4)_2$•$6H_2O$ (1.5×10^{-3} M, 100 μmol, 1 equiv.) was added.

Table 3-4. Conditions of each titration of axial ligands in section 3-6.

Host[a]	Guest	[Guest]	wavelength	Figure No.
1a	**LIm1**	2.4×10^{-2} M	611 nm	3-12
1a•Fe[c]	**LIm1**	2.4×10^{-2} M	614 nm	3-13
1b	**LIm1**	2.4×10^{-2} M	611 nm	3-14
1b•Fe[c]	**LIm1**	2.4×10^{-2} M	614 nm	3-15
1c	**LIm1**	2.4×10^{-2} M	611 nm	3-16
1c•Fe[c]	**LIm1**	2.4×10^{-2} M	614 nm	3-17
1a	**LIm2**	3×10^{-2} M	611 nm	3-18
1a•Fe[d]	**LIm2**	3×10^{-2} M	614 nm	3-19
1b	**LIm2**	3×10^{-2} M	611 nm	3-20
1b•Fe[d]	**LIm2**	3×10^{-2} M	614 nm	3-21
1c	**LIm2**	1.2×10^{-2} M	611 nm	3-22
1c•Fe[c]	**LIm2**	1.2×10^{-2} M	614 nm	3-23
1a	**LIm3**	3×10^{-2} M	611 nm	3-24
1a•Fe[d]	**LIm3**	3×10^{-2} M	614 nm	3-25
1b	**LIm3**	3×10^{-2} M	611 nm	3-26
1b•Fe[d]	**LIm3**	3×10^{-2} M	613 nm	3-27
1c	**LIm3**	1.2×10^{-2} M	611 nm	3-28
1c•Fe[c]	**LIm3**	1.2×10^{-2} M	614 nm	3-29
1a[b]	**LP2**	3×10^{-2} M	608 nm	3-30
1a•Fe[e]	**LP2**	3×10^{-2} M	610 nm	3-31
1b[b]	**LP2**	3×10^{-2} M	608 nm	3-32
1b•Fe[e]	**LP2**	3×10^{-2} M	611 nm	3-33
1c[b]	**LP2**	3×10^{-2} M	608 nm	3-34
1c•Fe[b, f]	**LP2**	3×10^{-2} M	612 nm	3-35
1a[b]	**LP3**	3×10^{-2} M	608 nm	3-36
1a•Fe[e]	**LP3**	3×10^{-2} M	610 nm	3-37
1b[b]	**LP3**	3×10^{-2} M	608 nm	3-38
1b•Fe[e]	**LP3**	3×10^{-2} M	611 nm	3-39
1c[b]	**LP3**	3×10^{-2} M	608 nm	3-40
1c•Fe[b, f]	**LP3**	3×10^{-2} M	612 nm	3-41

(a): $[\mathbf{1}]_0 = 2 \times 10^{-5}$ M, (b): $[\mathbf{1}]_0 = 5 \times 10^{-5}$ M, (c), (d), (e): $Fe(BF_4)_2 \cdot 6H_2O$ (1 equiv.) was added. (c): 6×10^{-4} M, 100 μmol, (d): 1.2×10^{-3} M, 50 μmol, (e): 1.5×10^{-3} M, 40 μmol, (f): 1.5×10^{-3} M, 100 μmol.

3-9. References

(1) *Spartan'08*, Wavefunction, Inc., Irvine, CA.

(2) (a) Nabeshima, T.; Yoshihira, Y.; Saiki, T.; Akine, S.; Horn, E. *J. Am. Chem. Soc.* **2003**, *125*, 28–29. (b) Nabeshima, T.; Tanaka, Y.; Saiki, T.; Akine, S.; Ikeda, C.; Sato, S. *Tetrahedron Lett.* **2006**, *47*, 3541–3544.

(3) Kato, M.; Hashimoto, E.; Kozaki, M.; Suzuki S.; Okada, K. *Tetrahedron Lett.* **2012**, *53*, 309–312.

(4) Rocha, M. A. A.; Gomes, L. R.; Low, J. N.; Santos, L. M. N. B. F. *J. Phys. Chem. A* **2009**, *113,* 11015–11027

(5) Frampton, M. J.; Akdas, H.; Cowley, A. R.; Rogers, J. E.; Slagle, J. E.; Fleitz, P. A.; Drobizhev, M.; Rebane, A.; Anderson, H. L. *Org. Lett.*, **2005**, *24,* 5365–5368.

(6) Nomura, N.; Ishii, R.; Yamamoto, Y.; Kondo, T. *Chem. Eur. J.* **2007**, *13*, 4433–4451.

(7) Fletcher, N. C.; Nieuwenhuyzen, M.; Rainey *J. Chem. Soc., Dalton Trans.* **2001**, 2641–2648.

~Chapter 4~
Development of an allosteric receptor with sterically bulky shielding units

4-1. Introduction

In **chapter 3**, allosteric receptors with various alkyl chain lengths and bulky ligands with different heterocyclic units were prepared. The degree of allosteric inhibition was significantly affected by the alkyl chain length, shape of ligands, and heterocyclic unit. We successfully increased the degree of allosteric inhibition by using a receptor with short alkyl chains and a sterically bulky ligand. In this chapter, sterically bulky shielding units were introduced to further increase the allosteric inhibition. A novel allosteric receptor **1e** with 9,10-diphenylanthracene skeleton as the bulky shielding units in the middle of the alkyl chains was designed and synthesized (Figure 4-1). These shielding units were forced to lie above and below the Zn porphyrin unit in the Fe complex **1e•Fe**. Therefore, the accessibility of a ligand to the Zn porphyrin was significantly limited, and the ligand-binding ability of the Zn porphyrin unit decreased.

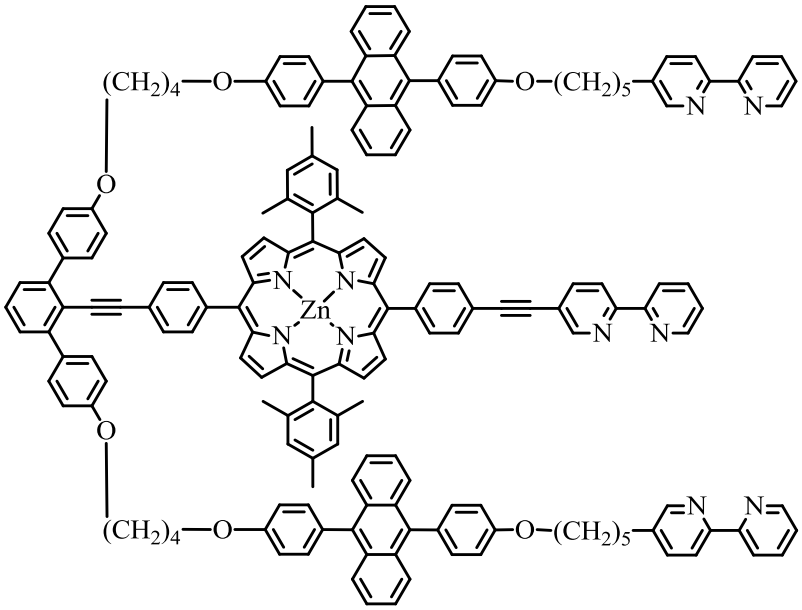

1e

Figure 4-1. Chemical structure of receptor **1e**.

4-2. Molecular mechanics force field (MMFF) calculations[1]

Before the synthesis, MMFF calculations of **1e** and its derivatives with different alkyl chain lengths were performed to estimate the suitable alkyl chain length to form a stable Fe complex and shield the Zn porphyrin unit efficiently. The steric energies of both Fe complex **1e•Fe** (E_{Fe}) and model complex

1e′•Fe (E_{cut}) were calculated as described in Section 3-2. The steric energies of Fe complex **1e•Fe** and model complex **1e′•Fe** were E_{Fe} = 915.89 kJ mol^{-1} and E_{cut} = 856.75 kJ mol^{-1}, respectively. The strain energy (subtraction of E_{cut} from E_{Fe}) was 59.14 kJ mol^{-1}, almost the same as that of **1a** (62.13 kJ mol^{-1}). This calculation result indicates that the alkyl chins in **1e** enabled both the formation of a stable Fe complex **1e•Fe** and the efficient shielding of the Zn porphyrin unit.

4-3. Synthesis of receptor 1e

Allosteric receptor **1e** was synthesized following a method similar to that for **1a** (see sections 2-2 and 2-3). Alkyl chain **7e** was synthesized by the successive formation of two types of ether linkages at the hydroxyl groups in 9,10-bis(4-hydroxyphenyl)anthracene (**15)** (Scheme 4-1). The Suzuki–Miyaura cross-coupling of side chain **7e** with main chain **11** was carried out by using [Pd(PPh$_3$)$_4$] as the catalyst that is sufficiently effective in the syntheses of **1a**, **1b**, and **1c**. Unexpectedly, the reaction was not successful under these conditions. Receptor **1e** was obtained as a purple solid in 57% yield when second-generation Buchwald precatalyst XPhos-Pd-G2 was used for the coupling reaction (Scheme 4-2).[2]

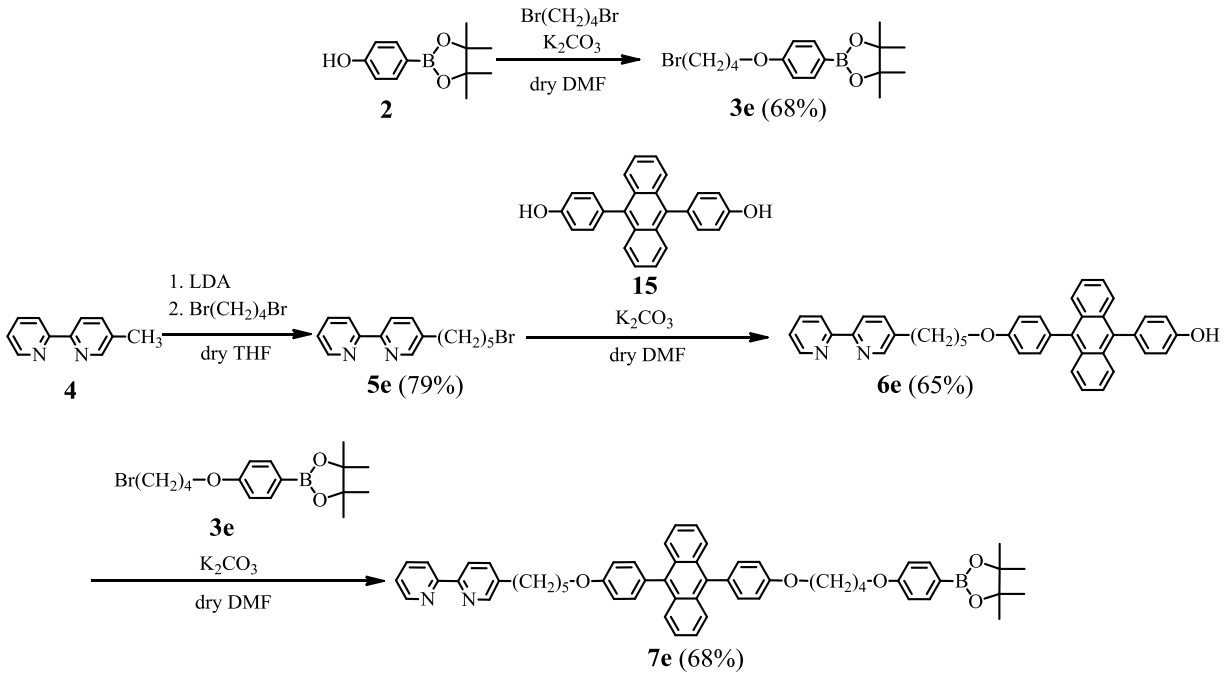

Scheme 4-1. Synthesis of side chain **7e**.

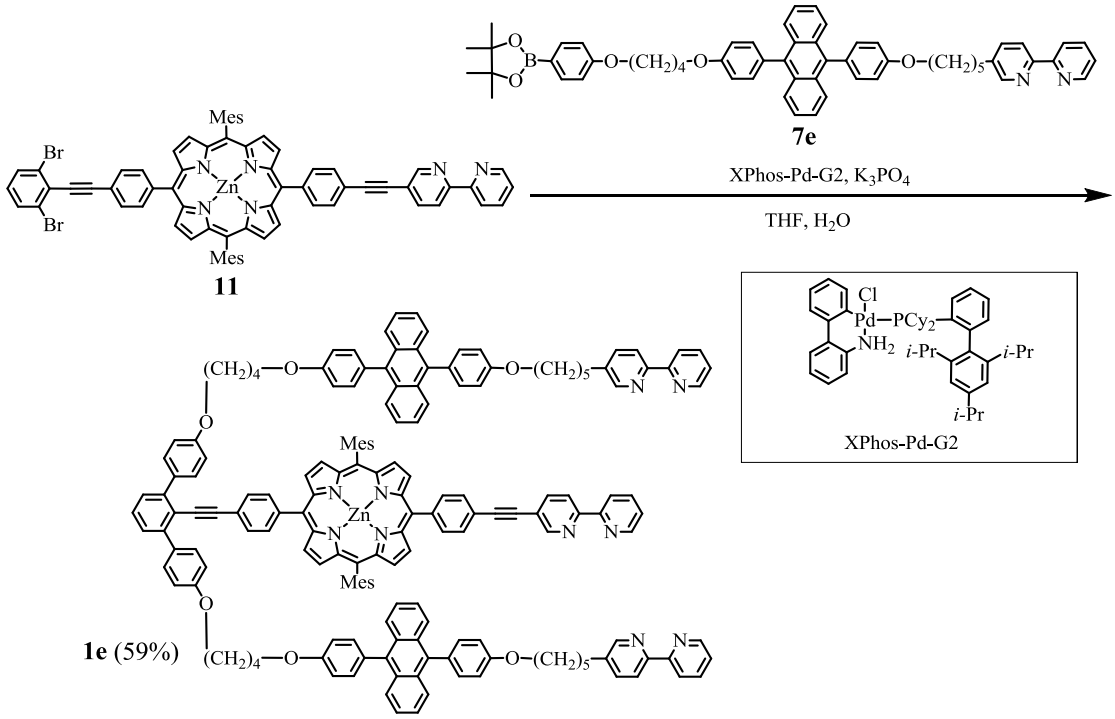

Scheme 4-2. Synthesis of receptor **1e**

4-4. Iron complexation

It was confirmed that allosteric receptor **1e** formed a stable 1:1 complex with Fe(II) ions as confirmed by UV–visible titration in a mixture of toluene/acetonitrile (1:1 v/v) at 20 °C. As shown in Figure 4-2a, when Fe(II) ions were added to a solution of **1e** (2×10^{-5} M), the characteristic MLCT absorption band of a Fe(II)(bpy)$_3$-type complex appeared at ~500 nm.[3] The absorption due to the MLCT band at 500 nm linearly increased in proportion to the amount of Fe(II) ions until the concentration of Fe(II) ions became the same as that of **1e** (Figure 4-2b). These results indicate the almost quantitative formation ($K_{1\bullet Fe} > 10^6$ M^{-1}) of Fe(II)(bpy)$_3$-type complex **1e•Fe**.

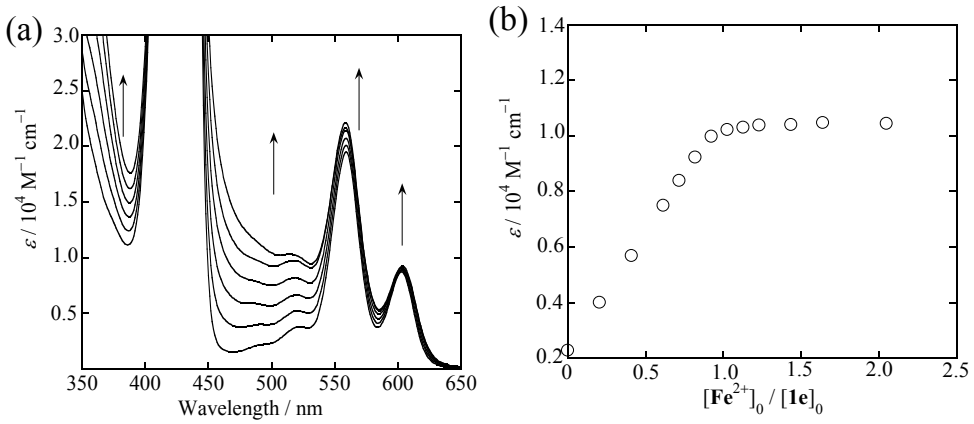

Figure 4-2. (a) UV–vis spectral change resulting from the titration of **1e** (2×10^{-5} M) with $Fe(BF_4)_2 \cdot 6H_2O$ (6×10^{-4} M) in a toluene/acetonitrile (1/1 (v/v)) solution at 20 °C. (b) The change in the molar extinction coefficient at 500 nm. $[Fe^{2+}]_0$: The concentration of Fe^{2+} when complexation is ignored. $[\mathbf{1e}]_0$: The initial concentration of **1e**.

4-5. Axial binding and allosteric inhibition

The binding constants of active receptor **1** ($K_{1 \cdot L}$) and inactive receptor **1•Fe** ($K_{(1 \cdot Fe) \cdot L}$) with axial ligands (see Figure 3-11) were determined by UV–visible spectroscopic titration in a mixture of toluene/acetonitrile (1:1 v/v) at 20 °C. Both the spectral change and the plot of the molar extinction coefficient vs. the relative concentration of the ligands are shown in Figures 4-3 to 4-12. The binding constants and degrees of allosteric effect ($K_{1 \cdot L} / K_{(1 \cdot Fe) \cdot L}$) are summarized in Table 4-1. Insignificant changes in the molar absorptivity of the MLCT band were observed during the titration of **1e•Fe**, indicating that the dissociation of **1e•Fe** did not occur under the experimental conditions.

Table 4-1. The binding constants of allosteric receptor **1e** and degree of allosteric effect.

Ligand	$K_{1 \cdot L}$ / 10^{-4} M^{-1}	$K_{(1 \cdot Fe) \cdot L}$ / 10^{-4} M^{-1}	$K_{1 \cdot L} / K_{(1 \cdot Fe) \cdot L}$
LIm2	5.02 ± 0.10	3.79 ± 0.13	1.32 ± 0.07
LIm3	7.11 ± 0.27	5.93 ± 0.36	1.20 ± 0.19
LP1	0.870 ± 0.011	0.500 ± 0.006	1.74 ± 0.04
LP2	0.605 ± 0.009	0.430 ± 0.016	1.41 ± 0.07
LP3	3.29 ± 0.10	0.348 ± 0.018	9.45 ± 0.78

in toluene/acetonitrile (1:1 v/v) at 20 ^{o}C

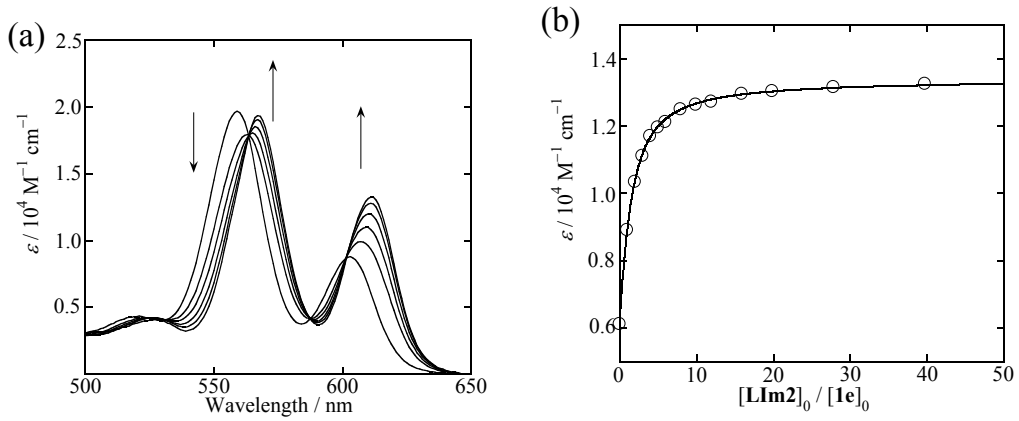

Figure 4-3. (a) UV−vis spectral change resulting from the titration of **1e** (2×10^{-5} M) with **LIm2** (1.2×10^{-2} M) in a toluene/acetonitrile (1/1 (v/v)) solution at 20 °C. (b) The change in the molar extinction coefficient at 611 nm. The solid line is a regression curve obtained by curve fitting. $[\mathbf{LIm2}]_0$: The concentration of **LIm2** when axial binding is ignored. $[\mathbf{1e}]_0$: The initial concentration of **1e**.

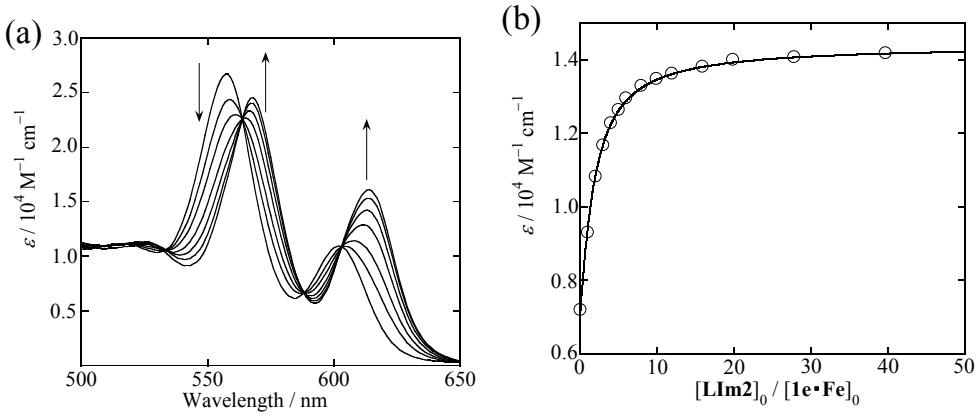

Figure 4-4. (a) UV−vis spectral change resulting from the titration of **1e•Fe** (2×10^{-5} M) with **LIm2** (1.2×10^{-2} M) in a toluene/acetonitrile (1/1 (v/v)) solution at 20 °C. (b) The change in the molar extinction coefficient at 613 nm. The solid line is a regression curve obtained by curve fitting. $[\mathbf{LIm2}]_0$: The concentration of **LIm2** when axial binding is ignored. $[\mathbf{1e•Fe}]_0$: The initial concentration of **1e•Fe**.

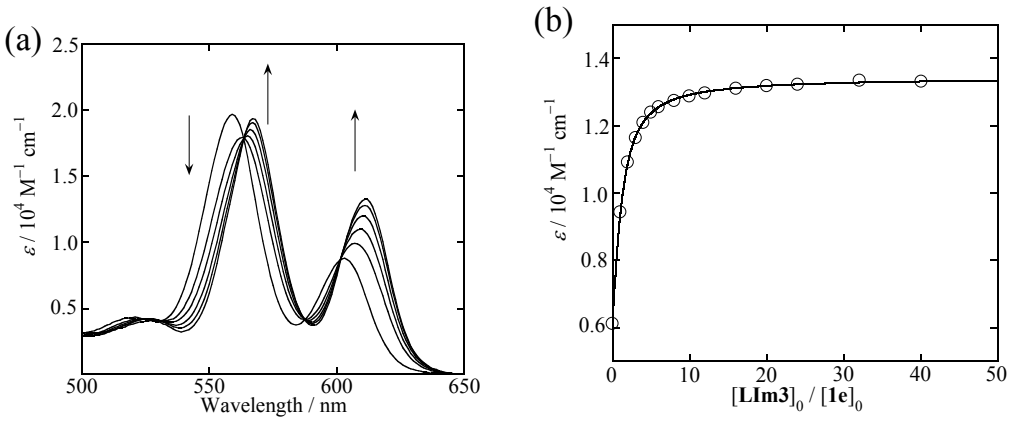

Figure 4-5. (a) UV−vis spectral change resulting from the titration of **1e** (2×10^{-5} M) with **LIm3** (1.2×10^{-2} M) in a toluene/acetonitrile (1/1 (v/v)) solution at 20 °C. (b) The change in the molar extinction coefficient at 611 nm. The solid line is a regression curve obtained by curve fitting. $[\mathbf{LIm3}]_0$: The concentration of **LIm3** when axial binding is ignored. $[\mathbf{1e}]_0$: The initial concentration of **1e**.

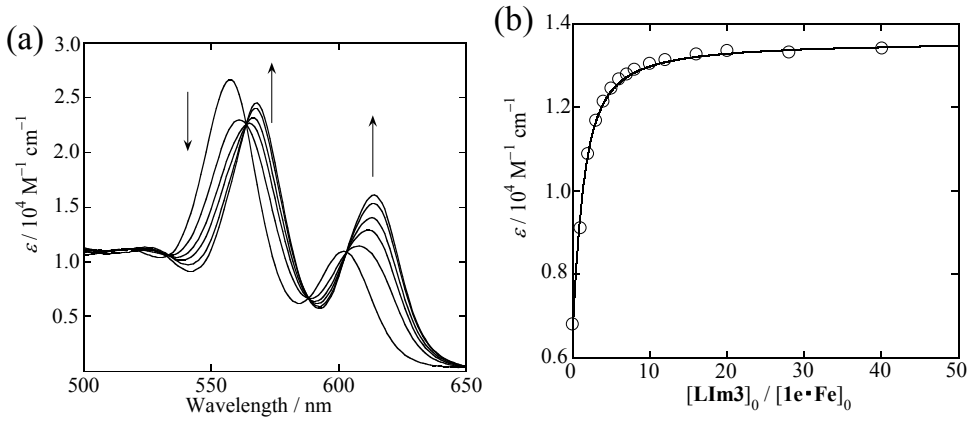

Figure 4-6. (a) UV−vis spectral change resulting from the titration of **1e•Fe** (2×10^{-5} M) with **LIm3** (1.2×10^{-2} M) in a toluene/acetonitrile (1/1 (v/v)) solution at 20 °C. (b) The change in the molar extinction coefficient at 613 nm. The solid line is a regression curve obtained by curve fitting. $[\mathbf{LIm3}]_0$: The concentration of **LIm3** when axial binding is ignored. $[\mathbf{1e•Fe}]_0$: The initial concentration of **1e•Fe**.

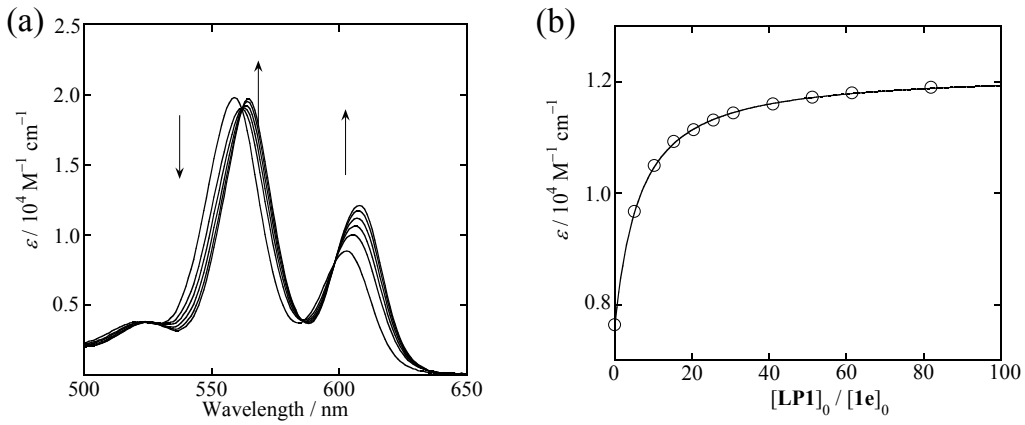

Figure 4-7. (a) UV–vis spectral change resulting from the titration of **1e** (2×10^{-5} M) with **LP1** (3×10^{-2} M) in a toluene/acetonitrile (1/1 (v/v)) solution at 20 °C. (b) The change in the molar extinction coefficient at 608 nm. The solid line is a regression curve obtained by curve fitting. $[\mathbf{LP1}]_0$: The concentration of **LP1** when axial binding is ignored. $[\mathbf{1e}]_0$: The initial concentration of **1e**.

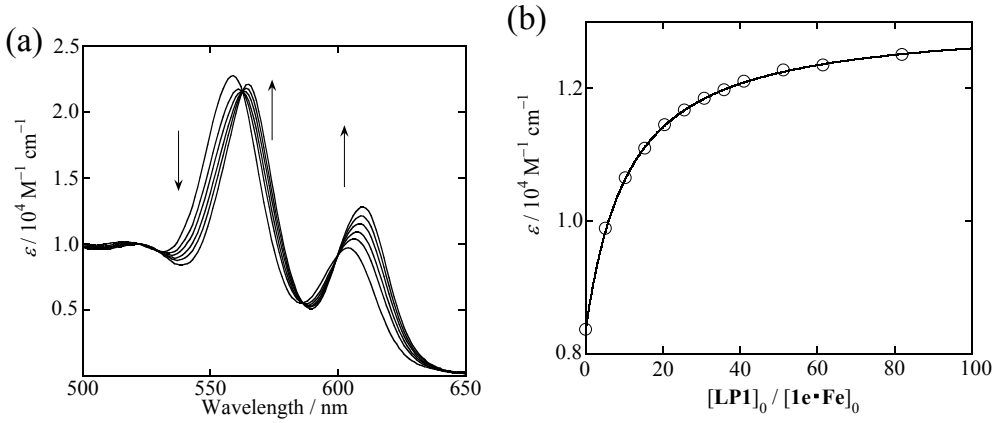

Figure 4-8. (a) UV–vis spectral change resulting from the titration of **1e•Fe** (2×10^{-5} M) with **LP1** (3×10^{-2} M) in a toluene/acetonitrile (1/1 (v/v)) solution at 20 °C. (b) The change in the molar extinction coefficient at 610 nm. The solid line is a regression curve obtained by curve fitting. $[\mathbf{LP1}]_0$: The concentration of **LP1** when axial binding is ignored. $[\mathbf{1e{\bullet}Fe}]_0$: The initial concentration of **1e•Fe**.

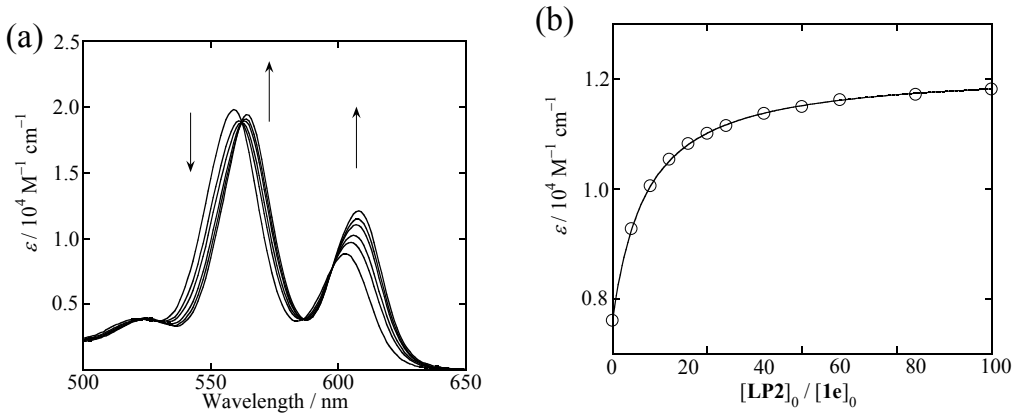

Figure 4-9. (a) UV–vis spectral change resulting from the titration of **1e** (2×10^{-5} M) with **LP2** (3×10^{-2} M) in a toluene/acetonitrile (1/1 (v/v)) solution at 20 °C. (b) The change in the molar extinction coefficient at 608 nm. The solid line is a regression curve obtained by curve fitting. $[\mathbf{LP2}]_0$: The concentration of **LP2** when axial binding is ignored. $[\mathbf{1e}]_0$: The initial concentration of **1e**.

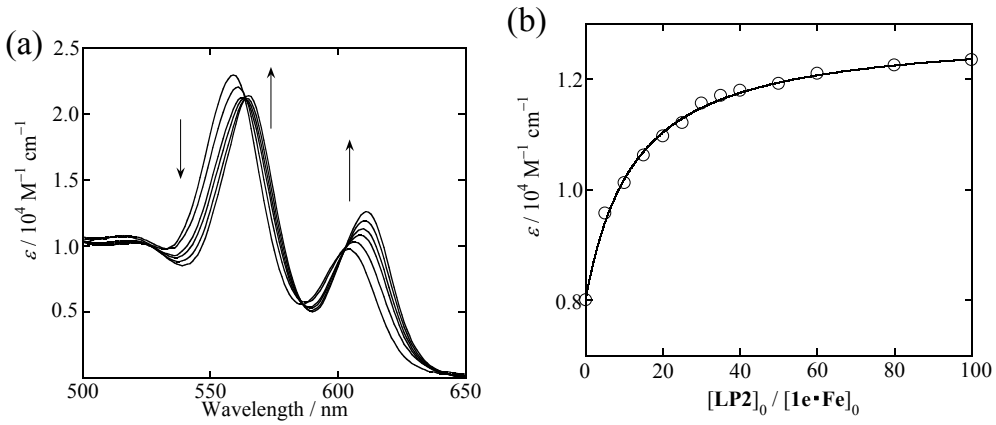

Figure 4-10. (a) UV–vis spectral change resulting from the titration of **1e•Fe** (2×10^{-5} M) with **LP2** (3×10^{-2} M) in a toluene/acetonitrile (1/1 (v/v)) solution at 20 °C. (b) The change in the molar extinction coefficient at 611 nm. The solid line is a regression curve obtained by curve fitting. $[\mathbf{LP2}]_0$: The concentration of **LP2** when axial binding is ignored. $[\mathbf{1e{\bullet}Fe}]_0$: The initial concentration of **1e•Fe**.

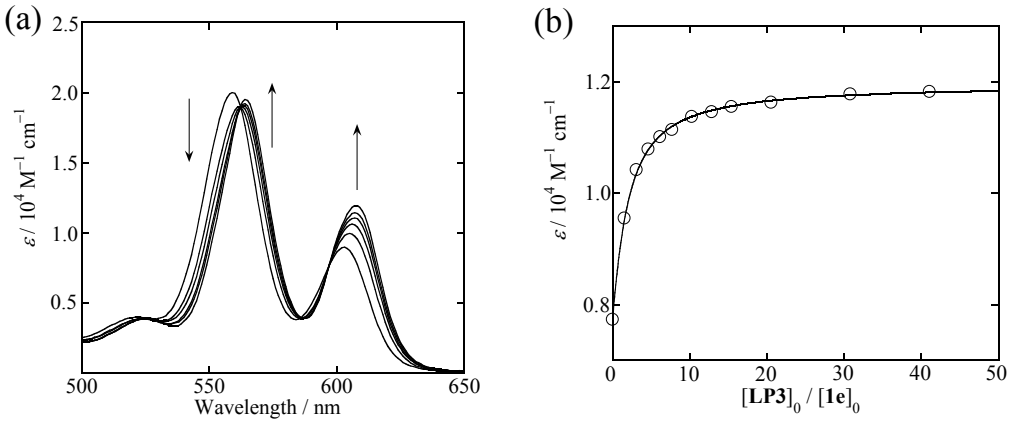

Figure 4-11. (a) UV−vis spectral change resulting from the titration of **1e** (2×10^{-5} M) with **LP3** (1.5×10^{-2} M) in a toluene/acetonitrile (1/1 (v/v)) solution at 20 °C. (b) The change in the molar extinction coefficient at 608 nm. The solid line is a regression curve obtained by curve fitting. $[\mathbf{LP3}]_0$: The concentration of **LP3** when axial binding is ignored. $[\mathbf{1e}]_0$: The initial concentration of **1e**.

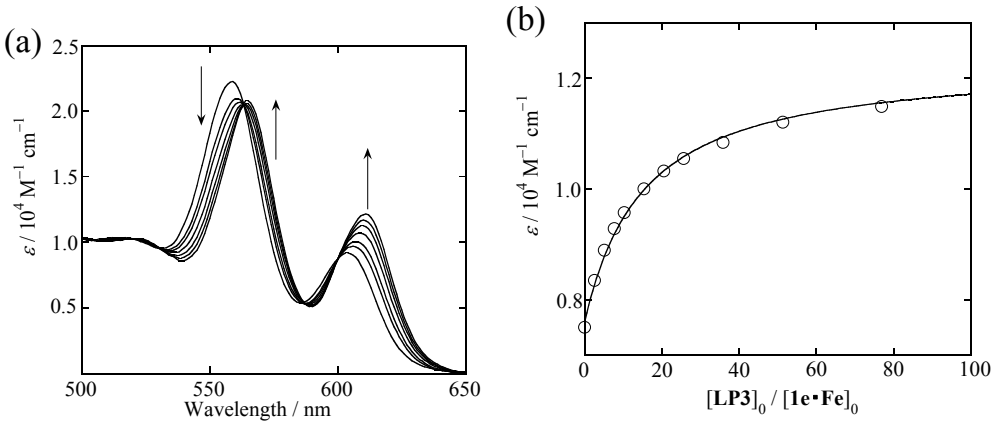

Figure 4-12. (a) UV−vis spectral change resulting from the titration of **1e•Fe** (2×10^{-5} M) with **LP3** (1.5×10^{-2} M) in a toluene/acetonitrile (1/1 (v/v)) solution at 20 °C. (b) The change in the molar extinction coefficient at 611 nm. The solid line is a regression curve obtained by curve fitting. $[\mathbf{LP3}]_0$: The concentration of **LP3** when axial binding is ignored. $[\mathbf{1e{\bullet}Fe}]_0$: The initial concentration of **1e•Fe**.

The degree of allosteric inhibition dramatically increased to 9.5 ± 0.8 when allosteric receptor **1e** and ligand **LP3** were used. The ligand containing an imidazole unit showed a degree of allosteric inhibition less than 2. These results indicate that the diphenylanthracene units in **1e** are not large enough to cause significant steric congestion between the shielding units and the dendritic unit in **LIm2** and **LIm3**. In other words, the dendritic units in these ligands are highly flexible. Although the addition of Fe ions decreases the binding constant of the Zn porphyrin unit in **1e** with pyridyl ligands **LP1** and **LP2**, the degrees of allosteric inhibition are less than 2. In contrast, the binding constant between **1e** and **LP3** dramatically decreased by adding Fe ions; the degree of allosteric inhibition was 9.5.

4-6. Thermodynamic analysis

Using the best combination of receptor **1e** and **LP3**, the thermodynamic parameters of axial ligand-binding reaction before and after the addition of Fe ions were determined. The binding constants of active receptor **1e** and inactive receptor **1e•Fe** with axial ligand **LP3** were determined by UV–visible spectroscopic titration in a mixture of toluene/acetonitrile (1:1 v/v) at 5, 10, 20, 30, and 40 °C. Both the observed spectral change and the plot of the molar extinction coefficient vs. the relative concentration of the ligands are shown in Figures 4-13 to 4-20. The binding constants and degrees of allosteric inhibition are summarized in Table 4-2. A plot of the natural logarithm of the equilibrium constants vs. the reciprocal temperature (Van't Hoff plots) was reasonably fitted by a straight line, as shown in Figure 4-21.

Table 4-2. The binding constants of allosteric receptor **1e** with **LP3** and degree of allosteric effect.

Temperature	$K_{1\bullet L}$ / 10^{-4} M^{-1}	$K_{(1\bullet Fe)\bullet L}$ / 10^{-4} M^{-1}	$K_{1\bullet L}$ / $K_{(1\bullet Fe)\bullet L}$
5 ^{o}C	8.41 ± 0.20	0.711 ± 0.024	11.8 ± 0.7
10 ^{o}C	6.33 ± 0.15	0.609 ± 0.033	10.4 ± 0.8
20 ^{o}C	3.29 ± 0.10	0.348 ± 0.018	9.45 ± 0.78
30 ^{o}C	2.25 ± 0.04	0.257 ± 0.010	8.75 ± 0.50
40 ^{o}C	1.58 ± 0.02	0.187 ± 0.010	8.45 ± 0.56

in toluene/acetonitrile (1:1 v/v)

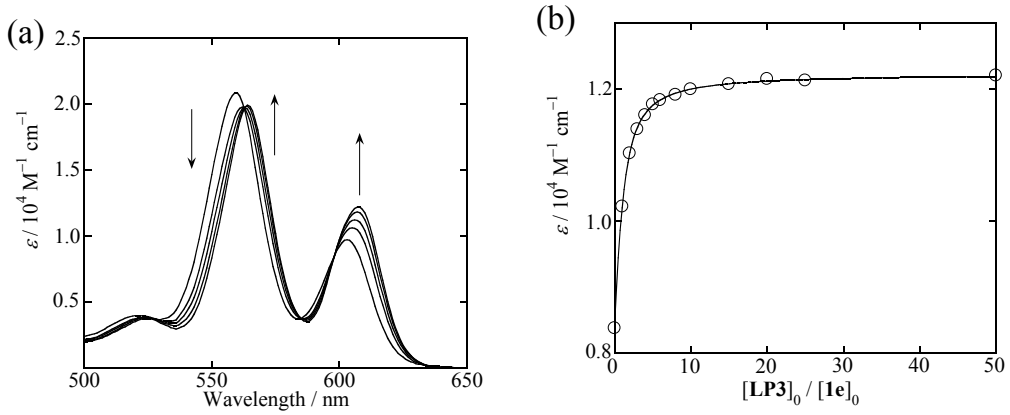

Figure 4-13. (a) UV−vis spectral change resulting from the titration of **1e** (2×10^{-5} M) with **LP3** (1.5×10^{-2} M) in a toluene/acetonitrile (1/1 (v/v)) solution at 5 °C. (b) The change in the molar extinction coefficient at 608 nm. The solid line is a regression curve obtained by curve fitting. $[\mathbf{LP3}]_0$: The concentration of **LP3** when axial binding is ignored. $[\mathbf{1e}]_0$: The initial concentration of **1e**.

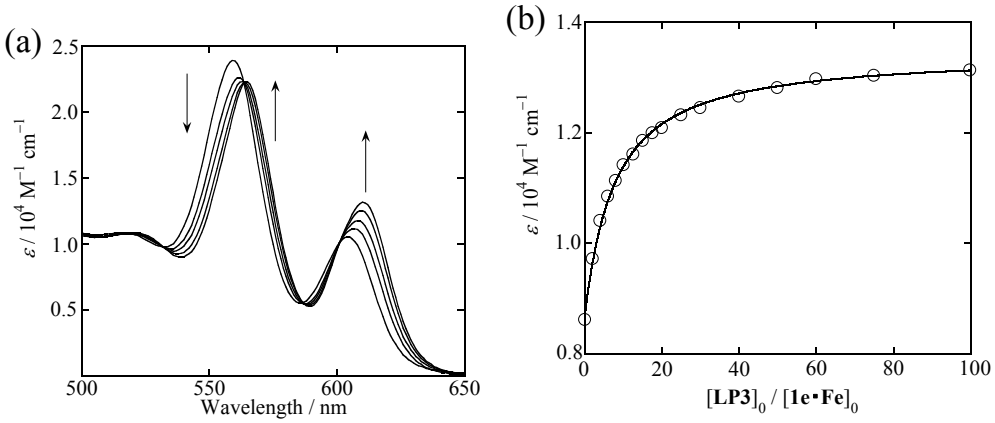

Figure 4-14. (a) UV−vis spectral change resulting from the titration of **1e•Fe** (2×10^{-5} M) with **LP3** (1.5×10^{-2} M) in a toluene/acetonitrile (1/1 (v/v)) solution at 5 °C. (b) The change in the molar extinction coefficient at 611 nm. The solid line is a regression curve obtained by curve fitting. $[\mathbf{LP3}]_0$: The concentration of **LP3** when axial binding is ignored. $[\mathbf{1e{\bullet}Fe}]_0$: The initial concentration of **1e•Fe**.

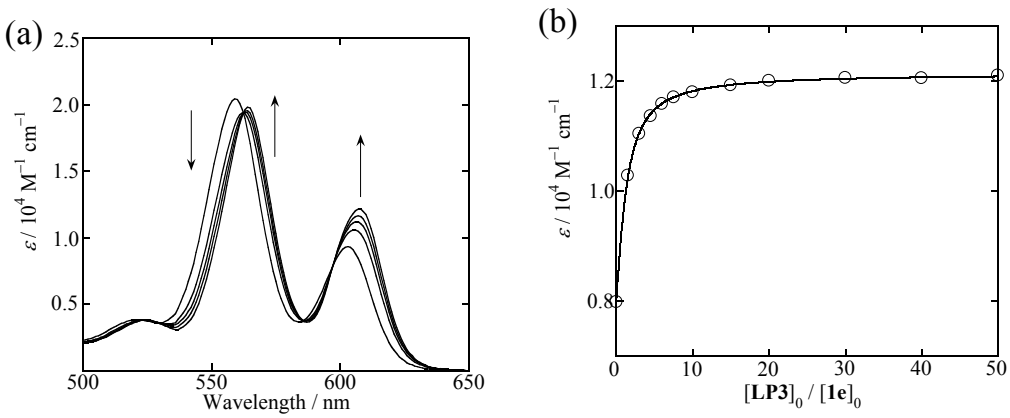

Figure 4-15. (a) UV–vis spectral change resulting from the titration of **1e** (2×10^{-5} M) with **LP3** (1.5×10^{-2} M) in a toluene/acetonitrile (1/1 (v/v)) solution at 10 °C. (b) The change in the molar extinction coefficient at 608 nm. The solid line is a regression curve obtained by curve fitting. $[\mathbf{LP3}]_0$: The concentration of **LP3** when axial binding is ignored. $[\mathbf{1e}]_0$: The initial concentration of **1e**.

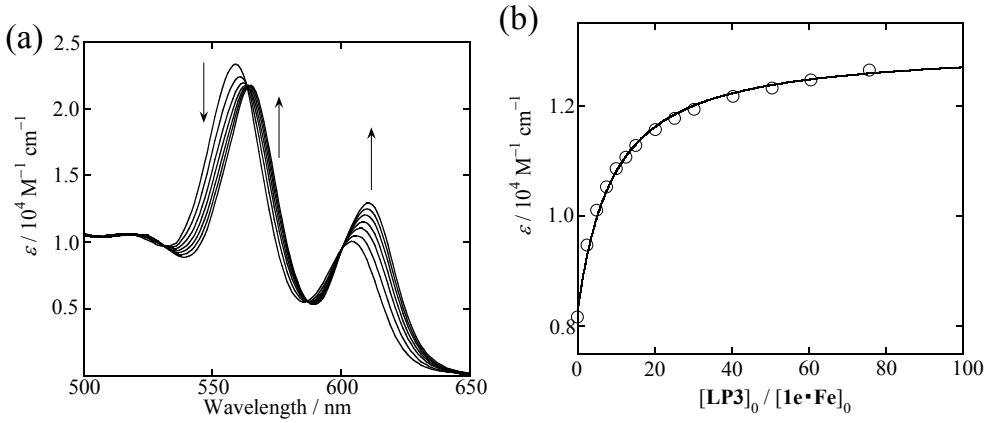

Figure 4-16. (a) UV–vis spectral change resulting from the titration of **1e•Fe** (2×10^{-5} M) with **LP3** (1.5×10^{-2} M) in a toluene/acetonitrile (1/1 (v/v)) solution at 10 °C. (b) The change in the molar extinction coefficient at 611 nm. The solid line is a regression curve obtained by curve fitting. $[\mathbf{LP3}]_0$: The concentration of **LP3** when axial binding is ignored. $[\mathbf{1e{\bullet}Fe}]_0$: The initial concentration of **1e•Fe**.

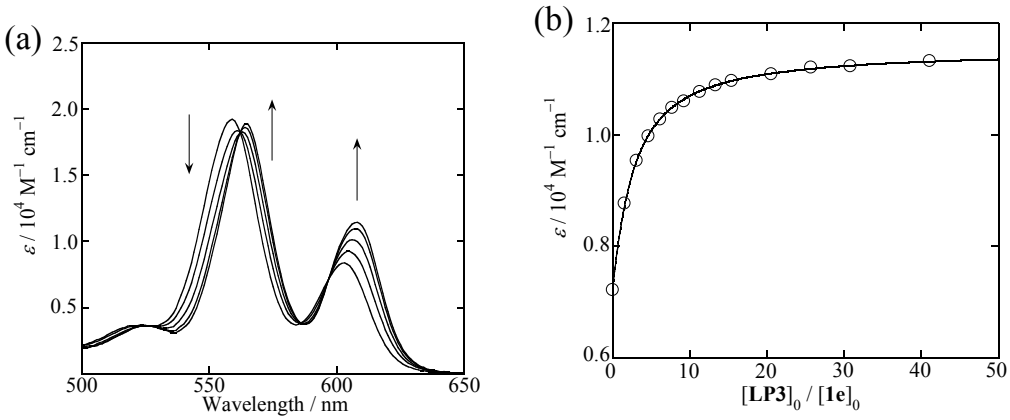

Figure 4-17. (a) UV−vis spectral change resulting from the titration of **1e** (2×10^{-5} M) with **LP3** (1.5×10^{-2} M) in a toluene/acetonitrile (1/1 (v/v)) solution at 30 °C. (b) The change in the molar extinction coefficient at 608 nm. The solid line is a regression curve obtained by curve fitting. $[\mathbf{LP3}]_0$: The concentration of **LP3** when axial binding is ignored. $[\mathbf{1e}]_0$: The initial concentration of **1e**.

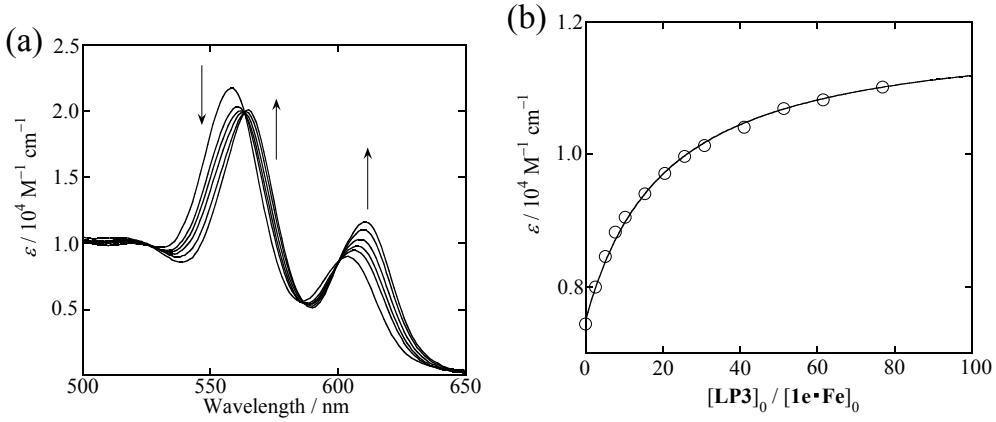

Figure 4-18. (a) UV−vis spectral change resulting from the titration of **1e•Fe** (2×10^{-5} M) with **LP3** (1.5×10^{-2} M) in a toluene/acetonitrile (1/1 (v/v)) solution at 30 °C. (b) The change in the molar extinction coefficient at 611 nm. The solid line is a regression curve obtained by curve fitting. $[\mathbf{LP3}]_0$: The concentration of **LP3** when axial binding is ignored. $[\mathbf{1e•Fe}]_0$: The initial concentration of **1e•Fe**.

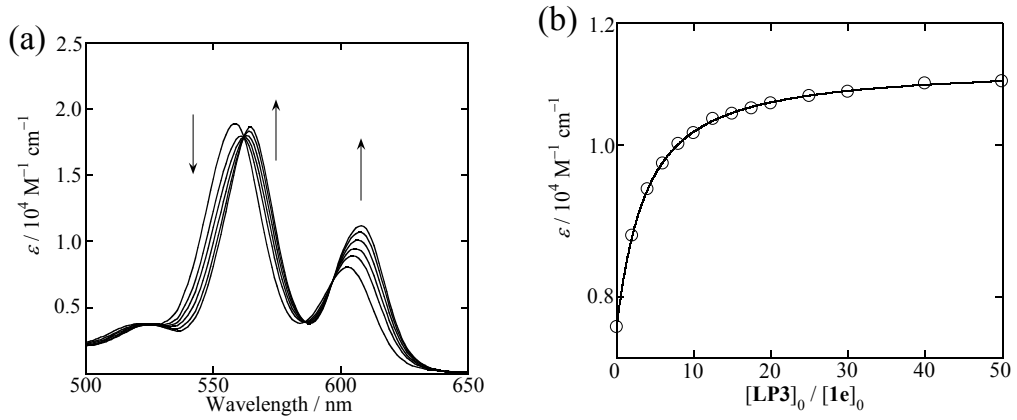

Figure 4-19. (a) UV–vis spectral change resulting from the titration of **1e** (2×10^{-5} M) with **LP3** (1.5×10^{-2} M) in a toluene/acetonitrile (1/1 (v/v)) solution at 40 °C. (b) The change in the molar extinction coefficient at 608 nm. The solid line is a regression curve obtained by curve fitting. $[\mathbf{LP3}]_0$: The concentration of **LP3** when axial binding is ignored. $[\mathbf{1e}]_0$: The initial concentration

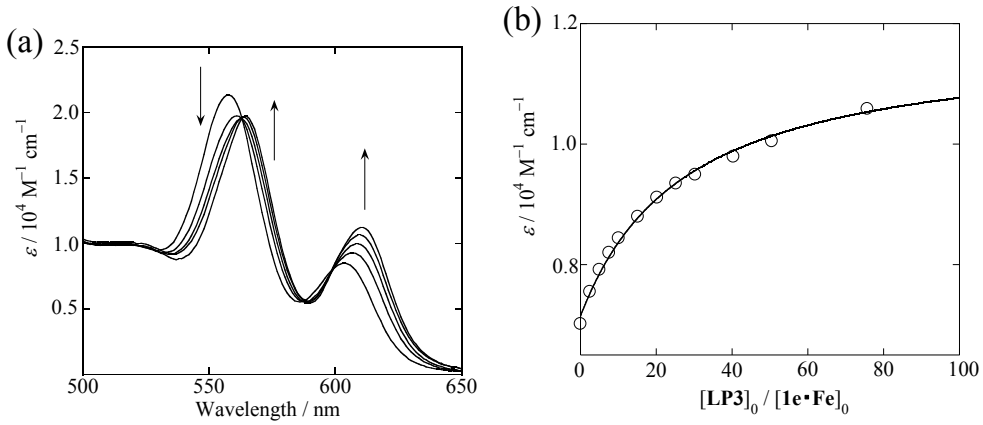

Figure 4-20. (a) UV–vis spectral change resulting from the titration of **1e•Fe** (2×10^{-5} M) with **LP3** (1.5×10^{-2} M) in a toluene/acetonitrile (1/1 (v/v)) solution at 40 °C. (b) The change in the molar extinction coefficient at 611 nm. The solid line is a regression curve obtained by curve fitting. $[\mathbf{LP3}]_0$: The concentration of **LP3** when axial binding is ignored. $[\mathbf{1e•Fe}]_0$: The initial concentration of **1e•Fe**.

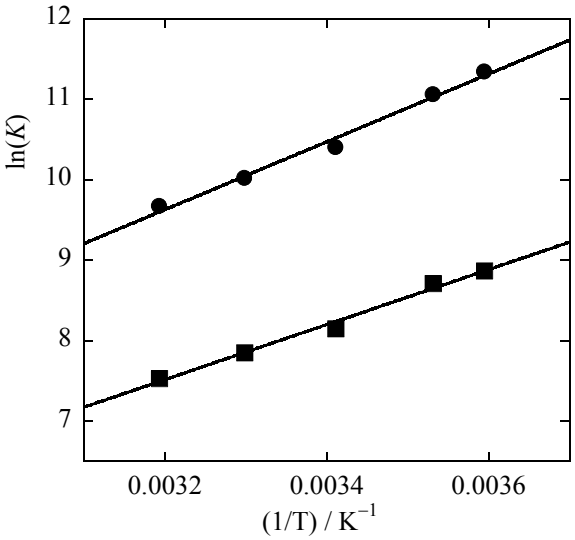

Figure 4-21. van't Hoff plots in the axial coordination reaction of **1e** with **LP3** (black circle) and **1e•Fe** with **LP3** (black square). Solid lines: $\ln(K_{\mathbf{1e•LP3}}) = 4216(1/T) - 3.861$ correlation coefficient (R) = 0.994, $\ln(K_{\mathbf{(1e•Fe)•LP3}}) = 3421(1/T) - 3.429$, R = 0.995.

The theoretical lines for the axial ligand-binding reactions before and after the Fe complexation can be expressed by the following equations: $\ln(K_{\mathbf{1e•LP3}}) = 4216(1/T) - 3.861$, correlation coefficient (R) = 0.994, and $\ln(K_{\mathbf{(1e•Fe)•LP3}}) = 3421(1/T) - 3.429$, R = 0.995. The enthalpy and entropy changes in the ligand-binding reactions were estimated to be $\Delta H_0 = -35.1 \pm 2.2$ kJ mol^{-1} and $\Delta S_0 = -32.1 \pm 7.4$ J K^{-1} mol^{-1}, respectively, for **1e** and **LP3**, and $\Delta H_0 = -28.4 \pm 1.6$ kJ mol^{-1} and $\Delta S_0 = -28.5 \pm 5.6$ J K^{-1} mol^{-1}, respectively, for **1e•Fe** and **LP3** (Table 4-3). The axial ligand-binding reaction between **1e** and **LP3** showed a larger enthalpy change than the corresponding reaction with **1e•Fe** and **LP3**, indicating that **LP3** is difficult to adopt the most stable arrangement because of the steric repulsion with the shielding units. Namely, the coordination bonds between the zinc centre in **1e** and nitrogen atoms in **LP3** were weakened because of the steric repulsion between **LP3** and the shielding unit. On the other hand, the entropy change was comparable in both the coordination reactions.

4-7. Conclusion

In conclusion, allosteric receptor **1e** with sterically bulky shielding units was designed and synthesized. Allosteric receptor **1e** formed a stable 1:1 complex with Fe ions as confirmed by UV–visible titration. The binding constants between **1e** and a series of axial ligands were determined by UV–visible spectroscopic titration before and after the Fe ion complexation. The binding constants of a sterically bulky pyridyl ligand **LP3** significantly decreased after the addition of Fe ions, indicating that the binding ability of the Zn porphyrin in **1** with the ligand were suppressed by adding Fe ions. The degree of allosteric inhibition was evaluated to be 9.5. The axial coordination reaction before the formation of the Fe(II) complex had a larger enthalpy change than the coordination reaction after the Fe(II) complexation, indicating that the steric repulsion between the shielding units and axial ligand plays an important role in this allosteric suppression.

4-8. Experimental section

4-8-1. Synthesis and characterization

General procedure.

Melting points were taken on a Yanako MP J-3 apparatus and are uncorrected. ^{1}H NMR and ^{13}C NMR spectra were recorded on Bruker Nanobay 300, JEOL Lambda 300WB, or JEOL Lambda 400 spectrometers. Chemical shifts were recorded in units of parts per million downfield from tetramethylsilane as an internal standard and all coupling constants are reported in Hz. IR spectra were obtained on a Shimadzu FTIR-8700 spectrometer. UV−vis spectra were obtained on a Shimadzu UV-2550PC spectrometer. The mass spectra were recorded on a JEOL JMS-700T and JMX-AX500 spectrometers. Elemental analyses were obtained from the Analytical Center in Osaka City University. TLC was carried out using 0.2 mm thick Merck silica gel (60 F_{254}) and 0.25 mm thick Merck aluminium oxide 60 precoated plates. Merck silica gel 60 (granulometry 0.063–0.200 mm) and Merck aluminium oxide 90 (granulometry 0.063–0.200 mm) were used for column chromatography. Recycling preparative GPC (gel permeation chromatography) was carried out using Japan Analytical Industry LC–908 with JAIGEL-1H and -2H GPC columns. 5-methy-2,2′-bipyridine (**4**)[4] and 9,10-bis(4-hydroxyphenyl)anthracene (**15**)[5] were prepared according to the reported methods. Commercially available reagents and solvents were purified and dried when necessary.

4, 4, 5, 5-Tetramethyl-2-(4-(4-bromobutoxyphenyl))-1, 3, 2-dioxaborolane (3e)

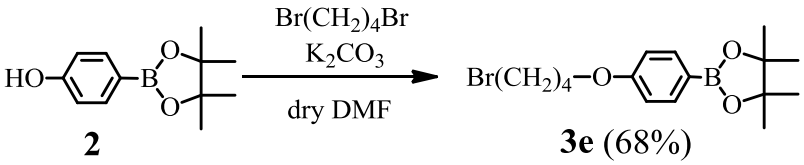

2 **3e** (68%)

To a mixture of **2** (660 mg, 3.0 mmol, 1.0 equiv.), 1,4-dibromobutane (3.24 g, 15 mmol, 5.0 equiv.) and potassium carbonate (1.77 g, 15 mmol, 2.0 equiv.), dry DMF (60 mL) was added under a nitrogen atmosphere. The suspension was stirred overnight at 40 ^{o}C. After cooling to room temperature, the reaction mixture was poured into water. The mixture was extracted with diethyl ether. The extract was dried over sodium sulfate and filtered. The solvent was removed under reduced pressure and the residue was purified by column chromatography on silica gel (hexane/dichloromethane = 2/1 (v/v)) to give **3e** as a white solid (720 mg, 68%).

3e: $C_{16}H_{24}BBrO_3$. White solid; MW 355.1; mp 54 ^{o}C; ^{1}H NMR (300 MHz, $CDCl_3$): δ 7.74 (d, 2H, J = 8.5 Hz), 6.88 (d, 2H, J = 8.6 Hz), 4.22 (t, 2H, J = 5.9 Hz), 3.49 (t, 2H, J = 6.5 Hz), 2.10-1.92 (m, 4H), 1.33 (s, 12H); ^{13}C NMR (75 MHz, $CDCl_3$): δ 161.42, 136.53, 113.79, 83.56, 66.59, 33.48, 29.43, 27.83, 24.86; MS (EI+): m/z 354 [MH^+]; IR (KBr, cm^{-1}): 3001(w), 2978(s), 2945(s), 2878(w), 1608(s), 1568(w), 1520(w), 1474(w), 1456(w), 1445(w), 1398(s), 1389(m), 1362(s), 1317(m), 1281(s), 1250(s), 1215(w), 1198(w), 1176(w), 1161(w), 1144(s), 1107(w), 1090(s), 1076(w), 1040(m), 1009(m), 960(m), 947(w), 854(m), 845(m), 812(m), 737(m), 671(m), 654(s), 634(w), 542(m), 518(m), 502(w); HRMS (EI+): m/z Calcd for $C_{16}H_{24}B^{79}BrO_3$: 354.1002. Found: 354.1009.

5-(5-Bromopentyl)-2,2′-bipyridine 5e[6]

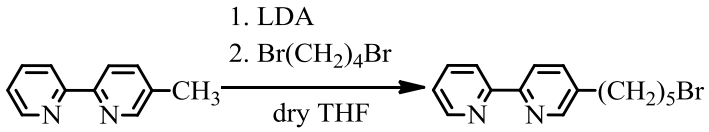

4 **5e** (79%)

To a solution of dry diisopropylamine (1.0 mL, 7.1 mmol, 1.8 equiv.) in dry THF (50 mL), *n*-butyllithium (1.6 M, in *n*-hexane, 3.8 mL, 6.1 mmol, 1.5 equiv.) was added dropwise at −78 °C under a nitrogen atmosphere. The solution was stirred for 1 h at −78 °C and 5-methyl-2,2′-bipyridine **4** (681 mg, 4.0 mmol, 1.0 equiv.) in dry THF (15 mL) was added at −78 °C. The temperature was allowed to raise gradually over 1 h to −40 °C. The solution was recooled to −78 °C and 1,4-dibromobutane (4.32 g, 20 mmol, 5.0 equiv.) in dry THF (15 mL) was added. The solution was allowed to warm up to room temperature and stirred overnight. After the addition of water, THF was evaporated under reduced pressure. Sodium hydrogen carbonate solution was added and the mixture was extracted with dichloromethane. The extract was washed with brine and dried over sodium sulfate. After filtration, the solvent was removed under reduced pressure. The crude product was purified by column chromatography on basic aluminium oxide (hexane/dichloromethane = 3/1 (v/v)) to give **5e** as a white solid (964 mg, 79%).

5e: $C_{15}H_{17}BrN_2$. White solid; MW 305.2; mp 31 °C; ^{1}H NMR (300 MHz, $CDCl_3$): δ 8.67 (d, 1H, J = 4.8 Hz), 8.51 (d, 1H, J = 2.1 Hz), 8.36 (d, 1H, J = 8.0 Hz), 8.31 (d, 1H, J = 8.1 Hz), 7.81 (td, 1H, J = 7.7, 1.6 Hz), 7.64 (dd, 1H, J = 8.1, 2.0 Hz), 7.31–7.29 (m, 1H), 3.41 (t, 2H, J = 6.7 Hz), 2.70 (t, 2H, J = 7.6 Hz), 1.91 (quintet, 2H, J = 7.1 Hz), 1.70 (quintet, 2H, J = 7.6 Hz), 1.57–1.49 (m, 2H); ^{13}C NMR (75 MHz, $CDCl_3$) δ156.22, 154.04, 149.29, 149.16, 137.68, 136.90, 136.79, 123.46, 120.82, 120.75, 33.63, 32.65, 32.54, 30.24, 27.68; MS (EI+): *m/z* 304 [M^+]; IR (KBr, cm^{-1}): 3067(m), 3053(m), 3011(m), 2962(m), 2943(s), 2928(s), 2866(s), 1585(s), 1574(m), 1557(s), 1460(s), 1429(s), 1392(m), 1350(w), 1304(w), 1258(m), 1230(m), 1205(m), 1190(w), 1148(w), 1092(w), 1065(w), 1042(w), 1030(m), 1013(m), 991(m), 860(s), 808(m), 785(s), 752(s), 737(m), 727(m), 640(s), 606(s); HRMS (EI+): *m/z* Calcd for $C_{15}H_{17}{}^{79}BrN_2$: 304.0575. Found: 304.0577.

Compound 6e

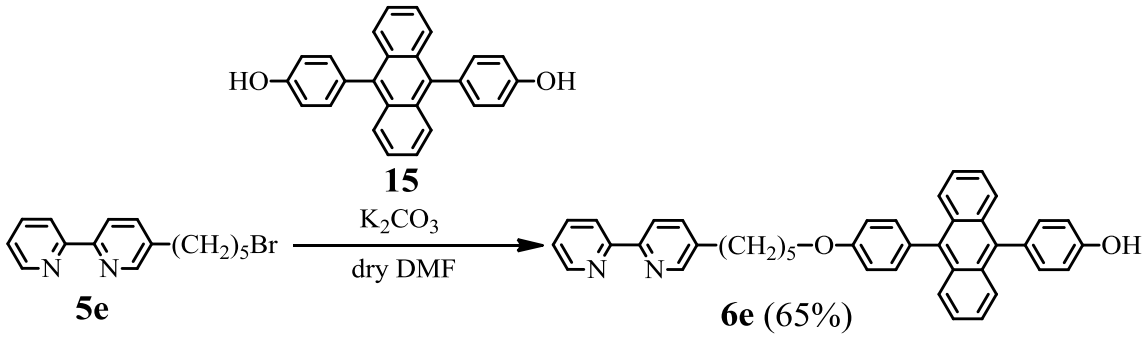

To a mixture of **5e** (244 mg, 0.8 mmol, 1.0 equiv.), 9,10-bis(4-hydroxyphenyl)anthracene **15** (1.45 g, 4.0 mmol, 5.0 equiv.) and potassium carbonate (473 mg, 4.0 mmol, 5.0 equiv.), dry DMF (80 mL) was added under a nitrogen atmosphere. The suspension was stirred overnight at 50 ^{o}C. After cooling to room temperature, the reaction mixture was poured into water. The mixture was extracted with diethyl ether. The extract was dried over sodium sulfate and filtered. The solvent was removed under reduced pressure and the residue was purified by column chromatography on basic aluminium oxide (chloroform) to give **6e** as a light yellow solid (299 mg, 65%).

6e: $C_{41}H_{35}N_2O_2$. light yellow solid; MW 586.7; mp 275 ^{o}C; ^{1}H NMR (300 MHz, d6-DMSO): δ 9.71 (br, 1H), 8.67 (d, 1H, J = 4.7 Hz), 8.59 (d, 1H, J = 1.8 Hz), 8.37 (d, 1H, J = 8.0 Hz), 8.34 (d, 1H, J = 8.1 Hz), 7.93 (td, 1H, J = 7.8, 1.7 Hz), 7.63 (dd, 1H, J = 8.0, 2.2 Hz), 7.68–7.60 (m, 4H), 7.45–7.33 (m, 7H), 7.25–7.18 (m, 4H), 7.03 (d, 2H, J = 8.4 Hz), 4.14 (t, 2H, J = 6.3 Hz), 2.76 (t, 2H, J = 7.3 Hz), 1.90–1.72 (m, 4H), 1.61–1.56 (m, 2H); ^{13}C NMR (75 MHz, d6-DMSO): δ 158.16, 156.90, 149.19, 141.44, 137.25, 136.99, 136.06, 132.05, 131.98, 129.94, 129.66, 129.60, 128.28, 126.64, 126.47, 125.25, 125.16, 123.86, 120.15, 115.43, 114.56, 67.47, 31.92, 30.29, 28.57, 25.23; MS (FAB+): *m/z* 587.2 [MH^+]; IR (KBr, cm^{-1}): 2922(s), 2856(m), 1699(w), 1684(w), 1653(w), 1607(s), 1558(m), 1516(s), 1489(w), 1464(s), 1437(m), 1392(s), 1364(w), 1269(m), 1242(s), 1178(w), 1154(w), 1067(w), 943(w), 829(m), 812(w), 796(w), 773(s), 727(w), 706(w), 675(m), 611(w), 575(w), 542(w); HRMS (FAB+): *m/z* Calcd for $C_{41}H_{35}N_2O_2$: 587.2694. Found: 587.2697.

Compound 7e (Side chain)

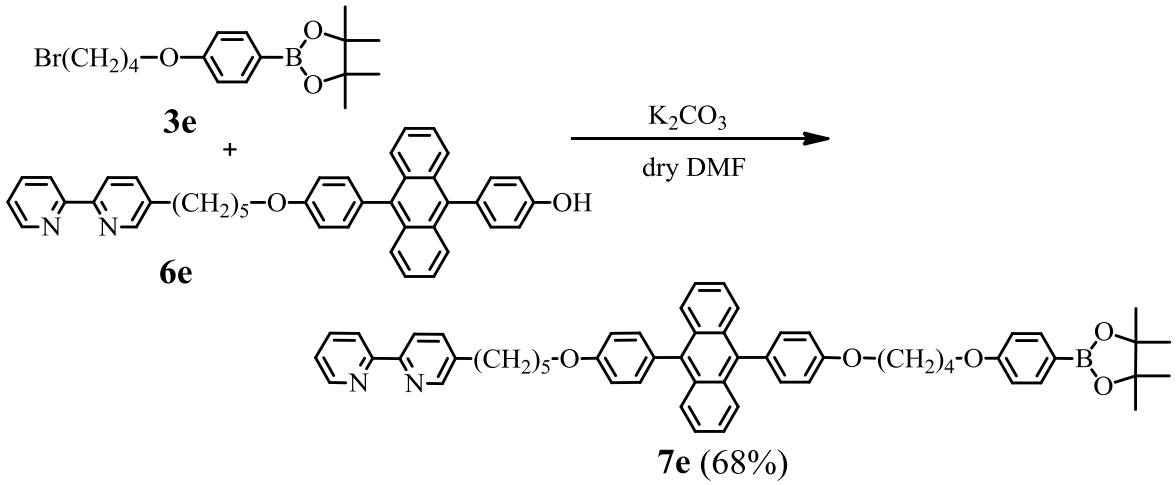

To a mixture of **3e** (178 mg, 0.50 mmol, 1.0 equiv.), **6e** (293 mg, 0.50 mmol, 1.0 equiv.) and potassium carbonate (296 mg, 2.5 mmol, 5.0 equiv.), dry DMF (100 mL) was added under a nitrogen atmosphere. The suspension was stirred overnight at 50 ^{o}C. After cooling to room temperature, the reaction mixture was poured into water. The mixture was extracted with dichloromethane. The extract was dried over sodium sulfate and filtered. The solvent was removed under reduced pressure and the residue was purified by column chromatography on hydroscopic (6wt%) basic aluminium oxide (dichloromethane / methanol = 1/ 0 ~ 9/ 1 (v/ v)) and washed with hexane to give **7e** as a light yellow solid (290 mg, 68%).

7e: $C_{57}H_{57}BN_2O_5$. light yellow solid; MW 860.9; mp 164 ^{o}C; ^{1}H NMR (300 MHz, $CDCl_3$): δ 8.68 (d like, 1H, J = 4.9 Hz), 8.56 (d, 1H, J = 1.8 Hz), 8.37 (d like, 1H, J = 8.0 Hz), 8.34 (d, 1H, J = 7.9 Hz), 7.84–7.68 (m, 8H), 7.39–7.31 (m, 9H), 7.13 (dd, 4H, J = 8.7, 3.0 Hz), 6.94 (d, 2H, J = 8.7 Hz), 4.19–4.10 (m, 6H), 2.78 (t, 2H, J = 7.6 Hz), 2.09 (s, 4H), 1.97–1.80 (m, 4H), 1.70–1.62 (m, 2H), 1.34 (s, 12H); ^{13}C NMR (75 MHz, $CDCl_3$): δ161.60, 158.46, 158.40, 156.26, 154.00, 149.35, 149.13, 137.91, 136.85, 136.82, 136.74, 136.73, 136.52, 132.36, 131.07, 131.01, 130.23, 127.03, 124.84, 123.40, 120.80, 120.74, 114.36, 114.34, 113.86, 83.52, 67.82, 67.52, 67.28, 32.81, 30.89, 29.68, 29.20, 26.10, 26.05, 25.77, 24.84; MS (FAB+): *m/z* 861.4 [MH^+]; IR (KBr, cm^{-1}): 2928(s), 2872(m), 1607(s), 1558(w), 1512(s), 1458(m), 1437(w), 1391(m), 1362(s), 1317(m), 1279(w), 1240(s), 1176(m), 1144(m), 1091(m), 1011(w), 943(w), 818(m), 795(m), 770(s), 656(m), 611(m); HRMS (FAB+): *m/z* Calcd for $C_{57}H_{58}BN_2O_5$: 861.4434. Found: 861.4439.

Compound 1e

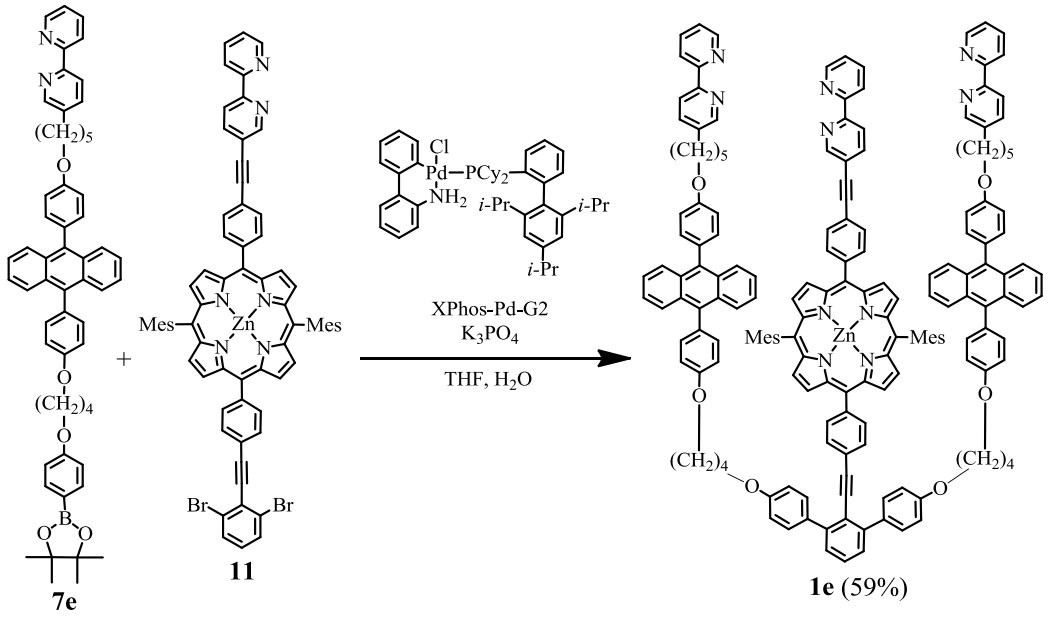

A mixture of **11** (48.0 mg, 40 μmol, 1.0 equiv.), **7e** (86.0 mg, 100 μmol, 2.5 equiv.), Xphos palladium (II) (6.3 mg, 8 μmol, 0.2 eq.) and tripotassium phosphate (212 mg, 1.0 mmol, 25 eq.) was dissolved in dry THF (8 mL) and distilled water (2 mL). The mixture was stirred overnight at 50 ^{o}C under an argon atmosphere. After cooling to room temperature, the mixture was poured into distilled water and extracted with dichloromethane. The solution was dried over sodium sulfate and solvent was removed under reduced pressure. The residue was purified by column chromatography on hydroscopic (6wt%) basic aluminium oxide (hexane/ dichloromethane = 1/ 4 ~ 0/ 1 (v/ v)) to give **1e** as a purple powder (57 mg, 57%).

1e: $C_{172}H_{138}N_{10}O_6Zn$; MW 2394.5; purple solid; mp 147 ^{o}C; ^{1}H NMR (300 MHz, $CDCl_3$): δ 8.96 (m, 1H), 8.85–8.79 (m, 4H), 8.76–8.73 (m, 5H), 8.68–8.66 (m, 2H), 8.55–8.54 (m, 2H), 8.51–8.46(m, 2H), 8.37 (d, 2H, J = 8.0 Hz), 8.32 (d, 2H, J = 8.1 Hz), 8.24 (d, 2H, J = 8.2 Hz), 8.11–8.07 (m, 3H), 7.94 (d, 2H, J = 8.2 Hz), 7.90–7.79 (m, 7H), 7.69–7.66 (m, 2H), 7.57–7.42 (m, 13H), 7.38–7.28 (m, 7H), 7.20–7.04 (m, 28H), 4.19–4.05 (m, 12H), 2.76 (t, 4H, J = 7.5 Hz), 2.61 (s, 6H), 2.07–1.61 (m, 32H); ^{13}C NMR (75 MHz, $CDCl_3$): δ158.74, 158.67, 151.74, 149.94, 149.77, 149.68, 149.32, 144.78, 143.66, 140.46, 139.46, 139.19, 139.00, 137.47, 136.90, 134.57, 134.29, 133.74, 132.27, 132.00, 131.00, 129.87, 129.22, 128.61, 128.16, 127.65, 127.47, 124.88, 123.34, 122.84, 121.65, 120.80, 120.45, 120.11, 119.42, 119.17, 114.20, 113.91, 83.87, 67.82, 67.63, 67.56, 32.80, 30.84, 29.68, 29.42, 29.13, 26.13, 25.73, 22.67, 21.63, 21.45; MS (FAB+): *m/z* 2504 [MH^+]; IR (KBr, cm^{-1}): 2922(s), 2854(s), 1716(w), 1653(w), 1608(s), 1576(m), 1558(m), 1541(m), 1512(s), 1491(w), 1458(s), 1437(m), 1242(s), 1204(w), 1178(s), 997(s), 908(w), 829(s), 796(s), 750(s), 727(w), 638(m); Elemental analysis: Calcd for $C_{180}H_{156}C_{l4}N_{10}O_6Zn$, [M + Hexane + 2 CH_2Cl_2]: C, 78.26; H, 5.69; N, 5.07. Found: C, 78.00; H, 5.89; N, 4.87.

4-8-2. UV–vis titration

General procedure.

UV-vis spectra were measured by a Shimadzu UV-2550 spectrophotometer using 1 cm quartz cuvettes and EYELA NCB-1200 Low Temperature Bath. A spectrochemical analysis grade of solvent was purchased from Wako pure chemical industries, Ltd. The curve fittings were calculated by using KaleidaGraph 4.1J.

Method

A solution of **1e** (2×10^{-5} M) in toluene-acetonitrile (1/1 (v/v)) was prepared by careful weighting using an analytical balance. Solution of **1e** (3 mL) was added in a quartz cell by using a whole pipette. The solution of **1e·Fe** was prepared by adding the solution of $Fe(BF_4)_2$ (1.0 equiv.) to the solution of **1e** (3.0 mL). A guest solution was added to the solution by using a micropipette. A solution of $Fe(BF_4)_2$ and axial ligands shown in Figure 3-11 were used as the guest solution for the determination of the complex formation constant and the axial binding constants, respectively. After each addition of the guest solution, the quartz cell was placed in the cell compartment of a spectrometer and allowed to come to thermal equilibrium. UV–vis spectra were measured with a spectrophotometer equipped with a temperature controller to keep the temperature at measurement temperature. This procedure was repeated until no change was recorded within the spectra. The association constants were determined by the curve fitting using expression 2n or 2q (see section 2-7-3) as a regression expression for the change of the apparent molar extinction coefficient ε (app) at appropriate wavelength. The conditions of each titration were summarized in Table 4-3.

Table 4-3. Conditions of each titration in section 4-4, 4-5 and 4-6.

Host[a]	Guest	[Guest]	wavelength	Temperature	Figure No.
1e	$Fe(BF_4)_2•6H_2O$	6×10^{-4} M	500 nm	20 °C	4-2
1e	**LIm2**	1.2×10^{-2} M	611 nm	20 °C	4-3
1e•Fe[b]	**LIm2**	1.2×10^{-2} M	613 nm	20 °C	4-4
1e	**LIm3**	1.2×10^{-2} M	611 nm	20 °C	4-5
1e•Fe[b]	**LIm3**	1.2×10^{-2} M	613 nm	20 °C	4-6
1e	**LP1**	3×10^{-2} M	608 nm	20 °C	4-7
1e•Fe[b]	**LP1**	3×10^{-2} M	610 nm	20 °C	4-8
1e	**LP2**	3×10^{-2} M	608 nm	20 °C	4-9
1e•Fe[b]	**LP2**	3×10^{-2} M	611 nm	20 °C	4-10
1e	**LP3**	1.5×10^{-2} M	608 nm	20 °C	4-11
1e•Fe[b]	**LP3**	1.5×10^{-2} M	611 nm	20 °C	4-12
1e	**LP3**	1.5×10^{-2} M	608 nm	5 °C	4-13
1e•Fe[b]	**LP3**	1.5×10^{-2} M	611 nm	5 °C	4-14
1e	**LP3**	1.5×10^{-2} M	608 nm	10 °C	4-15
1e•Fe[b]	**LP3**	1.5×10^{-2} M	611 nm	10 °C	4-16
1e	**LP3**	1.5×10^{-2} M	608 nm	30 °C	4-17
1e•Fe[b]	**LP3**	1.5×10^{-2} M	611 nm	30 °C	4-18
1e	**LP3**	1.5×10^{-2} M	608 nm	40 °C	4-19
1e•Fe[b]	**LP3**	1.5×10^{-2} M	611 nm	40 °C	4-20

(a): $[\mathbf{1e}]_0 = 2 \times 10^{-5}$ M, (b): $Fe(BF_4)_2•6H_2O$ (1.5×10^{-3} M, 100 μmol, 1 equiv.) was added to a solution of **1e**.

4-8. References

(1) *Spartan'08*, Wavefunction, Inc., Irvine, CA.

(2) Kinzel, T.; Zhang, Y.; Buchwald, S. L. *J. Am. Chem. Soc*. **2010**, *132*, 14073−14075.

(3) (a) Nabeshima, T.; Yoshihira, Y.; Saiki, T.; Akine, S.; Horn, E. *J. Am. Chem. Soc.* **2003**, *125*, 28−29. (b) Nabeshima, T.; Tanaka, Y.; Saiki, T.; Akine, S.; Ikeda, C.; Sato, S. *Tetrahedron Lett.* **2006**, *47*, 3541−3544.

(4) Kato, M.; Hashimoto, E.; Kozaki, M.; Suzuki, S.; Okada, K *Tetrahedron Lett.* **2012**, *53*, 309−312.

(5) (a) Fudickar, W.; Linker, T. *Chem. Commun*. **2008**, 1771−1773. (b) Barve, K. A.; Raut, S. S.; Mishra, A. V.; Patil, V. R. *J. Appl. Polym. Sci.* **2011**, *122*, 3483−3492.

(6) Fletcher, N. C.; Nieuwenhuyzen, M.; Rainey *J. Chem. Soc., Dalton Trans.* **2001**, 2641−2648.

Conclusion

Inhibition-type allosteric molecular systems **1** were developed using metalloporphyrins as the active site. The shielding strategy was successfully applied to achieve the allosteric inhibition of the receptor activity of **1** using Fe ions as the effector. UV–visible spectroscopic titration of **1** was performed to estimate both the thermodynamic stability of the Fe complexes and the degree of the allosteric inhibition of axial binding ability.

In **chapter 2**, molecule **1a** was designed as an artificial allosteric receptor. The synthetic route and evaluation method for the performance of allosteric receptor **1** were established. These results provide a basic technique to conduct the subsequent investigations. Allosteric receptor **1a** formed a stable 1:1 complex with Fe ion. The binding constants of **1a** with axial ligand **LP1** were determined before (active form) and after the Fe(II) complexation (inactive form). The addition of Fe ions considerably decreased the binding constant; the degree of allosteric inhibition was 1.64.

In **chapter 3**, artificial allosteric receptors **1b**, **1c**, and **1d** with shorter alkyl chains than **1a** were designed. Molecular mechanics force field (MMFF) calculations indicated that **1b** and **1c** afford stable Fe complexes, and the formation of Fe complex **1d·Fe** is probably not possible. Receptors **1b** and **1c** were synthesized. Allosteric receptors **1b** and **1c** formed a stable 1:1 complex with Fe ion. The binding constants of **1a**, **1b**, and **1c** with various types of axial ligands were determined before (active form) and after the Fe(II) complexation (inactive form), and the degrees of allosteric inhibition were determined. When receptor **1c** with the shortest alkyl chain and sterically bulky ligand **LP3** was used, a stronger allosteric inhibition (4.5) was observed.

In **chapter 4**, artificial allosteric receptor **1e** with sterically bulky shielding units was designed and synthesized. The binding constants of **1e** with many types of axial ligands were determined before (active form) and after the Fe(II) complexation (inactive form), and the degrees of allosteric inhibition were determined. When receptor **1e** and **LP3** was combined, the strongest allosteric inhibition (9.5) was observed. The thermodynamic parameters of axial ligand-binding reaction before and after the addition of Fe ions were determined by Van't Hoff plot. The absolute value of the entropy change became smaller when the Fe complex was formed. These results indicate that the axial coordination between the nitrogen atom of axial ligand and the zinc atom of porphyrin centre is destabilized by Fe complexation because of the steric repulsion between the shielding units and axial ligand. This destabilization plays an important role in the allosteric inhibition of artificial allosteric effector **1e**.

Acknowledgement

I would like to express my deep gratitude to Professors Keiji Okada, Masatoshi Kozaki, and Shuichi Suzuki (Lecturer at Osaka City University until September of 2015, Associate Professor at Osaka University from October 2015). They provided great instructions and wide-ranging advice to me over many years. In particular, I would like to express my deepest gratitude to Professor Masatoshi Kozaki, my graduate advisor.

I would like to express my gratitude to all the member of the physical organic chemistry laboratory. Their helpful discussions and friendship supported me. I would like to express my gratitude to all the members of the Analytical Center in Osaka City University. They helped in my NMR measurements, MS measurements, and elemental analyses. I would like to thank all the friends inside and outside the university. In particular, I would like to specially thank Mr. Satoru Yamamoto for his support, friendship, and help in Physical Chemistry.

This work was partially supported by the Sasakawa Scientific Research Grant (No. 25−319) from the Japan Science Society.

Finally, I would like to express my deepest gratitude to my family. I might not accomplish this goal without their support and encouragement.